Dr. Mei Li
China university of Geosciences (Beijing)
29 Xueyuan Road, Haidian, Beijing 100083, P. R. China

Dr. Ahmed Nabih Zaki Rashed
Professor, Electronics and Electrical Engineering
Menoufia University, Egypt

Dr. Rungun R Nathan
Assistant Professor in the Division of Engineering, Business and Computing
Penn State University - Berks, Reading, PA 19610, USA

Dr. Taohong Zhang
School of Computer & Communication Engineering
University of Science and Technology Beijing, China

Dr. Haifa El-Sadi
Assistant professor
Mechanical Engineering and Technology
Wentworth Institute of Technology, Boston, MA, USA

Huaping Yu
College of Computer Science
Yangtze University, Jingzhou, Hubei, China

Ph. D Yubian Wang
Department of Railway Transportation Control
Belarusian State University of Transport, Republic of Belarus

Prof. Mansheng Xiao
School of Computer Science
Hunan University of Technology, Zhuzhou, Hunan, China

Prof. Ying Cuan

School of Computer Science, Xi'an Shiyou University, China

Qichuan Tian

School of Electric & Information Engineering

Beijing University of Civil Engineering & Architecture, Beijing, China

Ph. D MU JING

Xi'an Technological University, China

Language Editor

Professor Gailin Liu

Xi'an Technological University, China

Dr. H.Y. Huang

Assistant Professor

Department of Foreign Language, the United States Military Academy, West Point, NY 10996, USA

Would you like to be an Associate Editor? Simply send a request together with your Curriculum Vitae to xxwlcn@163.com. We will have a team of existing editors or at least three experts in your field to review your request and make a decision as soon as we can. The criteria to be an associate editor are: 1. must have advanced degree; 2. must be a leader or have outstanding achievements in the specific research field; 3. must be recommended by the review team.

Table of Contents

Research and Design of Planning Systems in the AORBCO Model

Chongtian Feng

School of Computer Science & Engineering
Xi'an Technological University
Xi'an, China
E-mail: 15829250509@163.com

Wuqi Gao

School of Computer Science & Engineering
Xi'an Technological University
Xi'an, China

Liping Lu

School of Computer Science & Engineering
Xi'an Technological University
Xi'an, China
Emile: llp21@126.com

Junmin Luo

School of Computer Science & Engineering
Xi'an Technological University
Xi'an, China

Abstract—**Planning research in artificial intelligence began earlier, dating back to 1969, and the general problem solver (GPS) designed by Newell and Simon [1]. Since then, other researchers have also proposed other planners, such as QA3 system using theorem proving method to construct planning[2], Fikes and Nilsson designed STRIPS planning system [3], until today STRIPS planning method is still only a very important research method in the field of planning. After more than 50 years of research, there have been many intelligent planning methods such as graph planning method, probability planning, timing planning, heuristic planning and perceptual planning. Although the existing intelligent planning methods have been able to solve some problems, the existing planning mainly focuses on the design of the planning algorithm, and the manual analysis preprocessing workload is large. Research has pointed out that the new generation of intelligent planners should be knowledge-based development of knowledge-based planning systems is a meaningful work [4]. Therefore, by analyzing the existing intelligent planning methods and AORBCO model, this paper gives the definition of intelligent planning with self-consciousness, and proposes an intelligent planning method based on self-consciousness based on behavior control.**

Keywords-Cloud Computing; Intelligent Planning; Intelligent Model; Self-Consciousness; AORBCO Model

I. RESEARCH STATUS

Intelligent planning is a research field with strong application in the field of artificial intelligence, which is widely used in practical problems such as industrial task scheduling and mechanical manufacturing planning. For practical problems, developing a domain-specific planner is the main goal of improving planning efficiency, and a general domain-independent planner is the ultimate goal of researchers.

In the field of intelligent planning, some mature planning methods have been proposed, and a planner with good performance has been designed according to this method, which has successfully solved some planning problems. In the International Intelligent Planning Contest (IPC), more efficient planners are constantly emerging. The following is a list and analysis of the current mainstream intelligent planning methods.

A. Intelligent planning method

At present, the academic community divides intelligent planning into two categories: classical intelligent planning and non-classical intelligent planning. Classical planning only refers to: Agent knowledge of the planning world is complete planning process action effect is determined at

each time step can only perform one action [5]. Non-classical intelligent planning refers to: Compared with classical planning, non-classical planning refers to planning that is carried out in an environment that is partially observable or random, considers time and resources, and relaxes other constraints. Many planning methods are proposed for two intelligent planning problems.

The classical methods in the field of intelligent planning mainly include state space planning method and planning space planning method.

The state space planning method regards the planning solution process of the problem as a state transition. The prime minister of the method regards the initial state of the problem as the current state, and selects a certain operator for application to obtain a new state. If the target state appears, the planning ends. If not, the current state is updated according to a certain search strategy to repeat the above actions. The search strategies applied when planning fails mainly include depth-first search, breadth-first search and A * search algorithm. The first two search algorithms are called uninformative search algorithms, that is, search according to a specified order during the search process. For example, depth-first search searches according to the maximum depth of the search tree. If the search is completed, the planning ends. If the deepest node state is not the target state, the previous node is backtracked for re-search. The A * search algorithm adds a search algorithm for guiding information. The guiding information is a defined evaluation function:

$$f(n) = g(n) + h(h)$$

Where $g(n)$ is the minimum cost from the starting node to the current node, and $h(n)$ is the minimum cost from the current node to the target node.

In the planning space planning, the planner searches the planning space, and the planning is defined as a set of planning operations with a certain order and bound by variables, which does not necessarily correspond to an action sequence [6].

Graph planning is to introduce the graph structure into the planning process. Based on the planning graph, the planning graph is composed of two nodes and three edges. The two nodes refer to the proposition node and the action node, and the three edges refer to the precondition edge, add effect edge and delete effect edge [7].

The problem conditions solved by non-classical programming are often more relaxed than those of classical intelligent programming, such as the planning problem with uncertain initial state and action results. Such planning is called uncertain planning. For example, heuristic planning makes some assumptions and simplification constraints on the original planning to obtain a simpler problem. In non-classical planning, some new planning methods adapted to specific problems are often proposed based on classical planning methods.

A. Blum and J. Langford proposed the probabilistic planning algorithm PGraphplan [8] based on the planning graph. The algorithm includes two stages, plan graph expansion and effective plan extraction. The probabilistic planning algorithm solves the uncertainty planning, that is, the result of the action is uncertain. The probability is used to represent the uncertainty, and the result of the action has its probability. In 2003, The Duy Bui and Wojciech Jamroga of the University of Twente in the Netherlands extended the planning graph to deal with multi-agent planning [9]. They defined three kinds of agent relationships: cooperative relationship, antagonistic relationship and independent relationship, and proposed corresponding algorithms for the planning between the three agents.

The heuristic planning uses the search strategy to realize the planning, and uses different heuristic strategies to guide the search direction in the planning process. The current heuristic strategy has HSP planner, which calculates the planning cost by accumulating the heuristic value in the planning process, while the FF planner uses the enhanced hill climbing algorithm to optimize the planning cost, and finally realizes the optimal planning.

B. *Analysis of Intelligent Planning Method*

Classical intelligent planning believes that all information is known and there will be no unexpected situations. Therefore, planning is regarded as a transition between states, so the planning process is a process of searching for the target state among many states. Classical intelligent planning requires that every link in the planning process is determined. Therefore, classical intelligent planning is often harsh in planning conditions. For example, it is necessary to ensure the uniqueness of action results. However, there may be many consequences of actions in the real world. In fact, the results may be different according to the probability. Therefore, non-classical intelligent planning is developed on the basis of classical intelligent planning. So far, classical intelligent planning and non-classical intelligent planning can solve most practical problems. Although its planning effect is good, the whole planning process from the definition of intelligence does not reflect the characteristics of intelligence. Therefore, on the basis of the existing intelligent planning algorithm, it is necessary to combine intelligent research to further propose a planning that can use intelligent theory.

The existing intelligent planning has a great relationship with the problem itself. The information contained in the planning problem is extracted and input into the existing algorithm flow, and finally the planning result is given. A relatively complete agent often needs to know the knowledge of multiple fields. When the agent solves the problems in different fields, it needs to process different domain knowledge. At present, there is no unified organization form for different domain knowledge, which leads to the need for the agent to manually participate in the preprocessing when dealing with multi-domain planning problems. Through in-depth analysis of the nature of intelligence and the representation of knowledge, AORBCO model gives a relatively unified knowledge representation and knowledge organization form. Therefore, the development of intelligent planning system based on AORBCO model is a reasonable way to develop general intelligent planning system.

II. DEFINITION OF INTELLIGENT PLANNING BASED ON SELF-CONSCIOUSNESS

The ultimate goal of artificial intelligence is to make the machine have human intelligence. At present, the research of artificial intelligence does not have a deep discussion and understanding of human intelligence. The current artificial intelligence only makes the computer have ' look ' intelligence, that is, the existing artificial intelligence is human: the intelligent performance of program algorithm developers. Developers summarize the steps and methods to solve the problem, and input them into the computer (program) in the form that the computer can recognize, and drive the computer to carry out intelligent activities. Therefore, the existing artificial intelligence is a weak artificial intelligence that performs well. Intelligent planning is an early-developed branch of artificial intelligence, which wants to embody intelligence in the planning process. At present, the more recognized definition of intelligent planning is as follows : to understand and analyze the surrounding environment, according to the predetermined goal, to reason about a number of alternative actions and the resource constraints and related constraints provided, and to comprehensively formulate the action sequence to achieve the goal. This sequence of actions is called a plan. The intelligence that can only be planned is mainly reflected in the complexity of the planning algorithm to deal with the problem, the processing efficiency, and whether it is optimal. This is only to evaluate the intelligence of the planning from the results of the problem, but the algorithm itself is a summary of the public planning.

Therefore, it is essential to discuss what intelligence is in order to design an intelligent planning framework.

The AORBCO model believes that knowledge is the understanding and description of ' knowledge '. And people's knowledge is divided into eight knowledge: eye knowledge, ear knowledge, nose knowledge, tongue knowledge, body knowledge, consciousness, the last knowledge, Alafia knowledge. Through the eight senses, the information in the real world is

received, understood and called, so as to carry out intelligent activities. In the literature [10], through in-depth analysis and research on what intelligence is, through the study of general psychology, reflective psychology, cognitive psychology and consciousness-only psychology, the four characteristics of intelligence are pointed out, and the four major knowledge components in the AORBCO model are studied. It is considered that knowledge is the understanding and description of "knowledge." Only with knowledge can intelligence be shown. We believe that intelligence and knowledge are actually equivalent.

Therefore, the intelligent planning of agent should be based on agent intelligence, that is, intelligent planning is based on knowledge. Combined with the intelligent theory of AORBCO model, the definition of intelligent planning based on self-consciousness is given: agent takes its own knowledge as the planning basis, and calls knowledge under the action of behavior control mechanism to give the knowledge sequence that agent can call in turn to solve the problem.

III. OVERALL FRAMEWORK DESIGN OF PLANNING SYSTEM IN AORBCO MODEL

By studying the existing intelligent planning algorithm, the overall framework of intelligent planning based on self-consciousness is given under the knowledge system of AORBCO model.
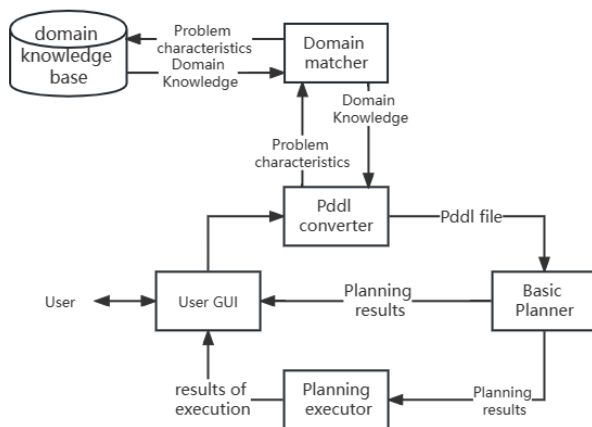
Figure 1.   System framework diagram

The above figure shows the overall framework of the planning system based on the AORBCO

model. The overall framework consists of six parts: domain knowledge base, user GUI, planning domain matcher, planning problem generator, general planning period and planning result interpreter.

The domain knowledge base is an agent's initialized knowledge stored in a non-relational database composed of nodes and relationships. The AORBCO model believes that domain knowledge is the result of Ego's abstraction of the real world, so there is more than one domain knowledge base for Ego;

User GUI: The user and system interaction interface, where the user can enter the problem to be solved into the system in a form that the user can understand.

Planning problem generator: It is the generation component of planning problem and the intermediate component of domain location. It has two main functions: convert the problem input by the user into an XML description format that the system can recognize, integrate it into the initial XML description of Ego, and then convert the XML format problem description file into a runnable pddl problem description file; extract key domain information from the problem.

Planning domain matcher: It is used to locate the components of the problem domain. After the planning problem generator obtains the key information of the domain, it locates the domain of the problem in many domain knowledge bases through the domain matcher, obtains the domain knowledge related to the problem and generates the domain PDDL file.

General planner: General planner is the core of the intelligent planning system based on self-awareness. The planning algorithm of the general planning period is not aimed at a specific domain knowledge. The core idea is: Based on the Ego knowledge organization form and storage form, the existing heuristic planning ideas are used to plan the problem. Because the knowledge organization form of Ego is fixed, that is, all domain knowledge is the same organizational structure, and the knowledge structure is universal, the planning algorithm on this basis also has domain versatility. When the user enters the

problem, because the problem itself has domain characteristics, the problem description file and domain knowledge file are needed to solve the specific problem.

Planning result interpreter: It is a part of processing planning results. The planning result interpreter has two functions: the first is to return the obtained action sequence to the user through the packaging display on the GUI; the second is to extract the obtained action sequence into strategic knowledge and store it in the knowledge base.

IV. DESIGN AOF GENERAL PLANNER BASED ON KNOWLEDGE ORGANIZATION

The design and implementation of the general planner is the core of the intelligent planning system based on self-consciousness. Based on the knowledge representation method of AORBCO model, the general planner is designed and implemented by referring to the idea of A-start algorithm. From the perspective of the agent in the AORBCO model, based on the idea of one person and one world, the general planning idea of the agent is as follows: After understanding the problem input and determining the domain to which the problem belongs, the agent first searches for related capabilities from the knowledge base. The correlation of capabilities is related to the representation and storage of capabilities in the knowledge base, and the emotion of the agent to the related capabilities during the search process will also affect the search results, which is the process of the agent's active matching capability. Another process is the agent's simulation of the action. The agent will simulate the ability to search. The ability to call will change the agent's current desire, that is, the state change of the ability object. The agent obtains the new state of the object through state reasoning. The gap between the new state and the target state is used as part of the agent's assessment of whether to select the ability. The design structure of general planner based on knowledge organization is as follows:
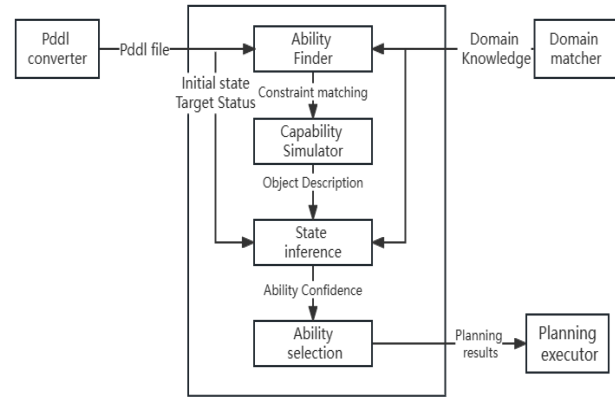
Figure 2.   Basic Planner Data Flow Diagram

This figure shows the transfer of data flow in the basic planning period. It can be seen that the original data is a pddl file and related domain knowledge. The initial state and target state are obtained according to the pddl file. First, it is sent to the capability searcher, and then selected the qualified capability through constraint matching. This capability is simulated, and the description of related topics after the simulation is state reasoned, Calculate the similarity between the target state and obtain the confidence level of the ability

The universality of the general planning period is mainly reflected in 1. The general field of the AORBCO model is only the representation. By analyzing the characteristics of AORBCO model and comparing the existing knowledge representation methods, the knowledge representation method based on AORBCO model is given in [11]. The descriptive representation framework of domain knowledge is given by XML markup language, and the general planner structure is designed based on this framework. The structure of the problem description file of different problems is consistent, and the domain knowledge representation structure of different fields is unified to design a general planner. The planning results can be integrated with the existing knowledge in the knowledge base and can solve other related problems. The following describes each part of the above figure.

The main function of the ability searcher is to search and match the current state of the object in the description of the problem based on the pre-condition, post-condition and ability object in the

domain knowledge base on the domain knowledge of the AROBCO model and the planning problem. The pre-post conditions of the ability in the AROBCO model are described by logical expressions. The constraint matching algorithm is used to match the pre-post conditions of the current state and ability of the object in the description of the problem, and the corresponding matching degree is calculated.

The action simulator is the result of the agent's ability according to the post-condition of the ability, that is, the action result described by the logical expression is related to the problem object, and the logical expression is applied to the object to observe the change of the object.

The state inference engine is the part of the agent to identify the current state of the object. When the agent simulates the ability, the state and attributes of the object may change. These changes may be close to the target state or far away from the target state. Therefore, the agent after the action simulation needs to understand and reason the current state attributes of the object to obtain a new state, and calculate the gap between the new state and the target state. After obtaining the gap between states and the ability matching degree, the confidence of the agent to the ability is obtained. The higher the confidence, the higher the possibility that the agent chooses the ability as part of the planning sequence, and vice versa.

The ability set obtained in the ability searcher is selected according to the confidence level. The degree of confidence will feed back to the emotional knowledge of the agent. The lower the ability to perform, the less the ability to solve the problem, so the agent's emotional weight is reduced accordingly.

Based on the above structure, there are three main algorithms involved in the general planner: object attribute and capability constraint matching algorithm, state similarity calculation algorithm and heuristic value (confidence) calculation algorithm. The following three algorithms are described:
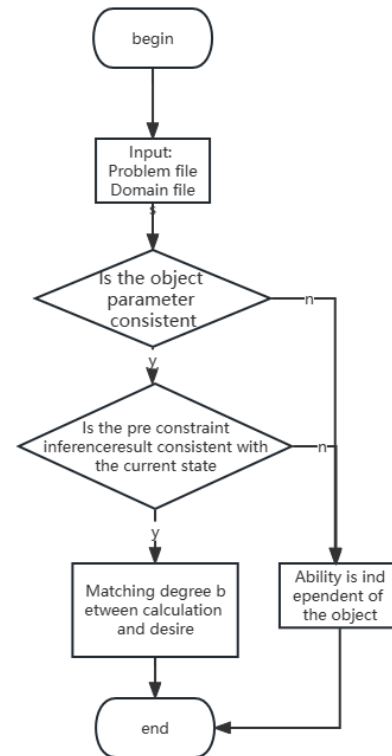
Figure 3.　Constraint matching algorithm flowchart

Figure3 shows the flowchart of the object capability constraint matching algorithm: The object attribute and capability constraint matching algorithm is mainly used to reduce the set of planning capabilities. The agent first determines whether the subject of the problem is the same as the capability topic through the entity alignment algorithm. Under the premise of the same subject, the knowledge reasoning technology is used to reason about the precondition of the capability. Calculate whether the precondition of the capability is semantically consistent with the current state of the object. After the above process, the object-capability matching degree is calculated by combining the emotional weight of the agent to the current capability.

the agent's ability is added when selecting the ability. Therefore, the emotional factor of the agent and the ability constraint matching value jointly generate the initial preference (the initial cost in A *), and the state similarity as the estimated heuristic value constitutes another part of the heuristic function.

Because the inference engine is the main component of the agent to update its own state, attributes and relationships, the inference engine in intelligent planning is described again. After the ability simulation of the agent, some characteristics of the object change. The change of the object characteristics means that the state of the object also changes. Therefore, it is necessary to redetermine the state of the object by analyzing and comparing the object characteristics, which is the main task of the state reasoning module.

This paper adopts rule-based reasoning strategy and uses Java rule engine technology to realize object state reasoning. Rule inference engine, also known as production system, is developed from rule-based expert system. Rule-based expert system is a branch of expert system in the field of artificial intelligence. It simulates human reasoning, uses tentative methods for reasoning, and uses human understandable terms to explain and prove its reasoning conclusions.

In the AORBCO model, the agent is an agent with reasoning ability, and the reasoning ability of the agent is mainly reflected in its knowledge organization and behavior control mechanism. The reasoning process of agent is based on knowledge and strategy, and the behavior control mechanism controls the whole process of reasoning.

The reasoning process of agent is based on rich knowledge base and scientific knowledge organization. In AORBCO model, ego knowledge is divided into descriptive knowledge, process knowledge, strategic knowledge and emotional knowledge. Descriptive knowledge is a description that represents the abstract knowledge of the real world and is used to represent the question of ' what ' ; process knowledge is the ability of agent to operate knowledge and have specific functions. Strategic knowledge is the action plan obtained by ego after matching descriptive knowledge, and its

Figure 4. Flow Chart of State Similarity Calculation

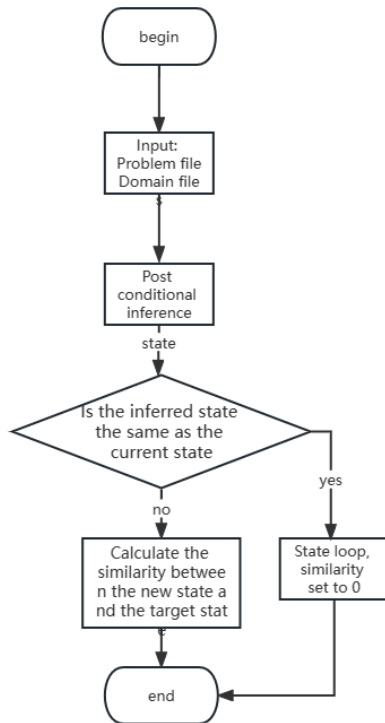This figure shows the flow chart of state similarity calculation: when the ability matching calculation is completed, the agent performs action simulation on the object according to the pre-condition and post-condition of the ability. Specifically, it refers to the reasoning of the state attributes of the object according to the post-condition description of the ability. After reasoning, a new expected state will be obtained. At this time, the state similarity calculation algorithm is used to calculate the gap between the expected state and the target state. The state similarity calculation mainly uses the cosine similarity to calculate the gap between the current object state and the target state.

Ability confidence algorithm: Based on the idea of A * algorithm, the confidence of ability is mainly composed of constraint matching value and state similarity. The higher the confidence is, the closer the ability is to the target state and the farther it is. The A * algorithm is mainly composed of the initial cost and the estimated cost. In the AORBCO model, the agent has self-consciousness, and the emotional weight factor of

core logic is if... else... matching mechanism; emotional knowledge is the knowledge of value judgment on the state of the world.
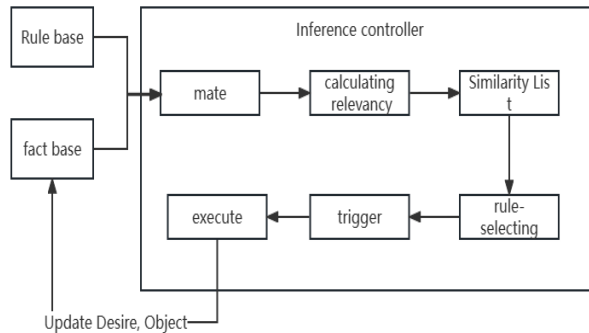

Figure 5.   State inference structure diagram

Figure5 shows the workflow diagram of the state inference engine in the AORBCO model: the inference controller of the agent is mainly composed of four modules, which are condition matchers; a similarity calculator; trigger and actuator. Condition matcher : compare facts and rules by comparing facts and rules, matching rules that meet the conditions, agents compare facts and rules from factors such as domain, object, object type, and object number ; similarity Calculator : There may be more than one rule matched according to the fact data. All the matched rules need to calculate the similarity between the behavior results in the rules and the target state. Trigger: The trigger maintains an ordered list, and the similarity of all matched rules is saved in the list. The trigger selects the rule with the highest similarity and hands the rule to the actuator; actuator: The actual and rules are given to the actuator, which executes the rules and changes the current desire and object.

Drools is an open source rule engine written in Java language, which uses Rete algorithm to evaluate the written rules. The rule writing format in Drools is:

rule "ruleName"

when

$message:Message(status == 0)

then

System.out.println("fit");

$message.setStatus(1);

update($message);

end

V.   CONCLUSION

By analyzing the intelligence and planning principles of the existing intelligent planning methods, the definition of intelligent planning based on self-consciousness is studied on the basis of AORBCO model intelligence theory. At the same time, the overall architecture of intelligent planning based on self-consciousness is given based on AORBCO model. The general planner is designed and implemented, and the planning algorithm in the general planner is designed by referring to the idea of A * algorithm. Although the existing intelligent planning algorithm can plan most of the problems, the algorithm itself does not reflect the intelligence and autonomy of the agent. The intelligent planning based on self-consciousness is a knowledge-based planning algorithm. The AORBCO model proposes the behavior control mechanism of the agent. The behavior control mechanism reflects the autonomy of the agent, and the knowledge participates in the behavior control mechanism to reflect the intelligence of the planning.

REFERENCES

[1] Ernst G, Newell A, Simon H. GPS: A case study in generality and problem solving [M]. New York: Academic Press, 1969: 102-104.

[2] Green C. Application of theorem proving to problem solving [C]. Proceedings of the First International Joint Conference on Artificial Intelligence, 1969: 219-239.

[3] Fikes R E, Nilsson J N. STRIPS: A new approach to the application of theorem proving to problem solving [J]. Artificial Intelligence, 1971(2): 189-208.

[4] Koukoulas P Kalouptsidis N. Blind identification of second order Hammerstein series [J]. Signal Processing 2003 83(1):213-234.

[5] Ding De Lu Jiang Yunfei. Intelligent Planning and Its Applications [J]. Computer Science 200229 (2): 100-103.

[6] Amndio Ana Margarida, Coelho das Neves José Manuel, Parente. Manuel Intelligent planning of road pavement rehabilitation processes through optimization systems [J]. Transportation Engineering, 2021, 5(10):81.

[7] Liu Ying. Research on several important problems in intelligent planning and planning recognition [D]. Northeast Normal University, 2013.

[8] Blum A, Langford J. Probabilistic planning in the Graphplan framework[C]. Proceedings of the Fifth European Conference on Planning. Durham, United Kingdom. 1999.

[9] Duy Bui, Wojciech J. Multi-Agent Planning with Planning Graph [C]. Proc. Of the 3rd European Symposium on Intelligence Technologies, Hybrid Systems and Their Impiementation Smart Adaptive Systems. 2003.

[10] Sun Chunhui.From Consciousness-only Learning to Consciousness-only Psychology[D]. Suzhou University.

[11] Xiao L, Luo J, Gao W. Research on Knowledge Representation based on AORBCO Model [J]. International Core Journal of Engineering, 2022, 8(10): 69-76.

Research on Fault Diagnosis System of IOT for Oil Well Pump Based on Machine Learning

Bozhi Xiao, Yangbing Lu, Miao Wang, Haojie Li, Hengyan Zhu, Xuan Cao, Shengquan Yang
School of Computer Science and Engineering
Xi'an Technological University
Xi'an, 710021, China
E-mail: xaitysq@163.com

Abstract—In order to realize automatic prediction and processing of remote fault diagnosis of oil well pumps distributed in different regions by crude oil production enterprises, a fault diagnosis system for oil well pumps based on machine learning was researched and designed. This fault diagnosis system is composed of three layers (perception layer, network layer and control application layer) Internet of Things structure. The function and characteristics of each layer are analyzed in this paper, and the hardware composition and control principle of sensor nodes and aggregation nodes of the measurement and control system are discussed and gives the node microcontroller program design flow chart and the main module content of the IoT central computer software design. This paper focuses on the principle of machine learning for fault diagnosis and prediction, and deeply explains the algorithm steps of using LSTM for fault diagnosis of oil well pumps. The enterprise application experiment results show that, compared with the traditional manual well patrol fault diagnosis method, this system has the advantages of convenient operation and maintenance, low labor intensity, high timeliness and accuracy of fault diagnosis, which can better reduce equipment maintenance costs for enterprises.

Keywords-Machine Learning; Oil Well Pump; Internet of Things; Fault Diagnosis

I. INTRODUCTION

The oil pump is an essential and important power equipment for oil wells to export crude oil[1]. Since most oil wells are distributed in desert mountains and wilderness, oilfield enterprises basically adopt on-site instrumentation display monitoring for their management, and carry out early warning management by manual line inspection, that is, patrol The inspectors check the operation status of the oil delivery pump of the well group regularly every day, record relevant data, and obtain information such as the flow, pressure and temperature of the oil pump during the period of operation [2-3]. As the scope of oilfield production sites and pipeline networks becomes wider and wider, and the number of oil wells continues to expand, this method gradually shows shortcomings in management. It shows shortcomings such as high labor intensity and obvious lag in dealing with problems, such as: If the operating pressure of the oil pump is abnormal, if the manual inspection method finds that the treatment is not timely, it may lead to the rupture of the oil pipeline, which will cause a series of serious problems such as property loss of oilfield enterprises and environmental pollution [4-5].

The Internet of Things is the "Internet of Things Connected", which is automatically generated through information such as various sensing devices, ZigBee wireless sensor network technology, 5G network transmission technology, RFID technology, video recognition technology, infrared sensing, global positioning system, and laser scanners. Acquisition equipment, according to the agreed agreement, realizes the network connection of interconnection and intercommunication of items according to the needs, and performs information exchange and communication, so as to realize the intelligent network system of intelligent identification, positioning, tracking, monitoring and management [6].

Machine learning is one of the branches of artificial intelligence, which refers to a method that enables computer systems to automatically learn and continuously improve performance

through computer algorithms and models [7-8]. The functions of machine learning include but are not limited to: classification, clustering, regression, dimensionality reduction, anomaly detection, association rule mining, etc. The advantages of machine learning in fault diagnosis are many. For example, machine learning can adaptively learn a machine's diagnostic knowledge from collected data, rather than utilizing the experience and knowledge of engineers. [9-11] This method can improve the accuracy and efficiency of fault diagnosis. LSTM [12-13] is an algorithm in machine learning. It is a special cyclic neural network that can solve the problem of gradient disappearance in traditional cyclic neural networks, and can also process long sequence data. In addition, the LSTM algorithm can also discover hidden patterns and relationships in large-scale data, thereby improving the ability of fault diagnosis.

II. DESIGN OF OIL PUMP MEASUREMENT AND CONTROL SYSTEM BASED ON INTERNET OF THINGS ARCHITECTURE

A. Overall Design of IoT System

The measurement and control of oil well pump data is the foundation of digital intelligent oilfield construction. Its goal is to detect the operating status and parameters of various components of oil pump equipment in real time, and transmit the collected operating data to the Internet of Things through intelligent instrument communication nodes and dedicated 5G networks. Control center machine [14]. On the one hand, the central computer conducts analysis and processing through the upper-level intelligent control software, makes decision-making control when necessary, and then outputs it to the equipment control mechanism through a dedicated 5G network; on the other hand, the central computer can convert and standardize the collected data through algorithms and store them to the database server, and at the same time serve mobile terminal or desktop terminal users through the public 5G network or Internet network [15]. The principle composition structure of the system equipment based on the Internet of Things architecture is shown in Figure 1. The system adopts a layered

design method to realize real-time data collection and monitoring of oil pipeline pressure, flow and temperature, and has low cost and strong automatic monitoring capabilities. It mainly consists of three layers: perception layer, network layer and application layer.
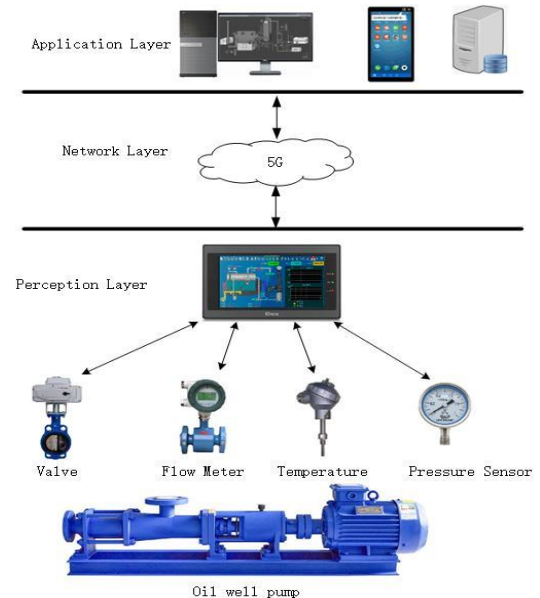
Figure 1. Organization structure of the system based on internet of things technology

B. Perceptual layer design

The sensing signals of this system for the measurement and control of oil delivery pumps in oilfield well groups mainly include: valve switches of various components, oil pump inlet and outlet pressure, oil pump inlet and outlet temperature, oil pump output flow, oil pump body temperature and other sensors. The sensing layer is composed of ZigBee wireless subnets of oil well pumps located in several areas, and the ZigBee wireless subnet is composed of sensor nodes with ZigBee communication modules and aggregation nodes (ZigBee well group control communicators, also known as gateway nodes). The convergence node in this system is the transfer station of each oil well's external communication, and its core component is the ZigBee wireless transceiver module. The aggregation node is a relatively independent processing unit. If the external network fails to contact the IoT control center, it can automatically adjust the operating status of the local oil pump according to the node's internal

operation logic rule base. In addition, it can also store the local data for a period of time. The measurement and control data can be queried locally to display the real-time or historical operation data of each sensor.

C. Network layer design

The network layer mainly completes the reliable transmission of the information collected by the oil pump or the control signal of the Internet of Things center [16-17]. It is essentially based on the wireless local area network (WLAN) or the wireless mesh protocol to form a larger network of multiple aggregation nodes to monitor the distribution of multiple areas. Oil well pumps. Specifically, its function is to receive the information from the aggregation node of the perception layer, which can be encrypted and transmitted to the control application layer through appropriate algorithms as needed [18]. In addition, the information and control output of the control application layer are reversely transmitted to the aggregation node of the perception layer. The network layer mainly acts as a bridge. Since the oil wells of oilfield companies are mostly located in uninhabited mountain areas, these places often do not have public communication 5G networks, and a dedicated wireless communication network needs to be set up to serve this system.

D. Application layer design

The application layer is the highest layer in the functional structure diagram of the system, and it is the remote control center of the system. It realizes the automatic safety control of the oil pump on the basis of receiving and analyzing the sensory information of each oil well [19-21]. The control application layer is mainly composed of IoT central computer, database server, desktop terminal, mobile terminal and so on. The central computer of the Internet of Things generally has a wireless transceiver module, which can receive the equipment information transmitted by the dedicated 5G network base station of the transport layer in real time, analyze and process it according to the requirements of the oil pump operation process parameters through the software system,

and store the data periodically in the database server [22-23]. Oil wells with different production volumes are equipped with different oil pump powers and different operating parameters. Various equipment parameters can be set through the man-machine interface of the control application layer. Spare. The data received by the control application layer from the network layer generally undergoes the steps of verification, unpacking, and anti-encryption conversion [24-25]. It can dynamically display data such as oil well temperature, pressure, and flow rate through a powerful host computer intelligent graphics software system, and it can monitor the abnormal operation of the equipment. It can predict in advance and make corresponding output actions quickly according to the equipment process. Mobile terminals such as mobile phones and handheld PDAs can access the web interface of the control system through the public 5G network, and can access the operating curves and data of the equipment under the permission of the authority; in addition, various departments of the oilfield enterprise can also access and browse the operating status of the system through the Internet Or remote control, which greatly facilitates the efficient management of oil pumps by oilfield companies.

III. OIL PUMP IOT MEASUREMENT AND CONTROL NODE HARDWARE

A. Sensor node

The main function of the sensor node is to collect current and voltage data, perform A/D conversion on the data and undergo a digital filtering process. These sensors are all equipped with wireless ZigBee communication modules. They can upload data to the sink node and accept commands from the sink node at the same time. Make the necessary adjustments to the output. A typical oil pump sensor node is usually composed of a sensor module, an analog filter module, an A/D conversion module, a D/A output module, an I/O control module, a node processor CPU, a wireless RFID module, a node storage module, and a power management module, etc [26]. Composition, the block diagram of its hardware composition is shown in Figure 2.
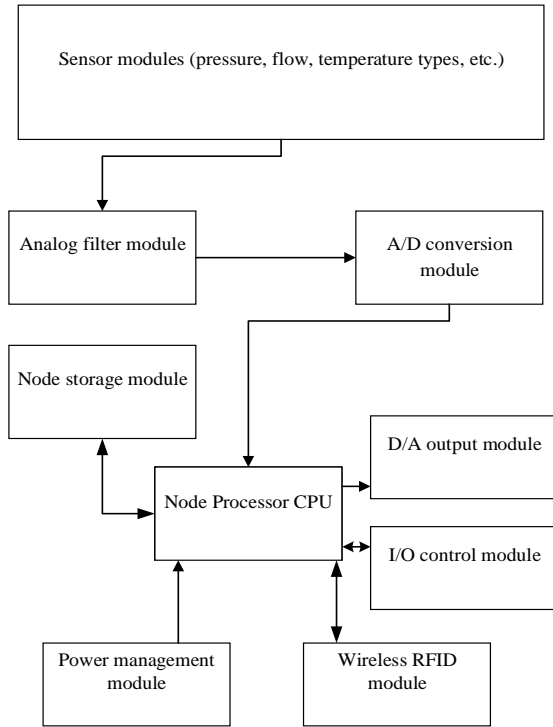
Figure 2.   Hardware components theory block diagram of the fuel pump sensor instrument node

The pressure sensor of this system adopts Rosemount sensor with a measurement accuracy of 0.1%, the measurement range is 0-10 Mpa, the DC power supply voltage is DC24V, the output sensing signal is 4-20mA, and the medium temperature is -20-90 ℃. The flow sensor adopts FD-M100AT sensor, the detection distance is 4-150 mm, the switching frequency is 1000 Hz, the output mode is NPN, and the response time is less than 0.5 ms. It can realize the detection of liquid flow in harsh environments, and is very suitable for oil pipelines in oil field enterprises, field arrangement environment. The model used for the temperature sensor is DS18B20, and its range is -55 to 125 ℃. It can sample and quantify the temperature data, and the resolution can generally reach 0.0625. The working voltage is 3.0 to 5.5V. The format only needs a maximum of 740ms, which is suitable for the low power consumption of sensor nodes.

B. Sink node

Convergence node (ZigBee well group control communicator, also known as gateway node) is responsible for collecting local sensor signals and interacting data with the IoT central computer through the network layer [27]. When the central computer of the Internet of Things sends a control command through data calculation, the sink node immediately sends it to the sensor node through wireless communication in real time after receiving it. After the sensor node unpacks the communication command, it specifically performs D/A output or I/O control. The aggregation node is mainly composed of the lower wireless communication module, the upper wireless communication module, the node processor CPU, the node LCD display module, the node key control module, the node storage module and the power management module [28-29]. The block diagram of its hardware composition is shown in the figure 3. The sink node itself is a relatively independent local oil pump control instrument. It has two modes: Remote and Local. Normally, it is in the remote mode. Once the communication delay or communication failure occurs, the sink node will automatically switch to the local mode according to the instrument backup rule base Automatic regulation of the oil pump.

The lower layer wireless communication module selects the CC1100 communication module, which can directly receive the information collected by the perception layer. The upper wireless communication module selects the SRWF508A wireless module, and the transmission distance between the node and the network layer base station can reach 3.5km. It is easy to realize long-distance transmission of collected information by building a wireless network. The node storage module uses the AT 24C256 chip, and the storage capacity can be easily expanded through multi-chip interconnection. The node LCD display module can display the oil pump operation collection information and equipment status transmitted by the current sensor node, which is convenient for users to directly view on site. The Key button control module is convenient to use direct local manual input to run the control rule library, set the working mode of the node, or directly issue control commands to start and stop the oil pump equipment, etc., and it uses the matrix scanning method to work.
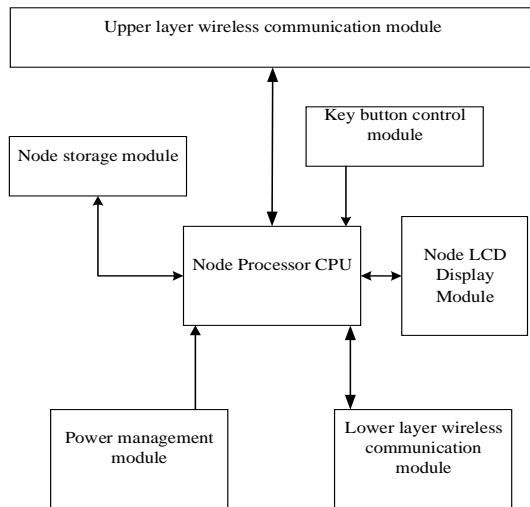
Figure 3.   Hardware components theory block diagram of the IOT aggregation instrument node

IV. SOFTWARE DESIGN OF INTERNET OF THINGS SYSTEM FOR OIL WELL OIL PUMP

The software design of the intelligent oil well pump wireless network monitoring system is based on the basic principles of reliability, safety, and control robustness, and is designed under the guidance of modularization and scalable upgrades [30-31]. The software design mainly includes the sensor node program design, the convergence node program design and the software design of the intelligent monitoring system of the central computer of the Internet of Things.

A. Node programming

The node program is mainly based on the design of the single-chip microcomputer program. In this system, the sensor node and the sink node have many similarities in their working principles, and their programming methods are similar. Due to space limitations, only the workflow of the sink node single-chip microcomputer program is given below, as shown in the figure As shown in figure 4, the node program uses a modularized subroutine design mode, which is composed of multiple relatively independent subroutines called by the main control loop program. Each round of cycle through these subroutines mainly completes the lower sensor data communication acquisition, data storage and processing, Key button processing, upper-layer wireless communication data submission, node data display and other tasks, set

the corresponding maximum running cycle time for each subroutine during the main loop running, so that if a node occurs during the running of a loop subroutine For exceptions, the system uses the stack to record the exception numbers in sequence, and unify to the last step to focus on popping the stack to execute the exception handling subroutine processing, which can improve the program operation efficiency and the timeliness of peripheral wireless communication response.
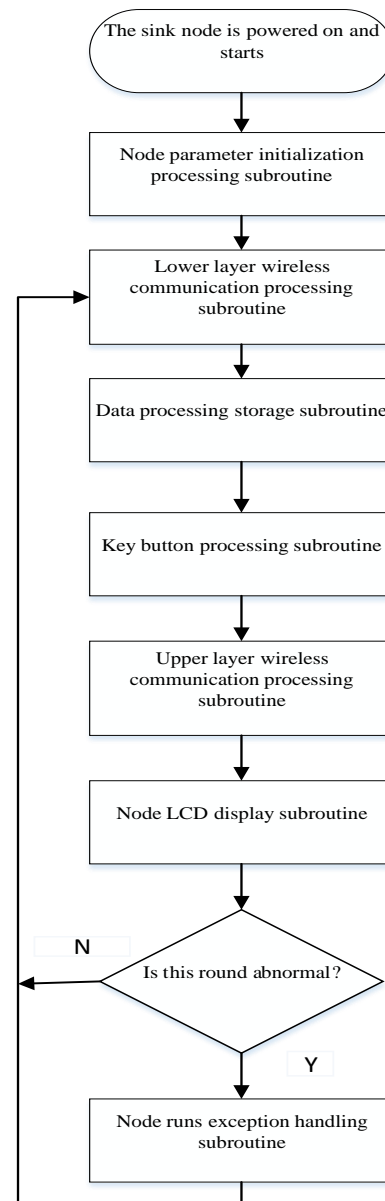
Figure 4.   MCU control program flow chart of the IOT aggregation instrument node

The single-chip microcomputer program of the aggregation node is written in an MCU development environment compatible with C language syntax, and the code of the main loop program is as follows:

```
    void main() /*main loop function definition*/
    {
    GatherGaugeLoad();/*Gathering node
power-on parameter initialization*/
        while (1) /*Infinite loop until the node is
powered off*/
        {
    DownWirelessComm();/*lower        layer
communication, collect oil pump data*/
        DataProcessSave();/*data    normalization
processing and saving*/
        KeyInService();/*User    Key    button
processing*/
        UpWirelessComm();/*upper        layer
communication, execute remote command*/
        KeyInService();/*Node    instrument    LCD
displays required data*/
        if (RunError()!=0) /*There is an exception
in this round*/
        Exceptionhand();/*Unified    processing
cycle exception*/
    }
    }
```

The wireless network communication between the sensor node and the aggregation node of this system is based on the traditional MAC protocol. It mainly realizes the establishment and maintenance of wireless data links between the devices of each layer of communication. The MAC data frame adopts the time slot CSMA/CA mechanism. It uses 3 the three parameters are the back-off index NB, the collision window CW and the back-off index BE to achieve reliable data transmission [32].

B. Central Computer Monitoring System Software Design

According to the actual needs of oil field enterprises for remote monitoring of well group oil pumps, the IoT central computer monitoring system software is mainly composed of 7 modules, as shown in Figure 5, including the system user

management module, network communication processing module, data record processing module, process screen A display module, a dynamic curve display module, a sensor node parameter module, and a convergence node parameter module.

The system user management module is used to control the user's authority to use the software, including remote desktop terminal and mobile terminal users, and can display or maintain basic information records of logged-in users. The network communication processing module is the key core module of the system. On the one hand, it performs real-time data exchange with multiple convergence nodes of the system through the dedicated network layer network, and on the other hand, it provides data services for enterprise remote mobile terminals and desktop terminals through the public 5G network and the Internet. . The system control center adopts the C/S design mode and adopts the TCP/IP asynchronous communication mode. It handles network-related work through proxy callback functions, so that there is no need to block or suspend threads when performing network operations. The system provides a standard Modbus TCP RTU-based interface for remote desktop or mobile terminal web-based page access.
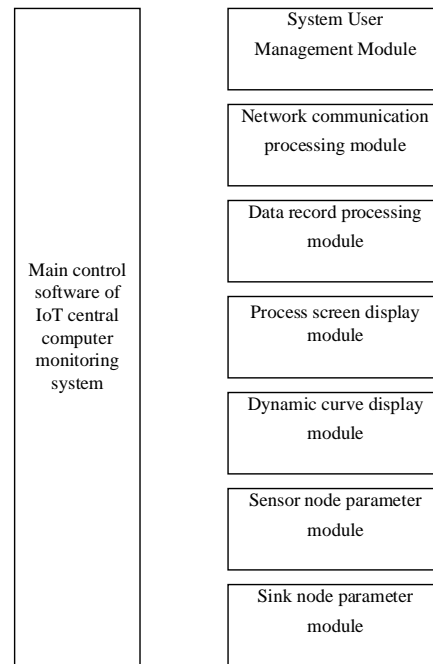

Figure 5.   Module structure diagram of the IOT center computer monitor system software

The main function of the data record processing module is to normalize the data of all oil pumps in the oil station monitored by the system, and then periodically (the time can be set, usually 5 minutes) record it to the database server [33-34]. The process screen display module is the most important man-machine interface of the system. It uses virtual instrument technology to display the operation status of each component of the oil pump and the corresponding position of the sensor parameters in real time, and can prompt whether the system has an alarm. The general refresh time of the screen is 5S. The function of the dynamic curve display module will display each sensor parameter in the form of a curve for each oil well. The dynamic curve has historical data curve display and a short-term operation trend graph in the near future. The built-in fault diagnosis algorithm of the system can predict whether the future will there will be a possibility of failure, which allows users to prepare in advance and prevent problems before they happen [35]. The sensor node parameter module can set a series of parameters such as the type of the system oil pump sensor, the working mode of the sensor, and the communication mode of the sensor network. The aggregation node parameter module can set a series of parameters such as the working mode of the aggregation nodes of each oil station in the system, the backup logic rule base, and the node network communication mode.

V. DESIGN OF MACHINE LEARNING FAULT DIAGNOSIS FOR OIL WELL PUMP

Fault Diagnosis System (FDS) [36-37] refers to a system that collects data, analyzes data, judges the cause of the fault, and predicts the development trend of the fault when the machine fails, so as to take corresponding measures to avoid or reduce the damage caused by the fault to the machine.

The working principle of the fault diagnosis system mainly includes the following steps [38]:

1) Data collection: The fault diagnosis system first needs to collect various data generated during the operation of the machine, such as temperature, pressure, flow, vibration and other data. This data can be collected by sensors, meters or other devices.

2) Data analysis: The fault diagnosis system analyzes the collected data to find out abnormal data. Anomaly data is an early warning sign that a machine is malfunctioning.

3) Fault judgment: The fault diagnosis system judges the fault type of the machine according to the abnormal data.

4) Fault prediction: The fault diagnosis system predicts the development trend of faults according to the types of faults.

5) Troubleshooting: The fault diagnosis system takes corresponding measures according to the fault prediction to avoid or reduce the damage caused by the fault to the machine.

6) The fault diagnosis system can help enterprises improve the operating efficiency of machines, reduce maintenance costs and prolong the service life of machines.

Following are some advantages of fault diagnosis system [39]:

It can improve the operating efficiency of the machine: the fault diagnosis system can prevent the occurrence or expansion of faults through early warning of faults, thereby improving the operating efficiency of the machine.

Can reduce the maintenance cost: the fault diagnosis system can accurately determine the cause of the fault and avoid false maintenance, thereby reducing the maintenance cost.

Can prolong the service life of the machine: the fault diagnosis system can prolong the service life of the machine by finding and handling faults in time.

A. Macro Design of Fault Diagnosis Expert System

Combining the operation characteristics of the oil well oil pump process and the user's fault diagnosis discovery and processing requirements, the fault diagnosis expert system structure shown in Figure 6 is designed.
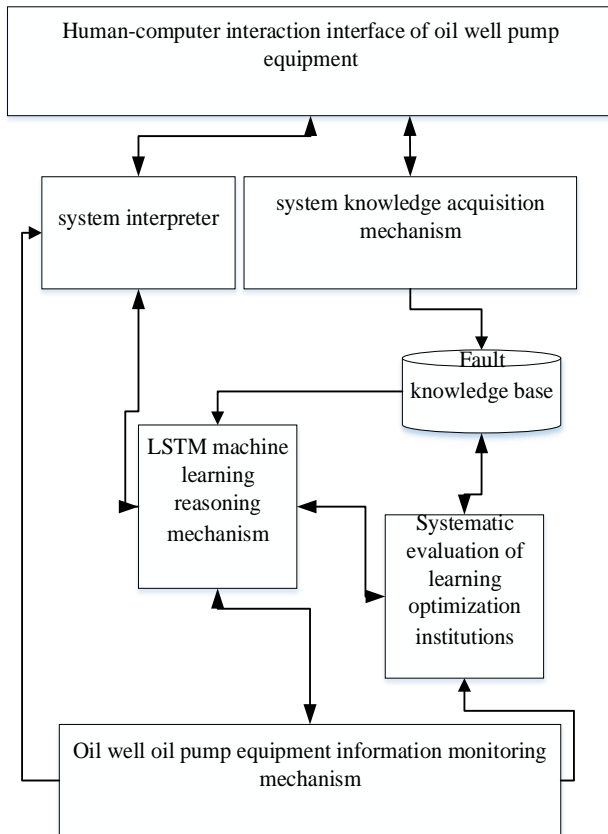
Figure 6.   The structure of the expert system for oil well pump LSTM machine learning fault diagnosis

It consists of 7 parts, including: oil well pump man-machine interface, system interpretation mechanism, system knowledge acquisition mechanism, fault tree structure knowledge base, LSTM machine learning reasoning mechanism, system evaluation learning optimization mechanism and oil pump skid status information monitoring mechanism. The description of each part is as follows:

1) Man-machine interface of oil well oil pump: The terminal for displaying various information for the system operation and the operation interface for the user to interact with the system. On the one hand, the user inputs the original device fault diagnosis rules, logic rules and other knowledge into the system through this interface; on the other hand, the system outputs the diagnosis results through this interface and asks or answers reasoning questions to the user. In addition, the operator can input the manual intervention parameters of the diagnosis system through this interface at any time according to experience and knowledge, so as to achieve real-

time manual correction of the diagnosis system, so that it can quickly enter the correct diagnosis track.

2) System explanation mechanism: Explain the cause of the fault and the reasoning process, and provide reasonable disposal suggestions to the user. It can answer various questions raised by users, and it can give necessary and clear explanations of the reasoning route and conclusion of the fault tree, so that users can understand the reasoning process. It is the main module to realize the transparency of reasoning. The system interpretation mechanism converts the information input by the user into the internal representation of the system, and then hands it over to the corresponding interpretation module for processing. The internal information of the system reasoning is also converted by the interpretation mechanism into an external form in the format understood by the user and displayed on the man-machine interface.

3) System knowledge acquisition organization: Domain expert knowledge engineers (mainly oilfield equipment experts) input all fault diagnosis experience knowledge and logical knowledge through the front man-machine interface, which will be processed by this organization and stored in the knowledge in a standardized form library to build fault trees.

In the fault diagnosis system, there are the original input rule knowledge, the rule knowledge generated by the system machine learning, and the intermediate rule knowledge generated during the reasoning process. Because there is an inevitable connection between this knowledge through the same attribute, it is necessary to eliminate their redundancy. That is to say, Jane. The basic idea of knowledge reduction is to use some measure to determine the importance of different attributes and construct the smallest subset of knowledge attributes [40]. The method of knowledge reduction based on rough set theory has good versatility, robustness and global search. There are two steps: one is to delete some columns from the decision table; the other is to delete redundant rows [41].

4) Fault knowledge base: Using production hierarchy rules to express the fault diagnosis reasoning logic function formulas of the phenomena and results of each component of the

oil well oil pump. The knowledge in this knowledge base must be expressed in the normalized form of the fault tree hierarchy, which is the core of this expert diagnosis system and the key to whether the quality of the expert system is superior. The quality and quantity of knowledge in the knowledge base determine the quality of the expert system [42]. quality level. There are two main types of knowledge stored in this knowledge base: one is the open knowledge of oil well pumps, including definitions, facts and theories in the field; the other is the knowledge obtained by oil field experts in long-term business practice Practical experiential knowledge.

5) *Machine learning reasoning mechanism:* The machine learning reasoning mechanism refers to the reasoning process of the machine learning model, including forward propagation and back propagation. Forward propagation refers to the process of calculating the input data through the neural network model to obtain the output result; back propagation refers to the process of calculating the gradient according to the loss function, and then updating the model parameters through optimization algorithms such as gradient descent. In the expert system, the advantages of reasoning based on machine learning include: automatic feature extraction, adaptive adjustment of model parameters, and ability to deal with complex nonlinear relationships. Compared with traditional expert systems, machine learning-based expert systems can handle complex problems better because it can automatically extract features from data and adaptively adjust model parameters to suit different data distributions and tasks Require. In addition, expert systems based on machine learning can also deal with complex nonlinear relationships [43], which cannot be handled by traditional expert systems. The machine learning reasoning algorithm of LSTM is adopted in this system.

6) *System evaluation learning optimization mechanism:* During the operation of the system, the system periodically evaluates the effect of using the knowledge source in the fault tree knowledge base in the process of fault diagnosis and reasoning to solve problems. Status information, suspend the knowledge with poor diagnosis and processing effect, and give warnings and prompts to users for reasoning with insufficient diagnosis knowledge; in addition, according to the summary of system evaluation and optimization and the quality of actions after

diagnosis and control instructions, it can monitor the system itself Constantly improve and innovate dynamically, and enrich the knowledge in the knowledge base in real time, and self-correct or delete the knowledge with poor performance and relatively large control deviation[44].

7) *Oil well pump status information monitoring mechanism:* This mechanism is mainly used to monitor the operating parameters of each equipment during the operation of the device through interface modules (such as I/O, A/D, D/A, and TCP/IP, etc., such as pressure, flow rate, etc.) , valve opening, temperature, etc., as well as the parameters of the components themselves, such as the frequency converter itself, such as current and voltage. The information is processed by the system data information rules and handed over to various institutions for use.

B. Principle of BP Neural Network in Fault Diagnosis

This system plans to use the LSTM algorithm, and its core is the BP neural network, so it is necessary to introduce the principle of the neural network in advance [45].

The BP neural network module used in the bottom layer of machine learning in this oil well oil pump fault diagnosis system is divided into four layers: input layer, fuzzy layer, fuzzy reasoning layer and output layer. The BP neural network input layer nodes correspond to the parameters that need to be controlled by the oil pump system, and the BP neural network output layer nodes correspond to the future measurement data predicted by the sensor. The function of the BP neural network module is to train and learn a large number of historical data of oil well pump sensors. The BP neural network controller can continuously optimize the real-time parameters of the machine learning fault diagnosis of the oil well oil pump by adjusting the weight coefficients of each layer, so as to realize the self-adaptive adjustment of fault diagnosis, prediction and alarm. The structure diagram of BP neural network is shown in Figure 7.
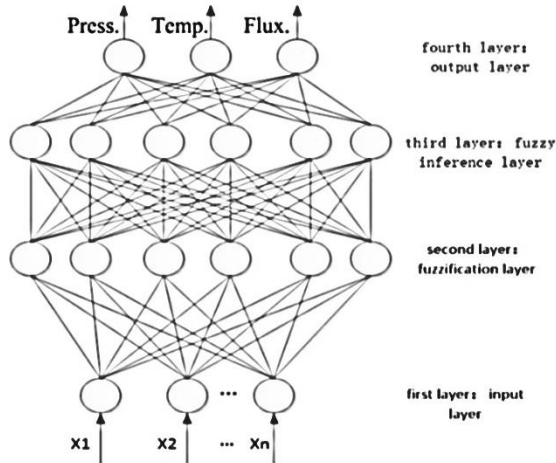
Figure 7.   Neural network module structure diagram

In this network diagram, the first layer is the input layer of the BP neural network module. Each neuron node in this layer represents an input variable of the system such as oil well pressure, flow rate, temperature and other information. Since the system needs to control the oil well pump Inlet oil pressure, outlet oil pressure and output oil flow, so the neural network module of the input layer fuzzy neural network LSTM machine learning control is composed of three neurons, that is, three nodes, and the main function of this layer is that the neurons will input the variable The value is passed to the neurons in the fault diagnosis and prediction layer through the action function, and the input and output in this layer are as follows:

$$I_i^{(1)} = x_i \qquad (1)$$

$$O_{ij}^{(2)} = x_i \qquad (2)$$

The second layer in the BP neural network is the fuzzy layer of fault diagnosis prediction. Each neuron in this layer is used to simulate the membership function of the input variables of fault diagnosis prediction. The input and output of fault diagnosis prediction in this layer are expressed as:

$$I_{ij}^{(2)} = -\frac{(x_i - c_{ij})^2}{b_{ij}^2} \qquad (3)$$

$$O_{ij}^{(2)} = \exp(I_{ij}^{(2)}) \qquad (4)$$

C. LSTM Machine Learning Model Design in Fault Diagnosis

LSTM is short for Long Short-Term Memory Neural Network. It is a variant of Recurrent Neural Networks (RNN) that excels at processing sequential data. LSTM was proposed by Hochreiter and Schmidhuber in 1997. LSTMs work by using gates to control the flow of information in the network. A gate is a structure in a neural network that controls the flow of information. LSTM has three gates: input gate, forget gate and output gate. Input gates control the entry of new information into the network. Forget gates control the deletion of old information from the network. The output gate controls the information output by the network. The structural principle of the LSTM machine learning model is shown in Figure 8.
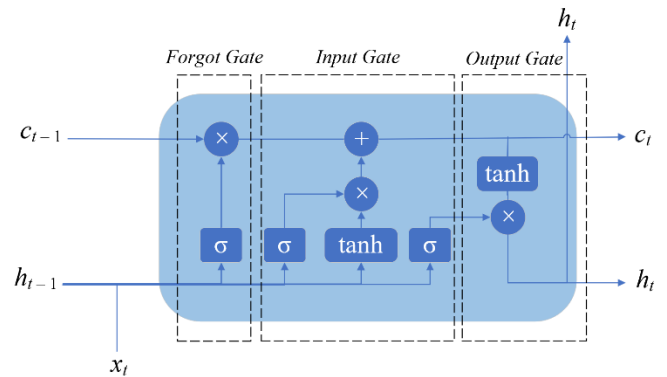
Figure 8.   LSTM machine learning model structure principle

LSTMs process sequence data through the following steps:

1) The input information is fed into the LSTM network.

2) Input gates control the entry of new information into the network.

3) Forget gates control the deletion of old information from the network.

4) The output gate controls the information output by the network.

5) LSTM can learn parameters through the backpropagation algorithm. The backpropagation

algorithm updates the parameters of the network by calculating the error of the network.

LSTM has been widely used in natural language processing, machine translation, speech recognition, time series prediction and other fields. LSTM is a very powerful neural network model that has achieved excellent performance in many tasks.

Here are some advantages of LSTMs:

- Can handle long sequence data
- Can learn long-term dependencies
- Achieved excellent performance in many tasks
- Here are some disadvantages of LSTMs:

Many parameters require a large amount of data for training, easy to overfit, Overall, LSTM is a very powerful neural network model that achieves excellent performance in many tasks.

The data basis formula adopted by the LSTM algorithm is as follows:

$$f_t = \sigma\left(U_f h_{t-1} + W_f x_t + b_f\right) \tag{5}$$

$$i_t = \sigma\left(U_i h_{t-1} + W_i x_t + b_i\right) \tag{6}$$

$$\acute{c}_t = \tanh\left(U_c h_{t-1} + W_c x_t + b_c\right) \tag{7}$$

$$c_t = f_t c_{t-1} + i_t \acute{c}_t \tag{8}$$

$$o_t = \sigma\left(U_o h_{t-1} + W_o x_t + b_o\right) \tag{9}$$

$$h_t = o_t \tanh\left(c_t\right) \tag{10}$$

In Figure 8, the cell state c_{t-1} and hidden state h_{t-1} at the previous time step is tuned by the forget gate switch to generate the corresponding states c_t and h_t at the current time step, where the forget gate vector f_t is expressed in Formula 5.

In Formula 5, σ denotes the sigmoid function layer which determines the parameters to be updated, U and W denote the weight matrices to be applied to the hidden state vector h_{t-1} at the previous time step and input vector x_t at the current time step, respectively, and b denotes the bias vector to reduce inaccuracy during training.

In order to update the cell state, the input gate utilizes the sigmoid function σ and tanh function to process the cell state vector c_{t-1} at the previous time step to generate the cell state vector c_t at the current time step. The working expression of the sigmoid function σ and tanh function are illustrated in Formula 6 and Formula 7, respectively.

Then, the cell state c_{t-1} at the previous time step is processed by forget gate, and the product of tanh layer output and sigmoid layer output are added together to update to the cell state c_t at current time step, as illustrated in Formula 8.

Finally, after being processed by the same sigmoid function and tanh function in the output gate to determine the output parameters and the weighted value in Formula 9, the hidden state h_t at the current time step is output by an LSTM cell to transfer to the next one or use as the final output in Formula 10.

D. Using LSTM to predict oil well pump pressure experiment in fault diagnosis

This system builds a data set based on a large amount of historical data such as temperature, pressure, and valve opening monitored online by all sensors of the oil well oil pump. Through the LSTM machine learning neural network prediction model and effective training, the future of the oil well oil pump can be obtained more accurately. The occurrence temperature, pressure, valve opening trend curve and the probability of failure data, once the abnormality is predicted by the fault diagnosis machine learning reasoning mechanism, an alarm will be issued immediately.

In the process of system experiment, the construction of back-end server is a crucial step.

The back-end server is responsible for receiving and processing front-end requests, performing data processing, implementing business logic, and returning the results to the front-end. In this design, we need to build a reliable, efficient, and secure back-end server to support various functions and requirements of the system. We chose Python as the back-end development language, combined with the development of the Flask framework. Python is a concise and powerful programming language with rich library and framework support, suitable for rapid development and deployment. Flask is a lightweight web framework with flexible routing management and template rendering functions, easy to learn and use.

LSTM normalization refers to normalizing the input and output in the LSTM network to improve the training speed and performance of the network. Commonly used normalization methods include, but are not limited to: Batch Normalization, Layer Normalization, and Instance Normalization, etc.

Among them, Batch Normalization is a commonly used normalization method, which can normalize the input on each mini-batch to reduce the internal covariate displacement, thereby improving the training speed and performance of the network. Layer Normalization is another commonly used normalization method, which can normalize the input on each layer to reduce the internal covariate displacement, thereby improving the training speed and performance of the network. Instance Normalization is a normalization method for image processing tasks, which can normalize the input on each channel to reduce the internal covariate displacement, thereby improving the training speed and performance of the network.

The following takes oil well oil pump pressure as an example to carry out fault diagnosis and prediction. The algorithm steps are as follows:

Step 1: Obtain the historical data of oil well pump pressure to form a training data set;

Step 2: Normalize the data in the dataset;

Step 3: Divide the training set into the training set for machine learning LSTM model training to obtain model parameters;

Step 4: The verification set divided into the training set is verified by the machine learning LSTM model to obtain error data;

Step 5: The machine learning LSTM model is used to predict the pressure of the oil pump for a period of time in the future. If it exceeds the range, it will warn that there will be a failure in the future;

The algorithm formula used for normalization in this system is as follows:

$$x_{standard} = \frac{x - x_{min}}{x_{max} - x_{min}} \tag{11}$$

$$x_{scaled} = x_{standard} * (max\,?\,min) + min \tag{12}$$

In Formula 11 and Formula 12, max represents the maximum value, and min represents the minimum value.

In the LSTM prediction experiment of the oil well pump pressure in this system, the system uses the normalized root mean square error (n-RMSE) to characterize the pressure prediction performance of the oil well pump for different models given different lengths of input windows and prediction windows. In order to obtain the indicator data n-RMSE in Python, it is necessary to sum the deviation squares between the predicted value of the oil well pump pressure and the actual value of the oil well pump pressure, and then divide the sum by the size of the oil well pump pressure test sample to calculate the MSE. Then, the indicator RMSE of oil well delivery pump pressure machine learning can be calculated by taking the root of MSE. Finally, the metric nRMSE for machine learning of oil well pump pressure is calculated by dividing the RMSE by the mean value of the real dataset. Usually, a lower index nRMSE of oil well oil pump pressure machine learning will indicate that the model prediction performance is better, and at this time it can be used for real-time diagnosis of oil well oil pump pressure faults.

The main technical index parameters of the LSTM machine learning algorithm for oil well

pump pressure failure are shown in formula 13, formula 14 and formula 15:

MSE (Mean Squared Error):

$$MSE = \frac{1}{N}\sum_{i=1}^{N}\left(y_i - \hat{y}_i\right)^2 \qquad (13)$$

RMSE (Root Mean Squared Error):

$$RMSE = \sqrt{\frac{1}{N}\sum_{i=1}^{N}\left(y_i - \hat{y}_i\right)^2} \qquad (14)$$

n-RMSE (Normalized Root Mean Squared Error):

$$nRMSE = \frac{RMSE}{\overline{y}} \qquad (15)$$

This experiment is based on the Python development environment. The oil well pump pressure sensor recorded in the project is used as the data set, and the data is cleaned, and then normalized. There are more than 3,000 pieces of data in this dataset, and the first 20 pieces of data are shown in Table 1.
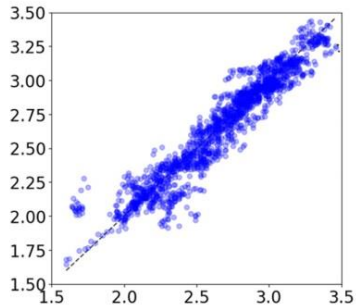
Figure 9.   Fault diagnosis and prediction scatter diagram of oil well pump oil delivery pressure training set

Then, the LSTM machine learning model is used for training to obtain the effective parameters of the model, and finally the prediction is made. The error of the training collection and distribution point is shown in Figure 9, the error of the testing collection and distribution point is shown in Figure 10, and the actual curve and predicted curve of the oil well pump are shown in Figure 11.
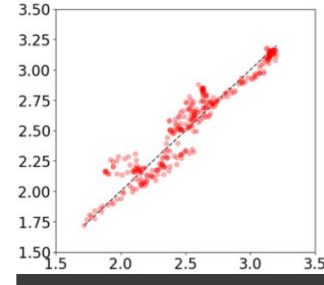
Figure 10. Oil well pump oil delivery pressure test set fault diagnosis and prediction scatter diagram

TABLE I.   TOP 20 RECORDS IN THE DATA SET USED BY OIL WELL PUMP MACHINE LEARNING

Code	Date	Time	Oil Pressure (Mpa)
1	6/1	0:00	1.69
2	6/1	1:00	1.81
3	6/1	2.00	2
4	6/1	300	1.97
5	6/1	4:00	1.84
6	6/1	5:00	2.01
7	6/1	6:00	1.62
8	6/1	7:00	1.89
9	6/1	8:00	2.14
10	6/1	9.00	2
11	6/1	10:00	2.06
12	6/1	1100	1.8
13	6/1	12:00	1.65
14	6/1	13:00	1.67
15	6/1	14:00	2.11
16	6/1	15.00	1.88
17	6/1	16:00	2.12
18	6/1	17:00	1.54
19	6/1	18:00	2.08
20	6/1	19:00	2.02
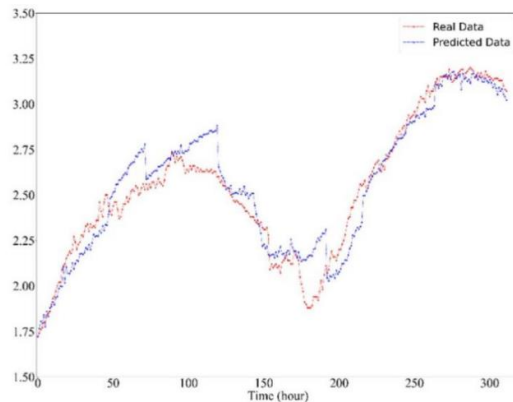
Figure 11. Comparison chart of machine learning actual value and predicted value of oil delivery pressure of oil well delivery pump

It can be seen from Figure 11 that the prediction accuracy of the LSMT machine learning algorithm is very high, which fully meets the needs of the oil well oil delivery pump for late pressure over-limit fault diagnosis and alarm.

According to the aforementioned evaluation indicators, the data obtained by machine learning operations are shown in Table 2.

TABLE II.   EVALUATION INDEX DATA OBTAINED BY MACHINE LEARNING OPERATIONS

Type	Train	Test
MAE	1.91	5.59
MSE	9.33	11.35
RMSE	5.42	7.41
nRMSE (%)	4.03	8.85

It can be seen from Table 2 that the machine learning model proposed in this paper has a very small error in the fault diagnosis and prediction of oil well pumps.

In the actual use of the system, when it is predicted that the pressure of the oil pump in the oil well will exceed the safety limit in the future, the oil pump will be diagnosed in advance and the engineer will be reminded to deal with it on site, so as to truly prevent problems before they happen.

VI. CONCLUSION

The author used the theoretical framework of the Internet of Things system proposed in this paper to successfully develop and experiment in the remote fault prediction and monitoring project of oil well digital oilfield of a subsidiary oilfield enterprise of PetroChina. The system can switch and control the output of four well groups distributed in different regions oil pump. The system's IoT central computer software is developed using the object-oriented integrated programming tool Embarcadero RAD Studio XE Community Edition, the database system uses SQL Server 2008, and the remote desktop and mobile terminal use Visual Studio 2020 to develop a B/S architecture Web system. Considering the safety of the special equipment controlled by the system, the mobile terminal can only browse the operating parameters and data of each oil pump, and cannot remotely control it. The system has been in trial operation for more than half a year. Compared with the early traditional manual inspection and management of oil pumps, the system is easy to operate, has a high degree of intelligence, and accurate and timely diagnosis and early warning of equipment operation faults. Strong guarantee. The experiment proves that the LSTM machine learning model has better prediction accuracy of oil well pressure failure.

The follow-up research recommendations of this project are as follows:

1) It is necessary to increase the complexity of the system, investigate the sensor data format and characteristics of most oil well pumps in China, connect the sensor data to the system in a standardized manner, expand and improve the monitoring software, in order to realize wide and comprehensive monitoring Comprehensive monitoring of the faults of oil well oil pumps, and the accumulation of data sets of many oil well oil pump sensors to provide a sufficient amount of data sets for machine learning.

2) The background of the system should use a variety of machine learning models other than LSTM to train and predict the oil well pump data set, and obtain the accuracy values predicted by different machine learning models, compare these values, and select the appropriate machine the learning model is finally used in this system.

REFERENCES

[1] Ma Hongjun. The research and application of key technologies and applications of offline monitoring and diagnosis of long-voltage pipeline oil pumps [J]. Water pump technology, 2023 (03): 29-35.

[2] Xu Jia, Hu Jiancun, Qin Ciwei, etc. Optimized high-pressure oil pump diagnosis based on parameter optimization VMD and distributed entropy [J]. Internal combustion engine Journal, 2023, 41 (02): 166-174.

[3]]Zhang Zongke, Dai Longxing. The application of the oil gas pump in the oil and gas collection system [J]. Comprehensive corrosion control, 2022, 36 (09): 34-35.

[4]　Li Yaping, Li Sujie, Ma Bo, etc. A method of failure diagnosis and health assessment of the oil pump unit [J].

[5]　Teacher Chaoguang. Based on the labView oil pump unit running noise noise, three -dimensional boundary sound field simulation research [D]. Northeast Petroleum University, 2022.

[6]　Liu Zhaoting. Study on the failure diagnosis method of the oil pump unit based on running noise analysis [D]. Northeast Petroleum University, 2022.

[7]　Zhang Xing, Zhang Yikun, Lin Mingchun, etc. The diagnosis and treatment of the resonance failure of the oil pump motor [J]. Chinese petroleum and chemical standards and quality, 2021, 41 (17): 47-49.

[8]　Confucius. Oil pump unit fluid power noise noise acoustic characteristics and their detection methods Study [D]. Northeast Petroleum University, 2021.

[9]　Fang Zhen. The design and realization of the chemical pump fault diagnosis system [d]. Anhui University, 2021.

[10] Wei Lixin, Chu Yongqiang, Liu Fang, etc. Oilfield station oil pumps fuzzy security evaluation [J]. Flow machinery, 2021, 49 (03): 68-73.

[11] [11] Xu Jia. Under the condition of complex working conditions, the diagnosis of fault diagnosis of high - pressure oil pumps for ships for ships under complex working conditions [D]. Nanjing University of Aeronautics and Astronautics, 2021.

[12] Xu Kai, Fushimi, Chen Shijun equivalent. Steaming generator status monitoring system based on LSTM neural network [J]. Application technology, 2020, 47 (06): 96-100.

[13] Wang Yizheng, Wang Yanwu, Gao Hongbin. Diagnosis of ship fuel pump-based fuel pump-based monitoring [J]. Mechanical and Electrical Engineering Technology, 2021, 50 (01): 163-165.

[14] Li Baisong, Su Jianfeng, Zhang Xing, etc. The diagnosis method of the oil pump inlet and export pipes [J]. Oil and gas storage and transportation, 2021, 40 (01): 21-25.

[15] Ning Shuangsheng. Pipeline pumps safety risk evaluation based on fuzzy FMECA [J]. Safety, 2020, 41 (08): 13-19.

[16] Xu Jing. The diagnosis of aircraft fuel pumps based on wavelets and migration learning [J]. Hydraulic and pneumatic, 2020 (06): 183-188.

[17] Guo Rui. ANSYS -based oil pump unit electromagnetic noise production mechanism and simulation research [D]. Northeast Petroleum University, 2020.

[18] Zhang Xinbo. Inquire about the vibration influencing factors and response strategies during the operation of the oil pump [J]. Chemical management, 2019 (33): 120-121.

[19] Zhang Dawei. The performance test exploration of the oil pump [J]. Technology Information, 2019, 17 (30): 70+72.

[20] Qin Jianan, Li Wenjin, Cheng Zhenxin, etc. The oil pump unit predicts the establishment and research of the maintenance decision model [J]. Equipment management and maintenance, 2019 (02): 182-184.

[21] Liu Zhaoquan. Oil pumps typical failure analysis and maintenance [J]. Chemical management, 2019 (03): 40-41.

[22] Xiao Bo ship. Explore the application of oil pump failure diagnosis technology in the refined oil pipeline system [J]. Contemporary chemical research, 2018 (10): 59-60.

[23] Zhao Jianghui. The application of status monitoring and fault diagnosis system in the oil pump unit [J]. Petrochemical technology, 2018,25 (08): 259.

[24] Baoxia L, Chenchen X, GANG L, et al. Application of Frequency Domain Analysis Method in Vibration Analysis and Fault Diagnosis of Oil Transfer Pump UNIT [J]. Journal of Physics: Conference Series, 2023, 2437 (1).

[25] liangliang d, qian x, yanjie j, et al. Review of reSearch on intelligent diagnosis of our transfer pump malfunction [J]. Petroleum, 2023,9 (2).

[26] Yao Sen, Dai Xingzheng, Cai Liang, etc. The research on the risk evaluation technology of the oil pump unit based on multi-level fuzzy analysis method [J]. Comprehensive corrosion control, 2021,35 (10): 53-56.

[27] He Min, Wang Xingru. Analysis and countermeasures for the causes of failure pump pump pump pumps in the long passing pipeline [J]. Equipment management and maintenance, 2021 (10): 55-57.

[28] Lin Yujun, Liu Yong, Zhao Shengsheng. Oil pump online monitoring mobile app design and development [J]. Science and education guidance (early journal), 2020 (28): 43-45.

[29] Ou Yonghong, Xu Lidong, Wang Lihong, etc.. Analysis and countermeasure study of the oil pipe oil pump failure pump [J]. Chemical management, 2020 (01): 181.

[30] Qiao Shijin, Qiao Linan. Analysis of the oil pump failure pump in the aircraft supply system [C] // Aviation Industry measurement and control technology development center, China Aviation Society testing technology branch, status monitoring special sensing technology Aviation Technology Key Laboratory. Tenth tenth tenth Sixth China Aviation Control and Control Technology Annual Conference Collection. [Unknown publishers], 2019: 455-456+461.

[31] Xu Guoping. Oil pipeline data collection and monitoring control (SCADA) system oil pump failure analysis of failure pumps [J]. Petroleum and gas stations, 2018,27 (05): 16-19+6.

[32] Analysis of Hou Nana. Oil pump failure diagnosis mode [J]. Chemical design communication, 2018,44 (04): 91+106

[33] Wu Peng. Analysis and countermeasures of the cause of the failure of the oil pipe oil pump pump [J]. Chemical management, 2018 (22): 128.

[34] liangliang d, qian x, yanjie j, et al. Review of reSearch on intelligent diagnosis of our transfer pump malfunction [j]. Petroleum, 2023,9 (2).

[35] Li Xiaoqing. Aquinus neural network and application in fault diagnosis [J]. Digital technology and application, 2022,40 (05): 150-152.

[36] Wang Lei. Diagnosis and health prediction of ore drainage pumps based on multi -source perception [D]. Anhui University of Science and Technology, 2022.

[37] Chen Yuhao. Study and application of typical industrial equipment health status prediction methods [D]. Chongqing University, 2022.

[38] Luo Shenghua. Research on the diagnosis and health state prediction method of hydraulic pump [D]. Jiangsu University of Science and Technology, 2022.

[39] Yin Jingtian. Filling in the diagnosis and health prediction of bearing fault diagnosis and health of the packaging system [D]. Jiangsu University, 2021.

[40] Shan Yahui. Research on the trend of vibration failure and health performance trends of hydropower units [D]. Huazhong University of Science and Technology, 2021.

[41] Ye Chunwei. Research on Early Equipment Diagnosis and Maintenance Strategy [D]. Nanjing University, 2021.

[42] Guli, Zou Yongsheng, Li Kaihong, etc. The ARMA model in the ARMA model in the research on the ectopic value trend of the oil pump vibration [J]. Fluid machinery, 2021, 49 (01): 22-28.

[43] Xu Kai. Research on the monitoring system based on the status characteristics [D]. Harbin Engineering University, 2020.

[44] Liu Jialong. Study on the diagnosis and health prediction of high -speed train steering racks based on data -driven high -speed trains [D]. Northeast University, 2020.

[45] Qiao Ningguo. High -speed train transmission systems based on multi -sensor data fusion prediction and health prediction [D]. Jilin University, 2019.

Research on Medical Dialogue Generation of External Knowledge

Na Liu

School of Computer Science and Engineering
Xi'an Technological University
Xi'an, 710021, Shaanxi, China
E-mail: 690879168@qq.com

Feng Huang

School of Computer Science and Engineering
Xi'an Technological University
Xi'an, 710021, Shaanxi, China
E-mail: 851072437@qq.com

Xiaohui Su

School of Computer Science and Engineering
Xi'an Technological University
Xi'an, 710021, Shaanxi, China
E-mail: 287099144@qq.com

Abstract—**Nowadays, the technology of medical dialogue generation has gradually attracted the attention of more researchers, and the demand for landing has gradually increased. Therefore, building a medical dialogue system that can automatically reply is conducive to improving the efficiency of clinical consultation and reducing the burden on doctors. This paper uses the method of fusing external knowledge to build a dialogue generation model, which greatly enhance the accuracy of the model and ameliorates the disadvantages of classical construction methods. Based on the large-scale pre-training model method, the doctor's response is generated by two-stage training, and the knowledge related to the medical background is added to generate the response that best fits the current context. In this paper, experiments were performed on the medical dialogue dataset KaMed and COVID-19, and the experimental data showed that compared with the traditional human-computer dialogue generation Seq2Seq model, the Perplexity value of this method decreased 1.91, compared with the VHRED model, B@1 value increased 0.3, and the B@2 value increased0.34, D@2 increased 2.14, it can be proved that the medical dialogue model proposed in this paper can provide doctors with response responses more effectively and enhance the accuracy of responses.**

Keywords-Medical Dialogue System; Knowledge Fusion Dialogue; Task-Oriented Dialogue Generation

I. INTRODUCTION

With the COVID-19 epidemic in 2019, an increasing number of businesses have launched a "home office" model, and online consultation has also become a new trend in the medical industry of various countries. In order to solve the problem of surge in user consulting demand and the shortage of medical personnel who provide online diagnosis and consultation services, it is imminent to develop a smart medical dialogue system that can provide users with online diagnosis and treatment solutions. These "online doctors" can greatly reduce the burden on human doctors, reduce the chance of cross -infection among patients, and improve the efficiency of medical resource operations.

The current task -type dialogue generation method can be divided into two types: traditional methods and deep learning methods. The advantage of using the traditional method to build a dialogue system is that it is simple, but only the answers to similar responses in the template can only be found, and high -skilled talent teams provide different templates in different fields. To other areas[2]. In deep learning methods, the method of decoder -based method creates a precedent for using neural network methods in task -type dialogue. At the same time, language models and neural network methods are used. The generated sentences have diversity and reduced artificial characteristics.

With the proposal and development of several large scale pre-training structures such as

Transformer and GPT, various variants in the field of task -type dialogue generation have also received widespread attention. This model can improve the ability of model modeling language through the pre -training mechanism to improve the model modeling language. , Cross -current -order attention mechanism can better process the structured MR (semantic information) input to achieve the best results at present. The filter mechanism is eliminated with medical knowledge with low historical compatibility with doctors and patients, enhance the selection of accurate knowledge in the reply, thereby improving the accuracy of the model, making it a more accurate and higher medical reference value.

II. RELATED WORK

In the task of establishing a task -oriented dialogue system, dialogue generation is an indispensable part of it. Many scholars are committed to studying various methods for dialogue generation. In 2015, we will be based on the decoder. The method is applied to the dialogue generation task, and a statistical language generator based on a combined cycle and convolutional neural network structure can be proposed. This structure can be trained on dialogue behavior and discourse. Essence Then in 2015, Wen et al. [4] referred to the research in the selection field, and proposed an Encoder-Decoder architecture that adapt to NLG based on a attention mechanism, which achieved a better effect than decoder-based methods.

In 2016, DUšEk et al. [5] explored the advantages and disadvantages of the two methods to generate sentence planning trees and directly generate natural languages with the SEQ2SEQ method. In the same year, Dukek et al. [6] introduced information about language models from the previous model. In the case of maintaining the overall framework of the model, they improved the input and spliced the user's words in front of the input MR (semantic information) three yuan group, as the front of the front; and the newly added one above Coder, coding user discourse alone.

In 2017, Van-Khanh Tran et al. [7] It proposed the encoder-polymer-decoder model based on the

extension of the encoder-decoder architecture of recursive neural network.

In 2018, Wei Z, LiU Q et al. [8] proposed a dialogue system for automatic diagnosis, constructed the Medical DS dataset, and proposed a framework of the dialogue system based on strengthening learning (RL). So as to improve the accuracy of automatic diagnosis.

In 2019, SHANG-Yu Su et al.[9] proposed a new type of language understanding and generating learning framework based on dual supervision and learning, providing a method that uses puppets. Experiments show that this method improves significantly improvement can be significantly improved. Language understanding and generating learning performance.

In 2020, PENG et al. [10] proposed the SC-GPT model to enter the MR tank into the GPT pre-training model, and directly obtain the results using the sequence to sequence method.

In 2021, Yangming Li et al. [12] proposed a new heterogeneous rendering (HRM) framework that explains how the nerve generator render the input dialogue (DA) as discourse. For each generation step, the mode switch is concentrated from the renderer to select the appropriate decoder to generate items (words or phrases). This model can well explain the rendering process of the nerve generator.

On the basis of predecessors' research and deep learning development, although the natural language generation (NLG) mission in the dialogue system has achieved good performance, it is still found that if only dialogue data is used to train the model during the dialogue generation process, the model is found to train the model for training. It is easy to produce such security responses such as "good" and "can". This type of reply has no reference value to the therapy of physician. Thus, to solve these challenges, this article adds and has added and added to predecessors' research. The symptoms described by patients have high-fitting medical knowledge, followed by effectively incorporating knowledge and tracking the patient's speech, testing the doctor's behavior entity, and eventually generated a reply through professional medical knowledge,

patient's condition and doctor behavior to help Patients provide diagnosis and treatment opinions and suggestions in effective ways.

III. RESEARCH METHODS

A. Task definition

Medical dialogue generation tasks are to help doctors provide diagnosis and treatment suggestions in the case of consultation. This needs to be based on the history of the doctor and patient dialogue and related medical knowledge, to generate the same text reply to the user's and conform to the context and meet the medical principles. This article uses the dialogue history $H = \{\{h_1, r_1\}, \{h_2, r_2\}, ..., \{h_i, r_i\}, ..., \{h_n, r_n\}\}$ and medical knowledge $K = \{k_1, k_2, ..., k_i, ..., k_n\}$ between patients and doctors. Among them, $\{h_i, r_i\}$ the history of the dialogue between doctors and patients, k_i is a collection of medical knowledge of the relevant dialogue history Each of these knowledge k_i contains head entities h, relationships r, and tail entities t that have some relationship with head entities. In the form of ternary groups, the model needs to generate a reply Y according to the history of dialogue H and related medical knowledge K Among them, $Y = \{y_1, y_2, ..., y_i, ..., y_n\}$, y_i it is the second in the reply. The goal of this article is to maximize the genetic reply Y, so that the response is accurate and referenceable.

B. Model overview

In this paper, a medical dialogue generation model that integrates external knowledge is proposed, as shown in Figure1. The model contains: doctor-patient dialogue coding, patient status tracking, doctor behavior detection, medical knowledge distillation, and reply generation. The model needs to obtain a vector with the context information of the doctor-patient dialogue by coding the doctor-patient dialogue to track the patient's condition status during the dialogue, and then predict the doctor's next round of actions, and finally fuse the medical knowledge extracted by the medical knowledge distillation module to produce relevant replies.
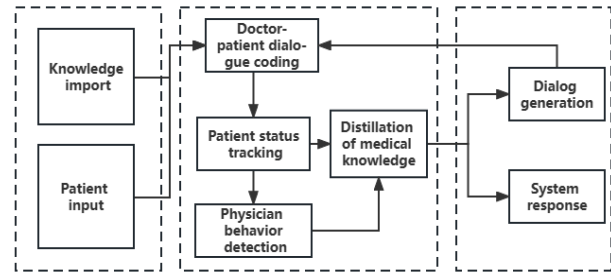
Figure 1. Structure diagram of knowledge-based medical dialogue generation

C. Doctor-patient dialogue coding module

For the doctor-patient dialogue coding module, this paper first uses the bidirectional gate circulation unit (BiGRU) to encode the doctor-patient dialogue history and convert it into a vector expression $\vec{H} = \{\{\vec{h}_1, \vec{r}_1\}, \{\vec{h}_2, \vec{r}_2\}, ..., \{\vec{h}_i, \vec{r}_i\}, ..., \{\vec{h}_n, \vec{r}_n\}\}$ with doctor-patient context information.
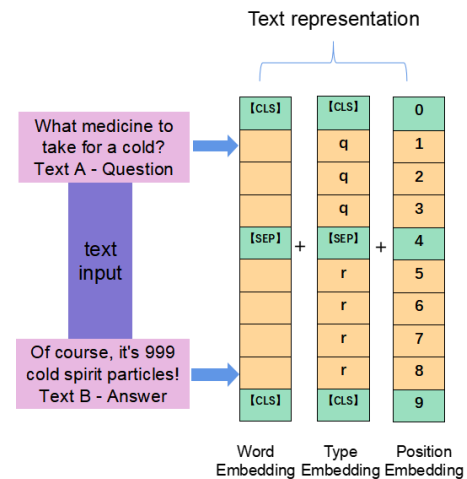
Figure 2. Input representation of doctor-patient dialogue coding module

The BiGRU neural network can greatly reduce the amount of calculation and complexity of the model. The input representation of its doctor-patient dialogue coding module is shown in Figure2.

After using BiGRU to encode the doctor-patient dialogue, a vector with the context information of the doctor-patient dialogue is obtained, where H is the doctor-patient dialogue history. Formally, the output of the encoder is shown in Equation (1):

$$E_h = BiGRU(H) \tag{1}$$

D. Patient status tracking module

The goal of the patient status tracking module is mainly to track the patient's condition status in the doctor-patient dialogue history, use tracking to the patient's state S to predict the doctor's next round of behavior B, and finally produce a response Y that is in line with the context of the doctor-patient dialogue. Therefore, a state tracker composed of variational autoencoder is added to the patient status tracking module to indirectly learn the posterior distribution $p(y|x)$ of the data to obtain the probability distribution of the patient state.
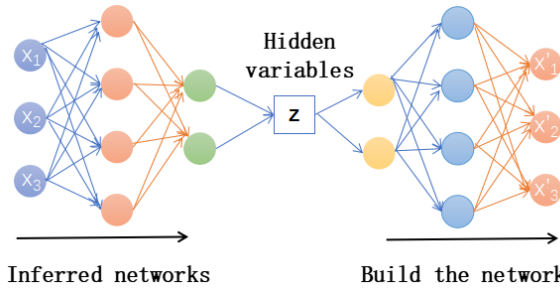
Figure 3.   (Variational autoencoder) Generates a model structure diagram

The learning process first learns the joint probability distribution $p(x,y)$ from the dialogue data, and then reverses the posterior distribution by solving the prior probability and categorical conditional probability of the patient's state, and the posterior probability obtained at this time is the probability of the patient's state tracking distribution at time t as sought in this module. The structure of the model is shown in Figure3.

In each round of medical conversation that tracks the patient's status, the status tracker first samples a previous round of patient status s_{t-1}^q from the approximate posterior distribution $q_{\phi_s}(s_{t-1})$ of the state, and then enters the previous round of patient status s_{t-1}^q into BiGRU to obtain the current round of patient status s_t^q, that is, the prior patient status s_t^q of the T round is combined from the patient status s_{t-1}^q of the T-1 round, the doctor's response R_{t-1}, and the patient description U_t of the T round. The formula is shown in Equation (2).

$$p_{\theta_s}(S_t) = p_{\theta_s}(S_t \mid S_{t-1}, R_{t-1}, U_t) \qquad (2)$$

Specifically, after obtaining the prior patient state $p_{\theta_s}(S_t)$ at time t, in the decoding stage, the model takes the doctor's behavior state $b_{t,0}^{S^p} = W_s^p[h_t^c; h_{t-1}^{S^q}]$ predicted at the very beginning moment (i.e., 0 moment) as the initial hidden state of the decoder (W_s^p in which a learnable parameter, $[\cdot;\cdot]$ is represented by a cascade operation of the vector), at the decoding moment of the ith word, the decoder decodes serially S_t, receives the encoding vector $e_{t,i-1}^{S^p}$ of the word of the previous moment as input, outputs the doctor's behavior state $b_{t,i}^{S^p}$ at the i moment, and maps it to the patient's state $b_{t,i}^{S^p}$ space. This article fixes the length of the patient state S_t to $|S|$, as shown in Equation (3).

$$p_{\theta_s}(S_t) = \prod_{i=1}^{|S|} soft\max(MLP(b_{t,i}^{S^p})) \qquad (3)$$

Where MLP represents a multilayer perceptron (MLP), the state tracker is inferred to be similar to the above process, but additionally combines a vector representation R_t (i.e.,) as input. The BiGRU decoder is used $b_{t,0}^{S^q} = W_s^q[h_t^c; h_{t-1}^{S^q}; h_t^R]$ to initialize, where W_s^q is a learnable parameter, and at the ith decoding moment, output the predicted doctor's actions $b_{t,i}^{S^q}$ in the t round. Among them, the approximate posterior distribution is formulated as shown in Equation (4).

$$q_{\phi_s}(S_t) = \prod_{i=1}^{|S|} soft\max(MLP(b_{t,i}^{S^q})) \qquad (4)$$

E. Doctor behavior detection module

The doctor behavior detection module is designed to predict the entity that the doctor will reply to in the next conversation, this paper builds a doctor behavior classifier in this module, which mainly divides the doctor behavior into four types

such as asking symptoms, diagnosis, prescribing drugs, small talk, etc., doctors should judge whether there is a shift between behavioral states according to the conversation history, that is, to determine whether the next sentence should continue to ask the patient's symptoms or give diagnostic suggestions, etc., the doctor behavior detection process is shown in Figure 4.
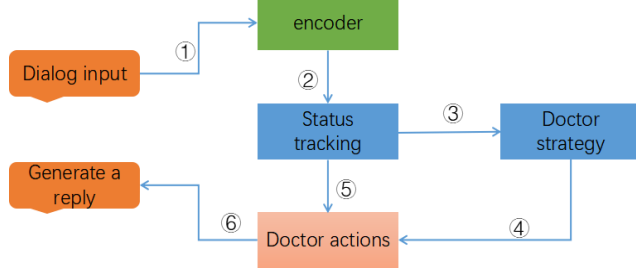

Figure 4. Flow chart of doctor behavior detection

Specifically, in this module, similar to the Patient Status Tracking Module, this paper models a priori distribution and an approximate posterior distribution of physician actions, and its prior strategy network and posterior strategy network are also based on encoder-decoder structures, and define the representation of physician behavior A_t at moment t as a physician action category A_t^c and a series of explicit keywords A_t^k, $A_t = \{A_t^c, A_t^k\}$, where A_t^k the length is fixed $|A|$.

For a priori strategy network, in the encoding stage, this paper first uses a BiGRU encoder to encode the patient state S_t^p at time t, and outputs a hidden vector $h_t^{S^p}$. In the decoding and reply stage, an action classifier A_t^c is designed to infer the doctor's action category, and the hidden layer vector h_t^c at time t is used to perform attention operations q_t on the obtained doctor's behavior, and an attention vector q_t about the doctor's behavior is calculated. Next, the action classifier combines the obtained attention vector to divide the physician's actions into four categories, namely, asking about symptoms, diagnosis, prescribing medication, and gossiping, and the doctor's prior behavior is formulaically described as shown in Equation (5).

$$P_{\theta_{a,c}}(A_t^c) = soft\max(W_c^p[h_t^{S^p}; h_t^c; q_t]) \quad (5)$$

Learners are described W_c^p, and the model samples the action categories $A_t^{c,p}$ from the prior behavior $P_{\theta_{a,c}}(A_t^c)$ of the doctor.

A_t^k are serialized by a BiGRU decoder, and at each decoding step, the context inference detector maps the output vector of the BiGRU decoder into the action space. The decoder is initialized by a doctor's behavior $b_{t,0}^{A^{k,p}} = W_k^p[h_t^{S^p}; h_t^c; e_t^{A^{c,p}}]$ at 0 moment, where $e_t^{A^{c,p}}$ is the embedded representation $A_t^{c,p}$. At the ith decoding step, the decoder outputs $b_{t,i}^{A^{k,p}}$. The contextual inference detector is based on the doctor's behavior output vector $b_{t,i}^{A^{k,p}}$ at i-moment, co-infers the action vector $A_{t,i}^k$ of the doctor at i-moment, learns from the original doctor-patient dialogue history and the detected patient state, and infers its prior distribution $A_{t,i}^k$ as shown in Equation (6) through a multilayer perceptron MLP.

$$p_{\theta_{a,d}}(A_{t,i}^k) = \frac{1}{z_A}\exp(MLP([h_t^{S^p}; h_t^c; e_t^{A^{c,p}}; b_{t,i}^{A^{k,p}}])) \quad (6)$$

Finally, the prior distribution of the doctor's behavior A_t is calculated as shown in Equation (7).

$$p_{\theta_a}(A_t) = p_{\theta_{a,c}} \cdot \prod_{i=1}^{|A|}[p_{\theta_{a,d}}(A_{t,i}^k) + p_{\theta_{a,g}}(A_{t,i}^k)] \quad (7)$$

The inference strategy network approximates the posterior distribution of action categories by extracting key information with directivity from previous doctors' responses R_t. Use a BiGRU encoder R_t to encode as a hidden vector h_t^R and a hidden vector S_t^q respectively $h_t^{S^q}$. Then obtain an approximate posterior distribution of the physician's action class at time t, as shown in Equation (8).

$$q_{\theta_{a,c}}(A_t^c) = soft\max(W_c^q[h_t^c; h_t^{S^q}; h_t^R]) \quad (8)$$

Finally, the model extracts the doctor's action vector to the T moment by approximating the posterior distribution $q_{\theta_{a,c}}(A_t^c)$ of the doctor's action category $A_t^{c,q}$ at time t. In order to enhance the influence of the information in the doctor's reply R_t at moment t, this paper inference policy network designs a posterior distribution A_t^k of contextual inference detector de-approximation. The decoder is represented by $b_{t,0}^{A^{k,q}} = W_k^q[h_t^c; h_t^{S^q}; e_t^{c,q}; h_t^R]$ initialization, where the word embed din e representation representing the doctor's behavior A. W_k^q is a matrix of learnable parameters. In the i-th decoding step, the decoder outputs a vector representation $b_{t,i}^{A^{k,p}}$, so the approximate posterior distribution of the i-th action keyword can be obtained in this paper, as shown in Equation (9).

$$q_{\phi_{a,d}}(A_{t,i}^k) = soft\max(MLP([h_t^c; h_t^{s^q}; e_t^{A^{c,q}}; b_{t,i}^{A^{k,q}}])) \quad (9)$$

Finally, the approximate posterior distribution of the doctor's behavior detection at the t moment is obtained by the doctor action category and the ith action keyword of the t moment, and the formula is shown in Equation (10).

$$q_{\phi_a}(A_t) = q_{\phi_{a,c}}(A_t^c) \cdot \prod_{i=1}^{|A|} q_{\phi_{a,d}}(A_{t,i}^k) \quad (10)$$

F. Medical Knowledge Distillation Module

The most important thing in the dialogue system that integrates knowledge is to screen the appropriate knowledge as the input of the dialogue system, but due to the large scale of external knowledge and many data types, all possible knowledge as input may lead to more noise and high computational intensity, so this paper adds a noise filtering mechanism in the medical knowledge distillation module to select better knowledge and generate a more accurate response.

Specifically, the medical knowledge distillation module of this paper first performs a global pooling operation on the encoded vector with dialogue history context information and the correct medical background knowledge vector information obtained to obtain the corresponding scalar representation sum $\{S_{k_1}, S_{k_2}, ..., S_{k_n}\}$, which uses the doctor-patient dialogue context vector and each dimension of information with medical background knowledge vector, so that the scalar obtained can represent the semantic information represented by the vector to a certain extent. Moreover, after the vector is converted to the corresponding scalar, the complexity of the feature representation is greatly reduced, and the complexity of the model calculation is greatly reduced.

Secondly, in order to allow simultaneous interaction between knowledge and knowledge and between knowledge and the historical context of doctor-patient dialogue, this paper stitches each piece of knowledge and the historical context of doctor-patient dialogue and performs a two-layer full connection operation to obtain the weight $r = \{r_1, r_2, ..., r_{N+1}\}$ assigned to each piece of knowledge and the historical context of doctor-patient dialogue, and the result of summing the weights of all knowledge is used k' as the representation of the selected knowledge. After global pooling and Layer 2 full connection operation, the model can learn more interactive information.

Where the weights can be expressed as shown in Equation (11):

$$r = \sigma(W_2 \delta(W_1(S_{k_1} S_{k_2}, ..., S_{k_N} S_x)) \quad (11)$$

Where W_1 and W_2 is the learnable parameter, δ is the ReLU activation function, σ is the sigmoid activation function.

The calculation method of k' is shown in (12) (13).

$$k_i' = r_i \cdot k_i (i = 1, 2, ..., N) \quad (12)$$

$$k' = \sum_{i=1}^{N} k_i' \qquad (13)$$

Where k_i' is the weight corresponding to each piece of knowledge, and the output k' of the knowledge distillation module is and will be used to participate in the generation of replies in the reply generation module.

G. Reply to the build module

The reply generation module is composed of the patient status obtained by the patient status tracking module, the next doctor behavior predicted by the doctor behavior detection module, and the knowledge that is highly consistent with the doctor-patient dialogue context screened out by the knowledge distillation module, and jointly generate a response through the reply generation module to give doctors a reference to the diagnosis and treatment response.

In the first stage of reply generation, the model uses a BiGRU encoder to encode the patient state S_t^q at t moment as an embeddable vector $\vec{S}_t^q$, followed by a word-level encoding matrix of the patient state S_t^q, in which $\vec{S}_t^q$ each row is represented as an embedding vector corresponding to a word. Similarly, physician behavior $A_t^{k,q}$ is encoded as an embeddable vector $\vec{A}_t^{k,q}$. Then the hidden vectors of the sum are calculated separately S_t^q and $A_t^{k,q}$ expressed as sum, and the reply decoder is based on a BiGRU unit in the decoding stage, $b_{t,0}^R = W_d[h_t^c; h_t^{S^q}; e_t^{A^{c,q}}; h_t^{A^{k,q}}]$ is initialized, where there W_d is a parameter matrix. In the i-th decoding step, the output $b_{t,i-1}^R$ of the decoder obtains a vector $b_{t,i}^h$ for the context representation H_t of the attention operation. At the same time, attention manipulation is performed for the patient's state S_t^q at time t and the doctor's behavior $A_t^{k,q}$ at moment t, and the hidden vector sum after attention operation is obtained, respectively. The relevant hidden vector and embedding vector $[b_{t,i}^h; b_{t,i}^s; b_{t,i}^a; e_{t,i-1}^R]$ are then fed

into the BiGRU unit of the decoder and output the i word $b_{t,i}^R$ in the i-moment, which $e_{t,i-1}^R$ is demonstrated. The probability $R_{t,i}$ of the model generating a reply is the sum of the generation probability and the probability of copying knowledge, which is formulated as shown in equation (14)(15)and(16).

$$p_{\theta_g}(R_{t,i}) = p_{\theta_g}^g(R_{t,i}) + p_{\theta_g}^c(R_{t,i}) \qquad (14)$$

$$p_{\theta_g}^g(R_{t,i}) = \frac{1}{z_R} \exp(MLP(b_{t,i}^R)) \qquad (15)$$

$$p_{\theta_g}^c(R_{t,i}) = \frac{1}{z_R} \sum_{j:W_j = R_{t,i}} \exp(h_j^{W^T} \cdot b_{t,i}^R) \qquad (16)$$

The generation probability is represented $p_{\theta_g}^g(R_{t,i})$ and the probability of copying knowledge is represented by $p_{\theta_g}^c(R_{t,i})$. z_R is a regular item shared with $p_{\theta_g}^c(R_{t,i})$. This article will write the sequence of $R_{t-1}, U_t, A_t^{k,q}$ and S_t^q to concatenate W, W_j to represent the j word in W.

IV. EXPERIMENTAL RESULTS AND ANALYSIS

A. Datasets

To validate the essentiality of the essay method, this paper uses large-scale medical datasets KaMed and a large-scale COVID-19 Chinese dialogue dataset proposed by Zeng et al. [10] in 2020. Among them, COVID-19 contains more than 1,088 conversations, covering common COVID questions and answers, and providing granular entity-level annotations; KaMed includes more departments and a wider variety of diseases, including more than 17K medical conversations and 5682 entities. The dataset used in this article is shown in Table1.

TABLE I.   DATASET STATISTICS

Datasets	Dialog	Utterances	Tokens	Knowledge
KaMed	17864	153,000	6,663,272	Y
COVID-19	1088	9494	406,550	N

B. Experiment setup

The experimental hardware environment in this article uses Intel I9-10900KCPU, Nvidia Geforce 2080Ti*2, 64G RAM, and SSD512G. The software environment uses the Windows 10 system, and at the same time uses Pycharm, Visual Studio Code, Pytorch, Neo4j, etc. for development, and uses TensorBoard for dialogue display.

C. Evaluation indicators

In order to evaluate the linguistic quality of the responses generated in this paper, the metrics BLEU@N, Distinct@N, and Perplexity confusion level (PPL) are used to evaluate the model proposed in this paper.

D. Experimental analysis

To validate whether the model proposed in this paper is better than the previous model, this article uses the Seq2Seq end-to-end model with attention mechanism, the HRED model and the model in this paper are experimented with KaMed, COVID-19 two datasets, first of all, in the experimental process, and the confusion matrix is used to summarize the generated results. The visual attention score obtained by different models obtained by the experiment can be seen: different models have different maximum attention scores for the context, the basic Seq2Seq model, for "cold" and "medicine" such entities are not high, and HRED and VHRED compared with the Seq2Seq model, the attention score of such entities has increased a certain accuracy, and finally the model that integrates knowledge in this paper has the most accurate attention score for the conversation context, which is for "cold" and "taking medicine" The high attention scores of such entities indicate that the method presented in this paper can track and speculate on medical entities. The results of medical dialogue generation under different datasets of different models are shown in Table 2 below.

TABLE II.　　EXPERIMENTAL RESULTS

Datasets	Model	B@1	B@2	D@1	D@2	Perplexity
KaMed	Seq2Seq	2.71	1.58	1.24	6.85	24.82
	HRED	2.59	1.59	1.17	6.65	27.14
	VHRED	2.49	1.55	1.15	6.42	28.65
	Ours	2.79	1.89	1.58	8.56	22.91
COVID-19	Seq2Seq	3.13	5.70	5.5	29.0	53.3
	HRED	2.56	5.73	5.21	32.39	49.6
	VHRED	3.31	5.65	5.65	34.56	47.2
	Ours	3.57	5.90	5.89	31.21	40.8

Experiments show that the proposed method performs well on two different datasets. Compared with the baseline Seq2Seq method, the Perplexity value of the proposed method is reduced by 1.91 compared with the baseline Seq2Seq method, and the smaller the value, the higher the accuracy of the proposed method. Compared with the VHRED model, the B@1 value of this method increased by 0.3, the B@2 value increased by 0.34, and the D@2 value increased by 2.14, all of which indicate that this method is better and still the same on the dataset COVID-19. Figure5 shows the following example of the conversation under test of the model in this document. Experiments show that the proposed method.
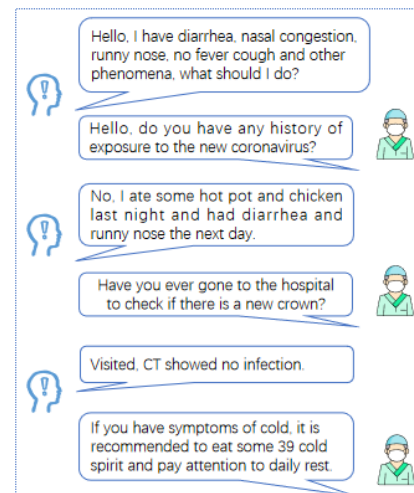

Figure 5.　Example of model generation

Model generation sample For example, when the patient proposes diarrhea, nasal congestion, runny nose and other symptoms and asks what to do, the doctor needs to look for knowledge related to the patient's disease in the knowledge triad through the patient's description of the disease, see which conditions the patient's symptoms are related to, further inquire about the patient's condition, and finally give a reply that the doctor can refer to.

V. CONCLUSION AND OUTLOOK

In order to solve the problem of surging demand for user consultation and shortage of medical personnel providing online diagnosis and treatment consulting services in the field of intelligent healthcare, this paper constructs a knowledge-based medical dialogue generation model, although the traditional template-based method is simple, but it requires high-skilled talents to write different templates in different fields, the labor maintenance cost is high, and the dialogue system built by slot filling patients can only find the existing answer set, can not be expanded, and the user utilization efficiency is low.

Therefore, this paper proposes a medical conversation generation model that adds external knowledge, and under the premise of using pre-trained models to enhance the scalability and portability of the proposed model, this paper pioneeringly combines external knowledge to improve the medical response generation task by tracking the patient's status and detecting the doctor's behavior. A large number of experiments on KaMed and COVID-19 show that the medical dialogue generation model based on this paper is superior to most baseline models in BLEU value, Discrete value and Perplexity value, which verifies the effectiveness of this model.

In the next study, it is planned to integrate patients' emotional variables into the dialogue generation model to enable the model to better understand the sentences expressed by the patient's spoken expression, hoping to generate more personalized and targeted responses and further improve the performance of the model in generating responses.

REFERENCES

[1] QIN Libo, LI Zhouyang, LOU Jieming, YU Qiying, CHI Wanxiang. Review of research progress on natural language generation in task-based dialogue systems [J]. Journal of Chinese Information Technology, 2022.

[2] ZHANG Xiaoyu, LI Dongdong, REN Pengjie, CHEN Zhumin, MA Jun, REN Zhaochun. Knowledge-aware medical dialogue generation based on memory network [J]. Computer Research and Development, 2022.

[3] Wen T H, Gasic M, Kim D, et al. Stochastic language generation in dialogue using recurrent neural networks with convolutional sentence reranking [J]. 2015.

[4] Wen T H, Gasic M, Mrksic N, et al. Semantically conditioned lstm-based natural language generation for spoken dialogue systems [J]. 1508.01745, 2015.

[5] Dušek O, Jurčíček F. Sequence-to-sequence generation for spoken dialogue via deep syntax trees and strings [J]. 2016.

[6] Dušek O, Jurčíček F. A context-aware natural language generator for dialogue systems [J]. 2016.

[7] Tran V K, Nguyen L M. Neural-based natural language generation in dialogue using rnn encoder-decoder with semantic aggregation [J]. 2017.

[8] Wei Z, Liu Q, Peng B, et al. Task-oriented dialogue system for automatic diagnosis[C]//Proceedings of the 56th Annual Meeting of the Association for Computational Linguistics (Volume 2: Short Papers). 2018: 201-207.

[9] Su S Y, Huang C W, Chen Y N. Dual supervised learning for natural language understanding and generation [J]. 2019.

[10] Peng B, Zhu C, Li C, et al. Few-shot natural language generation for task-oriented dialog [J]. 2020.

[11] Li Y, Yao K. Interpretable nlg for task-oriented dialogue systems with heterogeneous rendering machines[C]//Proceedings of the AAAI Conference on Artificial Intelligence. 2021, 35(15): 13306-13314.

[12] Sutskever I, Vinyals O, Le Q V. Sequence to sequence learning with neural networks [J]. Advances in neural information processing systems, 2014, 27.

[13] Radford A, Narasimhan K, Salimans T, et al. Improving language understanding by generative pre-training [J]. 2018.

[14] Radford A, Wu J, Child R, et al. Language models are unsupervised multitask learners [J]. 2019, 1(8).

Research on Iris Feature Extraction and Recognition Technology Based on Deep Learning

Yufei Chen

School of Computer Science and Engineering
Xi'an Technological University
Xi'an, 710021, China
E-mail: 18092589395@qq.com

Bing Zhao

School of Computer Science and Engineering
Xi'an Technological University
Xi'an, 710021, China
E-mail: 1574186102@qq.com

Yiyang Zhao

School of Computer Science and Engineering
Xi'an Technological University
Xi'an, 710021, China
E-mail: 2389369622@qq.com

Hao Wei

School of Computer Science and Engineering
Xi'an Technological University
Xi'an, 710021, China
E-mail: 3129943413@qq.com

Abstract—Certain biological information or behavioral information of a person can achieve the effect of characterizing an individual, and by combining the computer to extract the corresponding information, identity authentication is achieved. In a variety of biometrics, iris relative to fingerprints, handwriting and face, belongs to the structure within the human eye, if you want to steal is very difficult, in order to improve the safety factor, so the iris is used for authentication to achieve iris recognition. This study is based on deep learning iris recognition matching, in order to be able to effectively improve the accuracy of iris recognition, experiments are carried out. Evaluation metrics are performed through Hamming distance to calculate the correct recognition rate to ensure that the iris information can be accurately represented. This study mainly uses the improved PCHIP-LMD algorithm and CNN algorithm, the LMD algorithm is more context-aware, has better generalization ability, flexibility and scalability, while the CNN algorithm has the advantages of local awareness, parameter sharing and automatic parameter learning. In this study, we compare the correct recognition rate of iris recognition between improved PCHIP-LMD and CNN algorithms and get the conclusion that the correct recognition rate of the improved PCHIP-LMD algorithm is only 78%, which is much smaller than that of the CNN algorithm which is 92%, and we get the conclusion that LMD algorithm is suitable for iris recognition with few samples, and it is more suitable to use CNN algorithm when the sample images are too many. CNN algorithm. With the development of technology, the application of iris recognition will be more and more, I believe that soon will be widely popularized in daily life and work.

Keywords-Iris Recognition; Deep Learning; Normalization; Feature Extraction; LMD; CNN

I. INTRODUCTION

Today, with the rapid development of science and technology, biometric identification has begun to enter people's daily life and work. Biometric identification is a technology that collects the user's biometric features by means of modern technology and extracts the features through specific recognition algorithms, converts them into coded representations within the computer, and realizes identity authentication. Iris recognition is widely used in the field of identification by virtue of its uniqueness, stability and anti-counterfeiting features. Compared with other biometric identification, iris recognition is more secure, and is useful for safeguarding personal privacy and information security. Outstanding performance

In this paper, the iris feature extraction method based on traditional methods is firstly categorized into single feature and multi-feature fusion. Single feature is mainly for the acquisition of features in

the frequency domain, air domain, etc. Multi-feature fusion is based on single feature extraction, and multiple features are comprehensively extracted by using weighted summing or machine learning algorithms.

Secondly, the matching of iris recognition based on deep learning is added, which mainly includes distance recognition algorithms and neural network classification methods, which can use the Hamming distance, Euclidean distance, cosine distance, etc. to measure the distance between different iris image features, convert the extracted iris features into digital features, and compare the distance similarity with the template iris in order to determine the category. The neural network method is to input the extracted iris features into the network (e.g., BP, RBF, etc.), and then use the relevant classification function to complete the determination of the iris image category. In this paper, by comparing experiments on the CASIA-Iris-Syn dataset and CASIA-Iris Thousand dataset, which are commonly used in iris recognition tasks, we verified that the CNN test method can effectively improve the accuracy of iris recognition and achieve a low error rate.

Subsequently multi-feature fusion hierarchy is added. Depending on the different sources of data, the multi-feature fusion hierarchy can be categorized into, pixel hierarchy, feature hierarchy, matching hierarchy, and decision hierarchy.

Finally, iris feature matching test is performed. When recognizing the matching, the loss function layer of the network is removed, the rest of the network structure is retained, and the feature images extracted from the training model are expanded into one-dimensional feature vectors. The experimental results show that different iris feature vectors can be successfully extracted and the processed iris images are compared with those in the database for subsequent iris matching and recognition.

II.   RELATED WOEKS

In 2014, Zhen Nan Sun et al. encoded the texture of the captured iris images with a new representation of the texture, which brought together the advantages of vocabulary tree and local constraint line coding, resulting in further performance improvement over the previous one. In 2020, Bill Zeng regarded the iris recognition task as an iris classification task, and explored the effectiveness of various strategies on iris classification. In 2020, as the Belt One Road Policy is deeply implemented, Chinese iris vendors with independent intellectual property rights start to export iris technologies and solutions, and become the main suppliers for foreign iris universal registration programs.2021, Ding tong designs a multi-connected residual network can obtain feature maps of different scales in training, realizing multi-dimensional extraction of iris features.

Nowadays, deep learning algorithms are also different from traditional algorithms. In iris recognition, traditional algorithms still have certain dilemmas, in the use of traditional iris recognition algorithms, the need for the user to take the initiative to cooperate with a very high degree, requiring the user to follow the instructions for recognition; in the process of using the user experience is very poor. But deep learning has a different solution, compared to traditional feature recognition algorithms, deep learning methods in the premise of improving the recognition accuracy, but also improves the model of the image noise of the interference and resistance to the ability as well as the ability to generalize. This deep learning technique is data-driven, allowing the iris recognition system to be less demanding on image quality, than traditional algorithms. In the process of recognition, by adding different angles of eye posture and other changes, so that the system can recognize the iris features in different states, to ensure the system recognition efficiency, but also to improve the user experience.

In recent years, along with the continuous growth of computing power in China, deep learning has also been rapidly developed in the trend of the times, especially in the field of biometric identification systems, for example, the accuracy rate of face recognition technology based on deep learning has far exceeded that of human beings themselves.

III. MODEL AND METHOD

A. Iris

The iris is a part of the human eye, a flat, circular membrane located in the middle layer of the eye wall, between the cornea and the lens, visible through the cornea, commonly known as the "black eye". There is a small round hole in the center, called the pupil, from which light enters the eye. The iris is composed mainly of connective tissue containing pigment, blood vessels, and smooth muscle. The color of the iris varies depending on the amount and distribution of the pigment, and is generally black, blue, gray, and brown. Individual irises are biologically distinct and can therefore be used as an identifier.
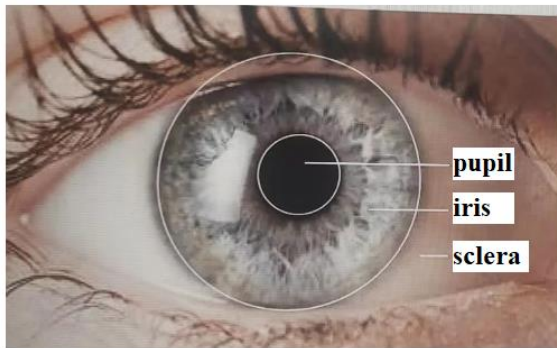

Figure. 1. The human eye

A complete iris recognition system consists of an acquisition device for collecting iris images and a recognition algorithm for extracting iris texture features. The iris image is first acquired by a high-precision iris capturing device, next the collected iris image samples are preprocessed, then the preprocessed iris image is feature extracted, followed by encoding the extracted texture features of the iris, and finally the features are saved in a database for subsequent recognition control.

B. Iris Recognition Key Technology

The acquisition of iris images is crucial because the image quality directly determines the accuracy of the recognition. The human iris and pupil are very close to a circle, and the iris is a region enclosed by the outer boundary of the pupil and the inner boundary of the sclera, which is a relatively small target, so a lot of work needs to be invested in the iris image acquisition part of the iris recognition research as well. The earlier algorithm used for iris image recognition is LMD and the recognition process is shown in Fig. 2.
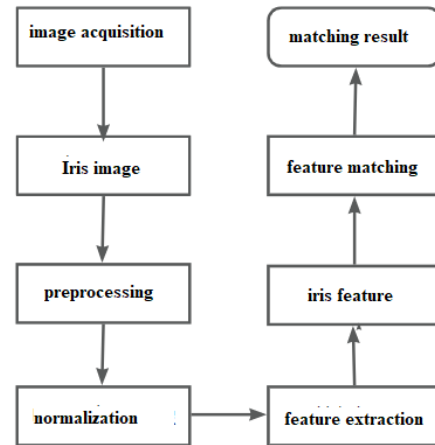
Figure. 2. Flowchart of iris recognition

C. Data sets

The more commonly used iris libraries in iris recognition related algorithms and systems are CASIA, UBIRIS, JLU iris library, IITD iris dataset, and MMU database. Among them, CASIA iris database is a free iris database provided by the Institute of Automation of Chinese Academy of Sciences (IAAS), which is acquired by the remote multimodal biometric feature acquisition and recognition system (LMBS) independently researched and developed by CASIA, and this device can capture images from a distance of 3 meters, and it is also one of the main databases applied to iris research in the world at the present time.

So far, the CASIA iris database consists of four versions, i.e., CASIA-V1~CASIAI-V4. The fourth version, CASIA-V4, was selected for this study.

CASIA-V4 contains a total of 54,601 iris images from more than 1,800 real people and more than 1,000 virtual people. All images are 8-bit grayscale images captured under near-infrared light and saved in JPEG format. CASIA Database Figure 3 shows two example iris images in CASIA-V4.

| (a)CASIA-Iris-Thousand | (b)CASIA-Iris-Syn |

Figure. 3.   Example of two iris images

D. Modeling Principles

The LMD model is a recognition algorithm that centralizes preprocessing, feature extraction, model training, and recognition in a single unit, and traditional LMD algorithms will show good performance on small datasets.

It has good recognition rate in iris recognition, which decreases in poor lighting, blurred images and too much test data. For this reason, the continuous improvement of the LMD method, named PCHIP-LMD, the flow of the algorithm is shown in Fig. 4, using this algorithm ensures the continuity and smoothness of the polynomial derivatives coming at each point, and improves its robustness and conformality.
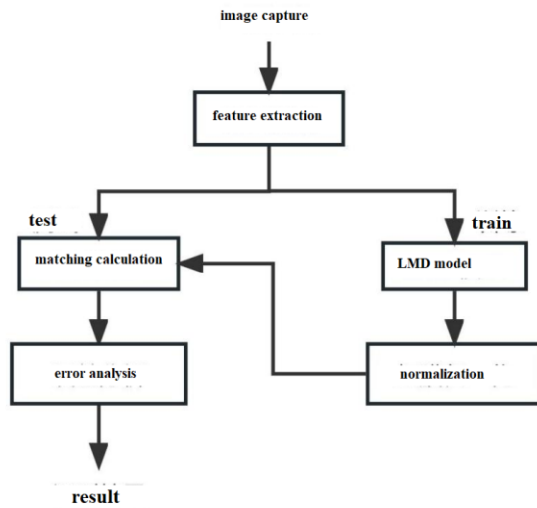

Figure. 4.   Flow of LMD improvement algorithm

Let there be a sequence of nodes ($x_i, i = 0, 1, 2, ..., n$) on the interval $[a, b]$, $a = x_0 < x_1 < ... < x_n = b$, whose corresponding function is y_i , $\int f'(x_i) = m_i, h_k = x_{k+1} - x_k, h = \max h_k$.

The segmented cubic interpolation function $I_h(x)$ satisfies.

$$I_h(x) \in [\alpha, \beta] \tag{1}$$

On any small interval $[x_{k+1}, x_k](k = 0, 1, ..., n-1)$, $I_h(x)$ is a cubic polynomial.

Satisfy the interpolation conditions $I'_h(x_i) = m_i$, $i = 0, 1, 2, ..., n$.

In the interval $x \in [x_{k+1}, x_k]$, the PCHIP function expression is

$$I_h(x) = y_i + c_{k,3}(x - x_k)^3 + c_{K,2}(x - x_k)^2 + (x - x_k)^3 \tag{2}$$

Among them,

$$\begin{cases} c_{k,1} = m_i \\ c_{k,2} = (\frac{3}{h_k}(y_{k+1} - y_k) - 2m_k - m_{k-1,1})\frac{1}{h_k} \\ c_{k,3} = (m_{k+1} + m_k - 2\frac{y_{k+1} - y_k}{h_k})\frac{1}{h_k^2} \\ x \in [x_k, x_{k+1}], (k = 0, 1, ..., n-1) \\ h_k = x_{k+1} - x_k, m_k = f'(x_k) \end{cases} \tag{3}$$

It decomposes the image into different frequency sub bands to extract the structural and textural information of the image. The PCHIP-LMD algorithm combines PCHIP interpolation and LMD decomposition, which can be used for image processing tasks such as image enhancement, denoising, and image synthesis.

PCHIP-LMD (Piecewise Cubic Hermite Interpolating Polynomial-Local Median Decomposition) algorithm is an algorithm used in the field of image processing and computer vision. The core idea of the algorithm is to combine PCHIP interpolation and LMD decomposition to achieve the tasks of image enhancement, denoising, and synthesis. PCHIP-LMD guarantees that the interpolated curves between two neighboring points are monotonic, which means that the curves will not have strange fluctuations or discontinuous parts.

LMD is an image decomposition technique that decomposes the input image into multiple frequency sub bands. This decomposition can be used to extract image structure and texture information for better handling and utilization of image features in subsequent processing.

In this study PCHIP-LMD algorithm combines two techniques PCHIP interpolation and LMD decomposition. First, the input image is smoothed and interpolated by PCHIP interpolation to obtain a smooth image representation. Then, LMD decomposition is applied to this smoothed image to decompose it into different frequency sub bands. The structure or texture of the image can be enhanced and the noise of the image can be reduced by adjusting the enhancement parameters of the different frequency sub bands. In this study, PCHIP-LMD is used for better feature image extraction, enhancing the robustness of the image and ensuring that the interpolation curve is smooth and monotonic between neighboring data points. The accuracy of the image matching results is improved.

E. Faster R-CNN

The Faster R-CNN model integrates feature extraction, frame extraction, frame regression and classification into one network, which greatly improves the overall performance of target detection. Compared with the traditional iris localization methods, the Faster R-CNN model for iris localization not only improves the accuracy of iris localization, but also adapts better to different lighting conditions and image quality.

The basic flow of Faster R-CNN model is shown in Fig. 5. Firstly, the input to the detection sample image is used to extract features by CNN mentioning the input image, and then several proposal windows are generated by RPN (Region Proposal Network) and the proposal windows are mapped to the last layer of CNN to convolve the feature maps. Finally, a fixed-size feature map is generated for each ROI through the ROI pooling layer, and the classification probability and edge regression are jointly trained.
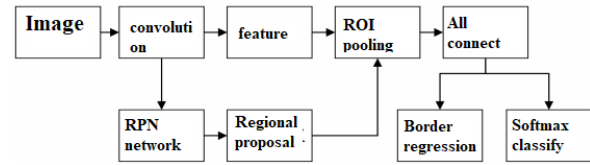
Figure. 5. Basic flow of Faster R-CNN model

When applying the Faster R-CNN model to iris detection, the training data need to be selected for labeling first. In order to better identify and locate the iris region in the test set, when labeling the iris images in the training set, the information of other objects in the labeling box should be minimized. When labeling, the outer boundary of the iris is labeled with a circle The ROI pooling layer labels the boundary of the pupil with a circle, and the outer rectangle of the pupil labeling circle is also labeled.

Combining the iris localization obtained from Faster R-CNN model detection and traditional iris localization and region segmentation algorithms can improve the localization and segmentation accuracy without decreasing the detection speed, which better solves the contradiction between accuracy and speed.
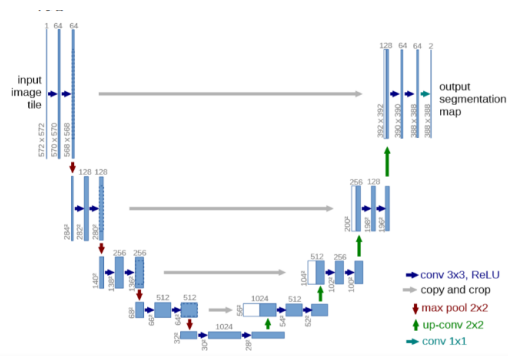
Figure. 6. U-net network structure

The U-net network structure is shown in Fig. 6. It is built using a U-shaped structure, and the hierarchy uses an encoding-decoding pattern, where the encoding part reduces the size while aggregating the image features, and the decoding part enlarges the size while mapping the image features. The encoding module aggregates the iris feature information through layer-by-layer convolution, which includes important feature information such as texture and pixel relationships. The decoding module gradually reduces the iris

feature map to the original image size through up-sampling while mapping the iris semantic information to the corresponding locations in the original image.

Meanwhile, Hamming distance is used as a comparison method for error analysis by setting J and K as the feature codes of two different iris images, respectively:

$$HD = \frac{1}{N}\sum_{i=1}^{N} J_i \oplus K_i \qquad (4)$$

Where N is the total number of bits encoded in the image and $\oplus$ is a different-or-relative operation, which is 0 when J and K are the same and 1 when they are different. The encoding of the same iris is similar with a small Hamming distance, while the encoding of the different iris is very different with a large Hamming distance, which can be used as a criterion for distinguishing whether the two iris images are the same iris or not. The experiment is set that if the Hamming calculated value is less than or equal to 0.2, then the scanned image matches with the iris that already exists in the database, and if the Hamming calculated value is greater than 0.2, then the scanned image cannot be matched with the iris that already exists in the database.

F. Evaluation indicators

On the basis of the whole iris recognition system, in order to determine the recognition performance of different recognition algorithms, it is necessary to determine the corresponding judgment standard, in the whole process of experimental analysis, the evaluation index will have an impact on the performance of the algorithm. The evaluation index of iris recognition algorithm is Correct Recognition Rate.

Correct Recognition Rate (CRR) indicates that a higher CRR during a single iris recognition indicates that the system is more capable of recognizing and making accurate judgments about the attribution of iris information. The correct recognition rate is calculated as shown in Equation X, which represents the ratio of the number of correctly recognized samples to the total number

of samples in a recognition task using a classifier. The correct recognition rate is a good response to the accuracy of the recognition algorithm and a good measure of whether the extracted features can accurately represent the iris information.

$$CRR = \frac{N_{correct}}{N} \times 100\% \qquad (5)$$

IV. EXPERIMENT AND ANALYZE

The software used in this study includes Python 3.7.13 and Matlab R2016a, the operating system used is Windows 10 Professional, and the hardware configuration of the computer is NVIDIA GeForce RTX 2060 graphics card, Intel(R) Core(TM) i5-10400F processor, 16GB of RAM and 6GB of discrete graphics memory. Intel(R) Core(TM) i5-10400F processor, 16GB of RAM and 6GB of discrete video memory.

In this study the advantages and disadvantages of two languages Python and MATLAB for iris recognition are compared along with the tools and libraries they provide.

Python is an interpreted language with rich scientific computing, deep learning and image processing libraries such as PyTorch, Keras and OpenCV. These libraries provide efficient data processing and analysis capabilities, and can help this study to achieve tasks such as training and optimization of iris recognition models, as well as image processing and feature extraction. At the same time, Python has GPU acceleration support, which can greatly improve the training and inference speed of deep learning models and help to improve the real-time performance of iris recognition. Python also has rich community support and open source code, which can help researchers to quickly develop and debug deep learning models. Python is used to implement the R-CNN model algorithm.

In contrast, Matlab is a specialized language for scientific and engineering computation, with powerful mathematical computation and matrix operations, as well as rich toolboxes, such as the image processing toolbox, the signal processing toolbox and the control system toolbox. These

toolboxes can easily implement a variety of scientific computing and engineering computing tasks, and can help this study to implement tasks such as segmentation, denoising, and enhancement of iris images. Matlab also provides some powerful visualization tools that can help this study to better understand and analyze the data. In addition, Matlab's syntax is simple and intuitive, easy to learn and use, and easier for researchers who do not have a programming background. The LMD model is implemented on Matlab.

A. Experimental data set

All the models in this paper are validated and compared uniformly on the CASIA-Iris-Syn dataset and the CASIA-Iris-Thousand dataset, where the CASIA-Iris-Syn dataset contains a total of 200 people, each of whom contains an iris image of the left and right eye, totaling 400 images, and the dataset is divided according to the ratio of 6:1. The CASIA-Iris-Thousand dataset contains a total of 50 people, in which each person contains 10 images of the left and right eyes, totaling 500 images, and the dataset is also divided according to the ratio of 6:1, and only the left eye image is used for Python based training and testing, and the dataset is divided as shown in Table 1.

TABLE I.　COMPARISON OF THE CONTENT OF THE TWO DATASETS

	Training Set	Test Set	Training Set	Test Set
Number of categories	50	8	45	6
Number of images/classes	20	20	10	10
Total number of images	342	58	342	58

The research in this paper aims to investigate the face recognition technology based on iris images. For this purpose, the iris images of the left and right eyes of 150 people, totaling 400 images, were randomly selected from CASIA V4.0 iris library as test samples for this experiment. On this basis, the experiment utilized the following research steps, the

First, this experiment normalizes the original captured iris images to obtain the feature maps. Next, the feature map is input into the convolutional neural network as the original

sample for training and testing. Finally, a threshold value of 0.200 is set in the experiment, and the recognition is performed according to this threshold value, and the recognition results are obtained as shown in Table 2 and Figure7.

TABLE II. ANALYSIS OF EXPERIMENTAL DATA

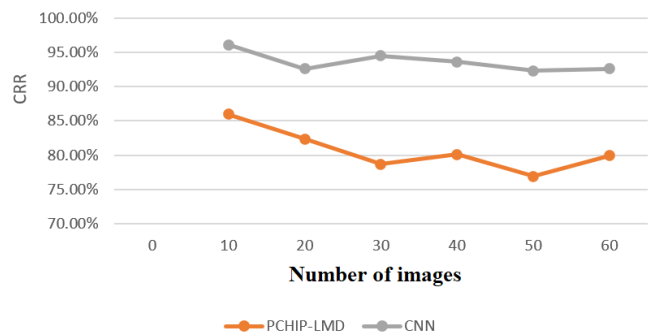| Test Methods	Training Set	Test Set	Number Of Correct Identifications	Recognition Rate % (Crr)
CNN	400	60	56	92
LMD	400	60	47	78

Figure. 7. CNN recognition result rate

Based on the analysis of the above results, it is concluded that the CNN algorithm yields a relatively high recognition rate of more than 90%, while the traditional LMD algorithm has a lower recognition rate of less than 80%.

B. Visualization of experimental results

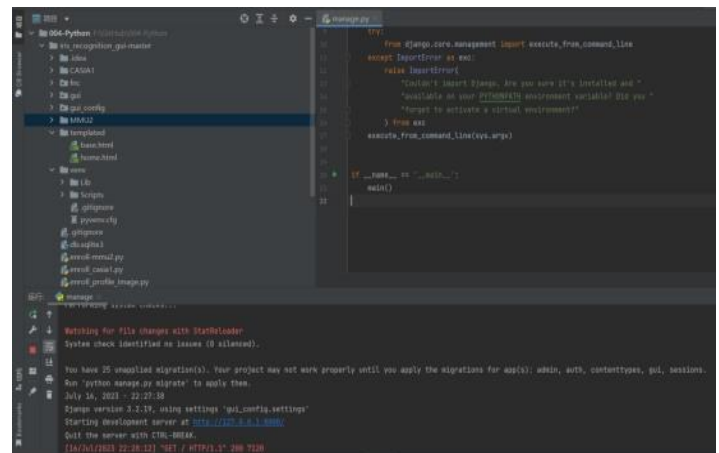The running code schematic is shown in Figure 8.

Figure. 8. Code Run Diagram

Figure 8 shows the R-CNN model implementation is based on Python3.7.13 Djanjo framework to realize the front-end interface, in the running results are displayed in the terminal interface will generate the local server address. The two html files in the middle are the iris interface administrator registration diagram and iris recognition system front-end interface diagram. The recognition function implements the iris verification function of an iris recognition system. The system is able to verify the input iris image by extracting iris features and performing iris matching to determine whether it matches the enrolled iris sample. First, the main function is set up, which obtains the path of the input image, the path of the template directory and the matching threshold from the command line parameters, and extracts features from the input iris image by calling the feature extraction related function to obtain its iris features. Then the matching function is called to match the extracted iris features with the registered iris samples. Finally, according to the matching result, the corresponding information is returned.
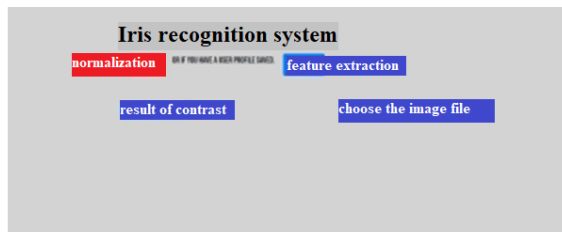
Figure. 9.   Front-end page display

Figure 9 shows the front-end page display diagram with five visualization functions, which normalize the collected images, feature extract the iris image at different angles, and extract different iris feature vectors for subsequent iris matching and recognition. Comparison of database images, the processed iris images are compared with those in the database, and the matching results are shown in Fig. 10, if there is a matching image in the database, it shows successful recognition. The database is added, you can click to select the file to add the un-deposited figure iris image, and the addition process is shown in Figure 11.
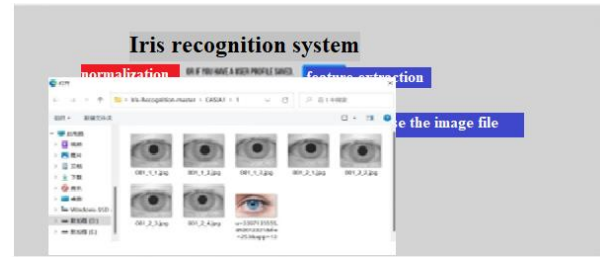
Figure. 10. Selecting the iris image to be matched against the image in the database
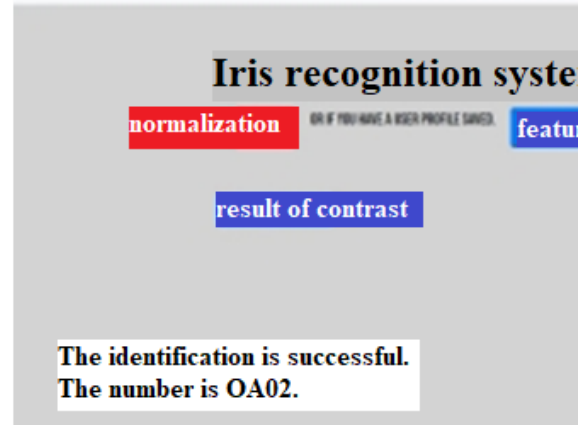
Figure. 11. Image matching demonstration

C. Matlab-based experimental analysis
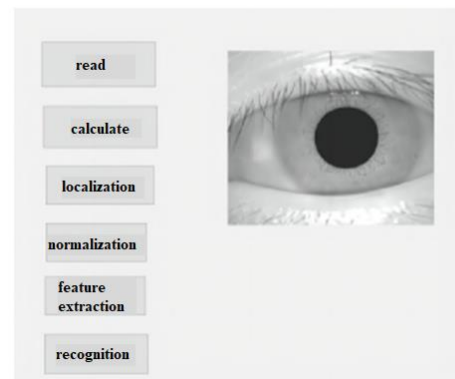
Figure. 12. Interface display

The experiment of LMD algorithm is based on Matlab R2016a for iris localization, extraction and recognition. Fig. 12 shows the runtime interface presentation, which contains the option of reading the image, selecting the image that you want to compare, and the image operation option, respectively. Canny edge detection algorithm is used for experimental implementation. The Matlab programming language was used to detect the

edges of the image by combining techniques such as Gaussian filtering (to remove noise), Sobel operator (to compute the gradient of the image). Moreover, different parameter settings are experimented and analyzed in the experiment to get the best edge detection results.

The result of the operation is shown in Fig. 13. The experiment implements an iris localization function. It obtains the positional information of the iris and pupil by reading an eye image, segmenting it into iris regions, and then drawing a localization circle on the image.

(a) canny edge extraction   (b) localizing iris image
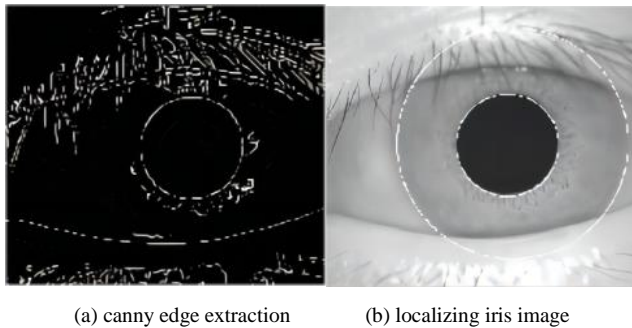
Figure. 13. Edge extraction to obtain iris

D. Localization

In terms of normalization process, this experiment consists of saving the normalized iris image and the noise array. Normalization removes distortion and rotation from the image by converting the original iris image into polar coordinate representation. The normalized image is displayed in the image control and saved in picture format. The noise array is also saved for subsequent processing. This step helps to improve the accuracy and stability of iris recognition system. The normalized image is shown in Fig. 14(a). Subsequently, the normalized iris image is subjected to feature extraction and coding method. The image is first processed using Gabor filtering to obtain a set of results. By processing the results, a biometric feature template consisting of binary values is obtained. In order to ensure the accuracy of the template, pixels with small amplitude are labeled as noise parts to reduce their effect on the template. With the method proposed in this paper, feature extraction and encoding of iris images can be performed accurately. The obtained feature extraction map is shown in Fig. 14(b)

(a) Normalized image   (b) Image after feature extraction
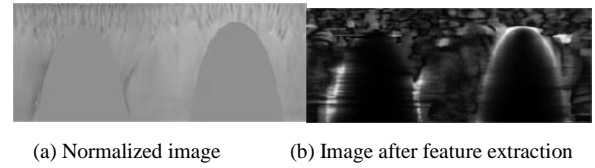
Figure. 14. Image after normalization and feature extraction
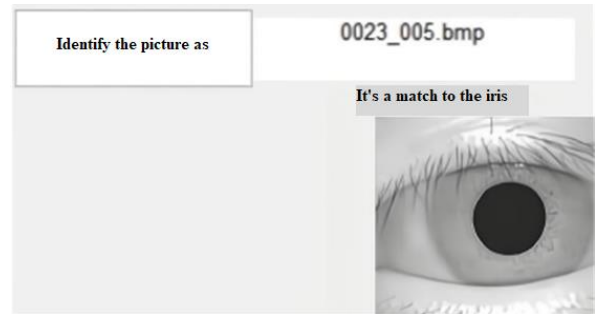
Figure. 15. Matching successful image

Figure 15 presents the interface of successful matching. The design of this experiment not only obtains good experimental results, but also provides a convenient user interface.

In this study, two languages, Python and MATLAB, are used to implement the iris recognition system, giving full play to their advantages and achieving good experimental results. Both Python and MATLAB have their own advantages and applicable scenarios. If deep learning model training and optimization are needed, or large-scale data processing and analysis are needed, Python is a better choice. If you need to perform scientific and engineering computing tasks, and need to visualize and analyze data, Matlab is also a good choice. Of course, the choice of language should also take into account the personal experience and proficiency of the researcher, as well as the specific needs of the project.

In research work, choosing the right language and tools is important for the development and implementation of iris recognition systems. Both Python and MATLAB have their own advantages and can provide efficient support for the development and implementation of iris recognition systems. By fully utilizing their advantages, the accuracy and real-time performance of iris recognition can be improved to better meet the practical needs.

In terms of modeling, the data performance of the LMD model is not as good as the R-CNN model, but the burden of its model, the complexity of its algorithm is relatively low, and appropriate algorithms and implementation paths are selected under different requirements.

V. CONCLUSIONS

Iris recognition is one of the most convenient and accurate of the current bio-information recognition technology; this paper combines the deep learning and applies the cutting-edge technology of deep learning to iris recognition. This paper mainly combines the convolutional neural network technology of deep learning with iris feature extraction and classification in iris recognition system, and uses this as the basis to introduce iris recognition based on CNN model. The current research status related to iris recognition technology at home and abroad clarifies the current research content and subject needs, and determines the research program of the subject. Combined with the iris recognition in recent years, the iris region is used as the input of the model based on the convolutional neural network model, and at the same time has a high recognition rate. It further promotes the development of iris recognition technology related fields. Iris has more advantages than others in terms of security and anti-counterfeiting, and the development prospect is getting broader and broader, so this research has great significance.

In this paper, we try to use the model generated by convolutional neural network in deep learning in iris recognition, and although we have achieved some results, there are still some deficiencies and shortcomings. For iris preprocessing, the traditional grayscale algorithm is still used for preprocessing, which may increase the computational difficulty. Therefore, future research can explore more advanced iris preprocessing techniques to improve the accuracy and real-time performance of iris recognition.

In addition, this paper selected the existing database CASIA v4.0 with a small amount of selected data and generated simulated iris images that can be used for network training. However, this may lead to data errors that affect the accuracy

and generalization ability of the iris recognition model. Therefore, future research can continue to collect more iris datasets and explore more data enhancement techniques to improve the generalization ability and robustness of iris recognition models.

Future research can explore more deep learning models and algorithms to improve the accuracy and real-time performance of iris recognition. In addition, more iris image preprocessing techniques can be explored to improve the robustness and generalization ability of iris recognition models. Through continuous improvement and optimization, iris recognition technology will have an advantage over other technologies in terms of security and anti-counterfeiting, promoting the development of related fields.

REFERENCES

[1] Mach. IntelH. Proenca, S. Filipe, R. Santos, et al, The UBIRIS.v2: A database of visible wavelength iris images captured on-the-move and at-a- distance[J]. IEEE Trans. Pattern Anal, 2010, 32(8):1529-1535.

[2] Fawzi A, Samulowitz H, Turaga D, et al. Adaptive data augmentation for image classification[C].2016 IEEE International Conference on Image Processing (ICIP). IEEE,2016.

[3] Carl M , Goldberg R .Iris biometrics: from segmentation to template security[J].Computing reviews, 2013, 54(11):672-673.

[4] Hu J, Shen L, Sun G. Squeeze-and-excitation networks; proceedings of the Proceedings of the IEEE conference on computer vision and pattern recognition, F, [C] Salt Lake City, UT, USA 2018.

[5] Ibrahim M T, Khan T M, Khan S A, et al. Iris localization using local histogram and other image statistics[J]. Optics & Lasers in Engineering, 2012, 50(5):645-654.

[6] Chen Y, Wu C, Wang Y. T-center: a novel feature extraction approach towards large-scale iris recognition [J]. IEEE Access, 2020, 8: 32365-32375.

[7] Leonard Flom, Aran Safir. Iris recognition system [P]. United States Patent No. 46413491987.

[8] Liu M, Zhou Z, Shang P, et al. Fuzzified image enhancement for deep learning in iris recognition [J]. IEEE Transactions on Fuzzy Systems, 2019, 28(1): 92-9.

[9] Zhao Z, Kumar A. Towards more accurate iris recognition using deeply learned spatially corresponding features; proceedings of the Proceedings

of the IEEE international conference on computer vision, F, [C] The Hong Kong Polytechnic University 2017.

[10] Nguyen K, Fookes C, Ross A, et al. Iris recognition with off-the-shelf CNN features: a deep learning perspective [J]. IEEE Access, 2017, 6: 18848-55.

[11] Lei Songze, Zhang Boxing, Wang Yanhong, et al. Object Recognition using Non-negative Matrix Factorization with Sparseness Constraint and Neural Network. information [J], 2019, 10(37):1-17(EI).

[12] Othman N, Dorizzi B, Garcia-Salicetti S. OSIRIS: An open source iris recognition software [J]. Pattern Recognition Letters, 2016, 82: 124-31.

[13] Raja K B , Raghavendra R , Vemuri V K , et al. Smartphone based visible iris recognition using deep sparse filtering[J]. Pattern Recognition Letters, 2015, 57:33-42.

[14] Mengjia Wang, Research on iris recognition algorithm based on deep learning [D]. Jilin University, 2022.

[15] Qi Zhao, Research on Iris Recognition Algorithm Based on Deep Learning [D]. Xidian University, 2020.

[16] Liu N, Zhang M, Li H, et al. Deepiris: Learning pairwise filter bank for heterogeneous iris verification [J]. Pattern Recognition Letters, 2016, 82: 154-61.

[17] Alinia Lat R, Danishvar S, Heravi H, et al. Boosting Iris Recognition by Margin-Based Loss Functions [J]. Algorithms, 2022, 15(4): 118.

[18] Roy K, Bhattacharya P Iris recognition with support vector machines[J]. Lecture Notes in Science. 2006, 3832: 486-492.

[19] Gangwar A, Joshi A. DeepIrisNet: deep iris representation with applications in iris recognition and cross-sensor iris recognition; proceedings of the 2016 IEEE international conference on image processing (ICIP), F, [C]. IEEE 2016.

Application of PanDict System Based on EPSEIRV and SI3R Models in Epidemic Forecasting and Healthcare Resource Planning

Bohan Liu

Phillips Exeter Academy

Exeter, USA 03833

E-mail: lbh833@126.com

Abstract—Global epidemics, such as COVID-19, have had a significant impact on almost all countries in terms of economy, hospitalization, lifestyle, and other aspects. Part of the reason is their high infectivity, but more importantly, due to the speed of virus transmission, the probability of new varieties appearing, and the conditions under which they appear, we cannot predict, making it a major challenge for us to arrange resources reasonably when the virus appears. Due to the inability of previous epidemic models to solve these three most important problems, we have developed the PanDict system, which can help solve all three basic problems discussed above. For a detailed explanation, our model consists of three key components that address the above issues: predicting the spread of new viruses in each local community and using our newly designed EPSEIRV model to calculate its R0 value; Creating and using the SI3R model to simulate variant competition; Predict the insufficient hospitalization in each state and use our IHOV model to generate a visual representation of the predicted demand. Compared to other vague and incorrect predictions/models, our EPSEIRV model accurately predicted the transmission of the severe acute respiratory syndrome coronavirus type 2 Omicron variant in the United States and South Africa before reaching its peak. In addition, the high infection rate of viruses allows them to spread widely among the population before vaccines are fully developed. As a result, the number of patients will inevitably surge, which will make hospitals overwhelmed, making the IHOV model particularly necessary. The PanDict model can quickly and accurately predict the speed of disease transmission, whether the disease will successfully mutate, and how to arrange hospitalization resources to most effectively alleviate pain. In addition, the PanDict model enables the hospitalization system to be more prepared for the upcoming surge in patients, which will greatly reduce excess deaths and insufficient hospitalization.

I. INTRODUCTION

Pandemics across the globe have long-lasting, profound impacts on all countries and on each individual. For instance, COVID-19 has crushed hospitalization systems worldwide and caused more than 6.3 million cumulative deaths, while H1N1 directly resulted in about 575400 deaths globally during its first year of circulation [2][3]. However, death and suffering are only the superficial consequences of a circulating epidemic, as its harmful effects permeate almost all aspects of people's lives. The International Monetary Fund (IMF) estimates that from 2019 to 2020, the global median GDP fell by 3.9%, the worst recession since the Great Depression, demonstrating an imperative need for designing a system that mitigates the harm of epidemics [1]. The unprecedented impact of COVID-19 can, in part, be attributed to the inability of previous studies to obtain essential information about a newly emerged virus. Without the support of that basic information, policymakers failed to establish practical measures against the virus, and individuals were misinformed or simply not informed, causing severe public concerns. The problematic areas are as follows.

For the Transmission forecast model, previous work has struggled to produce reliable transmission predictions because of some inherent flaws of the SEIRV model [4]. Even some authoritative organizations, including the CDC,

still cannot obtain the accurate value of the transmission coefficient (R0) of Omicron [5], let alone predict the growth of the epidemic. In addition, Dr. Fauci, one of the most trusted epidemiologists, has unexpectedly inaccurate and uninformative predictions in many well-known media, such as CNN [6].

For the Variant Prediction model, little to no work can be found about future variant prediction when confronted with a novel disease. For example, when the first wave of Omicron was close to an end, experts still had no clue what future variants would look like and under what conditions they could emerge [7]. Moreover, Dr. David Aronoff, an infectious disease expert and chair of the Department of Medicine at Indiana University School of Medicine, even said, "We really don't know if there's going to be another variant that may create a lot of havoc [8].

For hospitalization resources, highly contagious pandemics invariably threaten hospitalization systems, as the number of patients can grow exponentially in merely a few days. Omicron, for instance, caused substantial staffing and resource shortages in one-fourth of all US hospitals, resulting in delays in elective surgeries [9]. While most hospitals in the US had excess resources and staff, due to the rapid, exponential increase in the demand for hospitalization in certain states, officials had no other choice than to deploy the National Guard to "provide direct support to hospitals, care centers, and other medical facilities;" some even forced infected employees to keep working, putting patients at risk [10].

Realizing the urgent need to minimize the damage of global epidemics, this study devised PanDict (Pandemic PreDiction, a computer system that uses the EPSEIRV model, the SI3R model, and the IHOV model to produce accurate projections of future epidemic situations and to address the three pressing issues above with each model tackling one of those problems. The system provides its users with a reliable transmission forecast, an informative variant prediction, and a projection of the demand for hospitalization resources. PanDict allows its users to input some of the most basic parameters of a novel disease

and immediately receive the essential information needed to minimize its damage. Some detailed explanations of each part are as follows.

Realizing the urgent need to minimize the damage of global epidemics, this study devised PanDict (Pandemic PreDiction, a computer system that uses the EPSEIRV model, the SI3R model, and the IHOV model to produce accurate projections of future epidemic situations and to address the three pressing issues above with each model tackling one of those problems. The system provides its users with a reliable transmission forecast, an informative variant prediction, and a projection of the demand for hospitalization resources. PanDict allows its users to input some of the most basic parameters of a novel disease and immediately receive the essential information needed to minimize its damage. Some detailed explanations of each part are as follows.

First, to develop a reliable transmission forecast, the author formulated the EPSEIRV model. The original SEIRV model contains a variable, α, that can't be determined experimentally, for it contains no physical meaning. Hence, it has a preset value (average of past diseases), which skews information from the data and exacerbates the model's accuracy. Thus, the author replaced those variables with quantifiable variables that introduce population density and time of exposure into the system, allowing the system to conduct simulations in each local community and obtain accurate results. This study tested it with real-life data in South Africa and the United States, and our prediction of the infected population fits almost perfectly with the actual infected curve. This study yielded an R0 value around 18.9 for Omicron, substantially higher than the conclusion of previous studies, "above 7.05". The author published our findings on medium.com around mid-January, attached here. Secondly, to answer, "Will new variants emerge and how?" the author created the SI3R model, which simulates the competition between a mutant and a resident. After implementing it in the case of Omicron, the author concluded that for a new variant to emerge, it has to overcome the public's immunity against Omicron. Otherwise, it would die out almost immediately. The theoretical foundation regarding

super-infection and double-infection of the SI3R model references an article from The American Naturalist [11]. The article stopped at discussing variant evolution on the conceptual level, while the SI3R model allows for simulating competitions based on real-life data. Finally, the author devised the IHOV model to project the demand for hospitalization, extending an uncompleted Brown project [12]. The project initiated by Brown School of Public Health provides current hospitalization data, including the number of available beds, occupation rate, etc. However, that project simply listed some possible cases based on guessed situations, so it serves no forewarning purposes to the public. In contrast, EPSEIRV models the infected population of each state as a function of time produced and inputs those projections to the IHOV model, allowing us to predict and show exactly where, when, and how much, for example, beds are needed.

As far as our knowledge goes, the author was the first to develop an accurate simulation of the spread of Omicron. In a nutshell, our system serves two purposes. Firstly, it informs individuals, corporations, and the government about the future trends of newly emerged viruses. This helps reduce public concerns about the potential impact of pandemics and allows the health sector to better prepare for the emergence of new variants. Secondly, it assists hospitals in efficiently allocating resources, thereby minimizing unnecessary suffering and deaths. Currently, the author has only completed the IHOV model for the New England region. However, future work can easily expand the system's coverage to encompass the entire United States or even the entire globe.

II. PREVIOUS STUDIES

A. Transmission Forecast

Almost all mathematics-based disease transmission models are variants of the SIR model. This section explains the SIR model and presents some popular variations of it [4]. The SIR model separates the population into three compartments: Susceptible, Infectious, and Removed. Everyone who has neither obtained immunity against the disease nor been infected with the disease is considered Susceptible; everyone who is infected and can infect others is regarded to be Infectious, and everyone who is immune to the disease is defined in the Removed category.

The SEIRV model implemented two additional compartments to the SIR model, Exposed and vacant. The original Infectious group in the SIR model is elaborated into two, taking patients' latent period into account; the Exposed group contains all who have been infected but are not yet infectious. At the same time, the Infectious group includes those who were infected and have become infectious. The Vaccinated compartment comprises of people who have been vaccinated but have not yet gained immunity (those who have gained immunity are considered Removed). A more complete review of the SEIRV model is provided in the Method section.

In short, the SEIRV model has an exponent on the infection expression, α, which has no physical meaning, so it can't be determined with precision at all. It is pre-set to be around 1.2, a value that works best for most kinds of diseases. Thus, with α predetermined, the model only contains one degree of freedom: the contagiousness measure, β, which significantly undermines its accuracy. In contrast, the author improved the model by discarding the guessed variables and introducing two additional parameters derived from manipulating probability equations of encounters and the fraction of time people spend interacting with others. This improvement allowed us to accurately model the spread of the Omicron in January.

B. Variant Prediction

Most researchers use mathematical or biological approaches to predict the emergence of future variants of a disease. This section explores the deficiencies of each approach and how our system resolves this problem. The biological approach to predicting future variants requires an extensive amount of experimentation and often takes a large amount of time before attaining adequate information. In the case of Omicron, the infectious disease expert, Dr. David Aronoff, who attempted to use biological methods to predict future variant emergence, said after the surge of

Omicron that they still "really don't know if there's going to be another variant that may create a lot of havoc."8 This more mathematics-based article by Minus Van Baalen and Maurice Sabelis explored the competition between the resident strand and a mutant of a virus [11]. The study also explained the impact of that competition on the evolution of the virulence, as well as the infectiousness, of a disease. However, the study stopped on the theoretical level and did not provide a usable model for predicting variants. Thus, the author devised the SI3R model to simulate the competition between the resident strand and a hypothetical mutant of a virus to explore the conditions under which new variants could emerge.

C. Demand for Hospitalization

Before our project, the Brown School of Public Health was the only group that attempted to calculate the projected demand for hospitalization resources [12]. However, their study did not implement a disease transmission model that could estimate the spread of the disease; instead, they guessed the infected population and time and then calculated future demand according to the guesses. Thus, it has no specificity to the disease and will not be instructive to policymakers who need predictions of exactly where and when hospitals will hit their capacity to prepare for the exponential growth of the number of patients.

III.   METHOD

A. System Framework

The system aims to help minimize the damage of a newly emerged epidemic. It consists of three essential modules, each addressing one of the previous studies' problems.
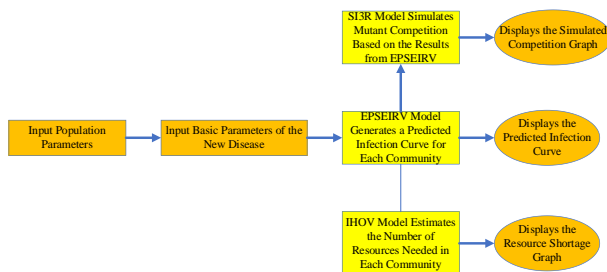
Figure 1.   System Usage Flowchart

As shown in Figure 1, the process of the system is as follows. The user first inputs the population statistics of the target country and enters the date of the first case in each local community. The basic parameters of the newly emerged disease are also required. Those mainly include the incubation period, infectious period, and vaccine efficacy. Subsequently, the system produces and displays an accurate prediction of the spread of the new virus according to those parameters. With the projected infection curve, the second module will test the condition and probability of the emergence of a new variant using the SI3R model. Lastly, the system uses the projected infection curve to calculate the demand for health resources in each individual county of the target country and displays the projected data on a map (you can download the actual numbers as well).

IV.   TRANSMISSION FORECAST – THE EPSEIRV MODEL

A. Review of the SEIRV Model

$$\frac{dS}{dt} = -\beta I \left(\frac{S}{N} \right)^{\alpha} - \psi \varepsilon S \qquad (1)$$

$$\frac{dE}{dt} = \beta I \left(\frac{S}{N} \right)^{\alpha} + \beta I \left(\frac{V}{N} \right)^{\alpha} - \sigma E \qquad (2)$$

$$\frac{dI}{dt} = \sigma E - \gamma I \qquad (3)$$

$$\frac{dR}{dt} = \gamma I + \iota V \qquad (4)$$

$$\frac{dV}{dt} = \psi \varepsilon S - \beta I \left(\frac{V}{N} \right)^{\alpha} - \iota V \qquad (5)$$

The SEIRV model is based on the following assumptions:

1) The total population remains constant (new births and deaths have trivial impacts and are not taken into account).

2) Measures against the disease remain unchanged.

3) People's living habits have no drastic changes.

4) The population is relatively homogeneous.

5) An individual can't catch the disease twice.

The exponent α in (1), (2), (5) has no physical meaning and thus cannot be obtained in any way other than estimating with infection data. For most kinds of diseases, the value of α = 1.2 works the best, so it was set to be around 1.2 for novel diseases as well without any other supporting experiment or evidence.

The model has only one degree of freedom (beta) with the exponent alpha predetermined; this lack of specificity significantly reduces its accuracy and robustness. In addition, this model does not account for changes in population density and social distancing. Thus, the author made the following changes to the model.

B. *Determining the Expression for Daily Infection*

This section summarizes the derivation of the daily infection expression.

Assuming that the probability of one person meeting an infectious individual and capturing the disease is λ and that an average person spends μ fraction of their time interacting with others, then the probability of the person catching the disease at all equals to:

$$\mu(1-(1-\lambda)^I) \qquad (6)$$

where I equal to the number of Infectious agents [13]. Because λ represents the probability of meeting one infectious individual and simultaneously receiving the disease, it should be almost infinitesimally small. Since $e = (1+\frac{1}{n})^n$ when n approaches infinity, author can approximate $e = (1-\lambda)^{-\frac{1}{\lambda}}$. Then, author may rearrange the expression as follows:

$$\mu(1-(1-\lambda)^I) = \mu(1-(1-\lambda)^{\frac{1}{\lambda}^{-\lambda I}}) = \mu(1-e^{-\lambda I}) \qquad (7)$$

This change in the expression connects daily infection numbers with population density and exposed time. Exposed time is associated with the model by μ, while this paragraph illustrates the model's connection to population density. Suppose r is the radius of a person's daily activity

range, p is the probability of catching the disease upon encounter, N is the population of the target community, and A is the area. Then, the author can express λ as $p\frac{\pi r^2}{A}$, Substituting A with $\frac{N}{D}$. D represents the population density. Finally, author yield $\lambda = p\frac{\pi r^2 D}{N}$. Showing that the infection coefficient λ is directly proportional to the population density.

C. *Equations of the EPSEIRV Model*

Thus, the system of differential equations in the EPSEIRV model is as follows:

$$\frac{dS}{dt} = -\mu\left(1-e^{-p\frac{\pi r^2 D}{N}I}\right)S - \psi\varepsilon S \qquad (8)$$

$$\frac{dE}{dt} = \mu\left(1-e^{-p\frac{\pi r^2 D}{N}I}\right)(S+V) - \sigma E \qquad (9)$$

$$\frac{dI}{dt} = \sigma E - \gamma I \qquad (10)$$

$$\frac{dR}{dt} = \gamma I + \iota V \qquad (11)$$

$$\frac{dV}{dt} = \psi\varepsilon S - \mu\left(1-e^{-p\frac{\pi r^2 D}{N}I}\right)V - \iota V \qquad (12)$$

S represents the number of people who are susceptible to the disease, E represents the number of people who have caught the disease but are not yet infectious, I represents the number of people who are infectious, R represents the number of people who have gained immunity against the disease, V represents the number of people who are under vaccination but are not fully vaccinated, t represents time in days, ψ represents the proportion of newly vaccinated individuals to the susceptible population, ε represents vaccine efficacy, σ represents the inverse of disease incubation period in days, γ represents the inverse of disease infectious period in days, ι represents the inverse of the time needed to gain immunity fro vaccines in days, p represents the probability of one person

capturing the disease upon encounter with an infectious agent, D represents population density, N represents the number of people in population, r represents the radius of an average person's daily activity range, and finally, μ represents the fraction of time an average person spends interacting with others. μ and p are social parameters in this model, while the rest are basic parameters.

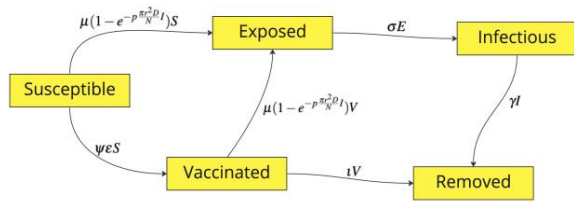The following chart elucidates the changing relationship between each compartment:

Figure 2.   Change between each compartment of the EPSEIRV model summarized in a flowchart.

On day 1, E is set to 1, R is set to the number of people who have received a booster shot before day -14 (14 days prior to the first case), V is set to the number of people who received a booster shot between day -14 and day 0, I is set to 0, and S is set to $N - E - V - R$.

Figure 3.   Comparison between the SEIRV model equations and the EPSEIRV model equations.

V.   DETERMINING PARAMETERS

The author will use the parameter determination process of the Omicron variant of Sars-CoV-2 as an example to demonstrate how each model parameter can be obtained.

A. Basic Parameters of Omicron

According to Centers for Disease Control and Prevention (CDC) investigations, the incubation period of Omicron is approximately three days, and the mean infectious period of Omicron is about 11 days [14]. CDC reports also reveal that the

effectiveness of unboosted vaccines is insufficiently low, and the British Broadcasting Corporation (BBC) claims that the efficiency of booster shots is roughly 80% [15][16]; therefore, the author decided only to include booster shots as an effective type of vaccination. In the United States, the boosted population has an average daily increase of 600,000 (0.18% of the entire population), while in South Africa, no one has received a booster shot yet, so the author decided to abandon the Vaccinated category when modeling the spread in South Africa [3].

B. Determining Social Parameters and Modeling

As shown by the United States Department of Labor statistics, below is a list of major daily activities and time spent by an average American (in hours) [17].

The activities marked red are the ones that potentially involve in-person interactions with others. However, for each activity, only a portion of the times listed above will imply in-person interactions. Supporting facts are as follows:

As shown in TABLE I. , Roughly 80 percent of the population shops online [18]. Forty-two percent of the workforce works from home [17]. About 40 percent of socializing time is online [19]. Private cars dominate the American Commute. Only 5% of US commuters use public transportation [20]. Forty-six percent of students receive only online instruction [21].

Therefore, the number of hours that involve potential interactions with others can be calculated as: $0.38 \times 0.2 + 0.14 + 3.02 \times 0.58 + 0.18 \times 0.54 + 0.18 + 0.54 \times 0.6 + 0.37 + 0.79 \times 0.05 \approx 2.97$ hours, which means $\mu = \dfrac{2.97}{24}$ With all the parameters specified, author graphed this system of differential equations by compiling it into a Python program. Then, the author utilized the least rooted mean squared error ($RMSE$) to determine the best representative p-value and the most accurate model for the spread of Omicron in the US. The amount of time people spends interacting with others in South Africa is not much different from that of the United States because it compares two groups with large populations and similar pandemic-control regulations.

TABLE I.   THE STATISTICS OF THE UNITED STATES DEPARTMENT OF LABOR

Major Activity	Average Time	Potential Fraction	Resulting Time
Personal Care Activities (Sleeping, Grooming...)	10.74	0	0
Household Activities	2.01	0	0
Purchasing Goods and Services	0.38	0.2	0.076
Caring for and Helping Household Members	0.43	0	0
Caring for and Helping Non-household Members	0.14	1	0.14
Working and Work-Related Activities	3.02	0.58	1.7516
Attending Class (Education)	0.18	0.54	0.0972
Homework and Research	0.19	0	0
Organizational, Civic, and Religious Activities	0.18	1	0.18
Socializing and communicating	0.54	0.6	0.324
Watching Television	3.05	0	0
Participating in Sports, Exercise, and Recreation	0.37	1	0.37
Telephone Calls, Email, and Mail	0.22	0	0
Travel	0.79	0.05	0.0395

VI. VARIANT PREDICTION – THE SI3R MODEL

A. Setting up the SI3R model

Upon the emergence of a novel virus, not only are authors concerned about the spread of the resident strand of the virus, but the public is also perturbed by the possibility of the appearance of new variants, particularly when the author can't obtain sufficient information about when and under what conditions new variants may emerge. Since little to no work has been done to investigate the competition between a mutant and a resident, the author devised the SI3R model to simulate the competition and thus determine the conditions under which a new variant might emerge.

The model consists of five compartments: Susceptible, Infectious1, Infectious2, Infectious, and Removed. The model's assumptions include those of the improved SEIRV model and that the mutated strand cannot evade the public's immunity against the resident variant. Therefore, the Susceptible compartment represents the portion of the population that has caught neither of the strands and is thus prone to receive the virus. Infectious contains those who have been infected with the resident strand and are capable of spreading it. Individuals in the Infectious2 compartment can spread the mutant, while those in the Infectious compartment can transmit both strands. Since both strands, the resident and the mutant, according to the prediction, cannot escape the immunity against the other strand, individuals removed from any of the three infectious compartments would be defined in Removed. This system of equations is not extremely detailed but is sufficiently functional to generate general results. More future work could be implemented to enhance the accuracy, for example, by adding the Exposed categories.

B. Generating Equations for the SI3R model

As established above, the expression for daily infection number of one variant can be modeled by $\mu\left(1-e^{-\alpha I}\right)S$. Thus, combining the infected number of the five possible transmission routes results in $\mu\left(5-e^{-a_1 I_1}-e^{-\alpha_1 I_a}-e^{-a_2 I_2}-e^{-\alpha_2 I_a}-e^{-\alpha_a I_a}\right)S$. Then, dividing up the infected population into one of the three Infectious groups yields the correct model.

C. Equations of the SI3R model

Below is the system of differential equations that describe the change of each compartment.

$$\frac{dS}{dt} = -\mu\left(5-e^{-a_1 I_1}-e^{-\alpha_1 I_a}-e^{-a_2 I_2}-e^{-\alpha_2 I_a}-e^{-\alpha_a I_a}\right)S \quad (13)$$

$$\frac{dI_1}{dt} = \mu\left(2-e^{-a_1 I_1}-e^{-\alpha_1 I_a}\right)S - \mu\left(1-e^{-a_2 I_2}\right)I_1 - \theta_1 I_1 \quad (14)$$

$$\frac{dI_2}{dt} = \mu\left(2-e^{-a_2 I_2}-e^{-\alpha_2 I_a}\right)S - \mu\left(1-e^{-a_1 I_1}\right)I_2 - \theta_2 I_2 \quad (15)$$

$$\frac{dI_a}{dt} = \mu\left(1-e^{-\alpha_a I_a}\right)s + \mu\left(1-e^{-a_2 I_2}\right)I_1 + \mu\left(1-e^{-a_1 I_1}\right)I_2 - \theta_a I_a \quad (16)$$

$$\frac{dR}{dt} = \theta_1 I_1 + \theta_2 I_2 + \theta_a I_a \quad (17)$$

S represents the number of people who are susceptible to both the resident and the mutant, I1 represents the number of people who are infected by the resident strand, I_2 represents the number of people who are infected by the mutated strand, I_a represents the number of people who are infected by both strands, R represents the number of people who have gained immunity, θ_I represents the inverse of the infectious period of the resident strand, θ_2 represents the inverse of the infectious period of the mutated strand, θ_a represents the inverse of the infectious period of individuals carrying both strands, α_1 represents the resident strand's transmission rate from a person in the Infectiousa compartment, α_2 represents the mutated strand's transmission rate from a person in the Infectiousa compartment, α_a represents the probability of an individual who carries both strands transmits all two to a susceptible individual, a1 represents the resident strand's transmission rate from a person in the Infectious1 compartment. a2 represents the mutated strand's transmission rate from a person in the Infectious [2] compartment, and finally, μ represents the fraction of time an average person spends interacting with others. On day 1, I_1 is set to the number of patients in reality, I_2 is set to 1, R is set to the number of people who have been infected and removed in reality, I_a is set to 0, and S is set to $(Population) - I_1 - I_2 - I_a - R$.
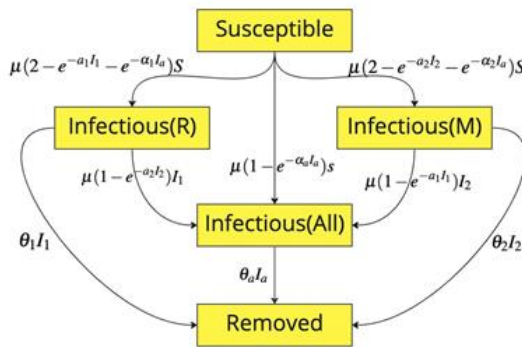

Figure 4.   Change between each compartment of the SI3R model summarized in a flowchart.

VII.   ESTIMATING THE DEMAND FOR HOSPITALIZATION − THE IHOV MODEL

Using the EPSEIRV model, the author can thus simulate the growth of the new variant in each local community as a function of time. Then, obtain the number of hospitalization resources needed (n) in each hospital using (18):

$$\frac{dR}{dt} = \theta_1 I_1 + \theta_2 I_2 + \theta_a I_a \qquad (18)$$

In which I represents the infected population of that target community as a function of time yielded by the EPSEIRV model, h represents the hospitalization rate, O represents the number of already occupied beds, V represents the emergency vacating rate, and T represents the total number of beds available. Established in the EPSEIRV section as part of our improvement, the infectiousness and transmission curve of a virus closely related to the population density and exposed period. Those factors tie closely to the individuality of each local community (e.g., Brooklyn, New York, would have a much denser population distribution than Exeter, New Hampshire). Hence, the $I(t)$ function yielded by the EPSEIRV model allows us to model the transmission data of each community accurately.

Due to our time limitation, the author was only able to implement the IHOV model on the state level in the New England region. However, with simple data gathering and inputting, future work can be done to implement the IHOV model in each county and even globally. The author has implemented all New England states' parameters to the code, including population, population density, number of beds available, bed occupancy rate, etc. Assuming that 40 percent (can be adjusted) of all occupied beds will be emptied for the steep increase in the number of patients, the system then calculates the number of beds.

VIII. RESULTS

The results section has three parts, each covering a part of the system. Since the system aims to generate useful guiding information when new diseases emerge, this section will discuss the results yielded from running the system on Omicron data in the United States.

A. Infection Forecast

The best-fitting p for the data obtained in the United States equals to 3.57×10−8. Please note that the author used positive test percentages

instead of new daily cases because the percentage better represents the status of the entire population, for only a small portion of the population is tested each day. In addition, the author subtracted the percentage of Delta variant positive cases (used the model on Delta as well) from the total positive percentage. Also, the author assumed day 0 to be November 22, 2021, since the first detected case in the US is a traveler who returned from South Africa on November 22 [22].
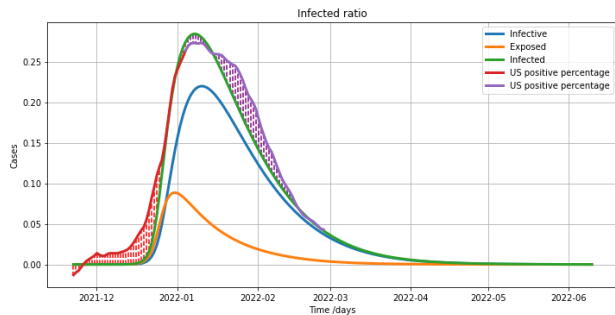

Figure 5.   Projected Positive Percentage as a Function of Time in the US Produced by the EPSEIRV Model

As shown in Figure 5, in which the vertical and horizontal axes respectively represent infected population percentage and time, the red line is the data the author used to generate our prediction (green line), while the purple line represents the real-life data of the ensuing days. Our prediction was generated on January 6 and based on the data before that day. Our model accurately predicted the peak of the infected percentage and produced a projected infection curve that is almost identical to that in real life. The dotted lines mark the error of our predicted trajectory, which, shown in the picture, is negligibly small.
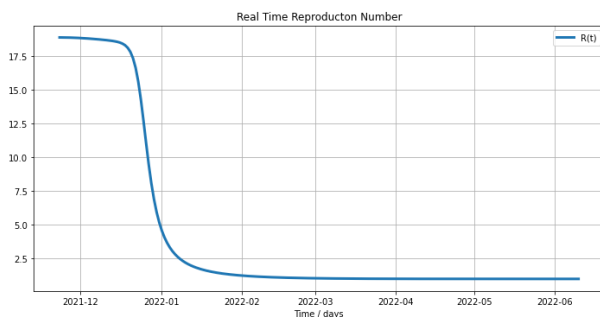
Figure 6.   Real-Time Reproduction Number as a Function of Time in the US Produced by the EPSEIRV Model

Figure 6 is the yielded real time reproduction number of Omicron in the US as a function of

time by the EPSEIRV model. This concludes that the R0 value of Omicron in the US is approximately 18.8, and its real-time reproduction number (R(t)) decreases as a larger portion of the population becomes infected or removed.   This is a reliable R0 value because the infection curve of this R0 value perfectly models the actual infection data. (Note: R0 is a concept in epidemiology that estimates an infectious agent's propensity for epidemic transmission. Simply explained, the R0 value of a disease means how many secondary infections were caused by the very first case in a fully susceptible population, while R(t) is defined as the average secondary infections caused by one patient relative to time [23].) An R0 value of 18.8 is extremely high for a disease, which is consistent with its absurdly quick circulation speed in the US. Before the author published our data on Medium.com, the CDC announced that the R0 value of Omicron was about 75. Now, with more projects examining the R0 number of Omicron in the US, an R0 number above 13 for Omicron has become somewhat of a consensus, reaffirming our produced result.

In contrast, Figure 7 shows the performance of the original SEIRV model when α, according to its published essay, is set to 1.2.   All other parameters were set the same way as the EPSEIRV model.   While also using the same amount of data, the SEIRV model performs significantly worse than our proposed EPSEIRV model (the shaded region also represents its prediction error). Apparently, Omicron's absurdly high contagiousness is not well considered in the 1.2 value of alpha in the original model.

B. Variant Prediction

Figure 7.   Simulation of the Competition Between Omicron and a Hypothetical Mutant

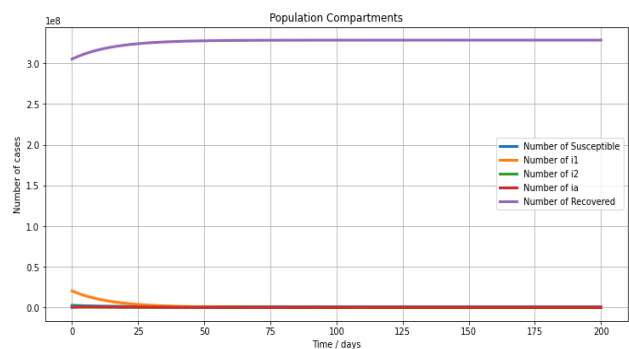Figure 6 models the increase of accumulative positive Omicron cases in the United States; it is found that the increase of accumulative positive Omicron cases will be slow until late December 2021. However, it will increase rapidly by March 2022, which more directly shows that most of the population will be infected with Omicron before the end of March 2022. After that, the cumulative number of cases will not increase and level off.

Since the existence of a mutant is hypothetical, the author can't determine the specific parameters of it. However, the model still produced illustrative results. Assuming that on March 5, 2022, a new mutant of Sars-CoV-2 appears, thus setting day 1 to March 5, 2022, the author obtained Figure 7. The purple line represents the Removed category, the orange line is Infectious1, the minuscule green tip is Infectious2, and the almost straight red line is Infectiousa. This study tested with a range of input parameters, from absurdly high transmission rate to low transmission rate and from long infectious periods to short infectious periods. Nonetheless, it had a negligible impact on the growth of the number of patients in each Infectious compartment, for both strands died out very quickly in all scenarios due to the large number of removed individuals. Thus, under the assumptions of the model, it is not likely that a new mutant of Omicron can prevail. In conclusion, assuming that no drastic changes happen to the US population, for a new variant to prevail, it has to overcome the immunity against Omicron.
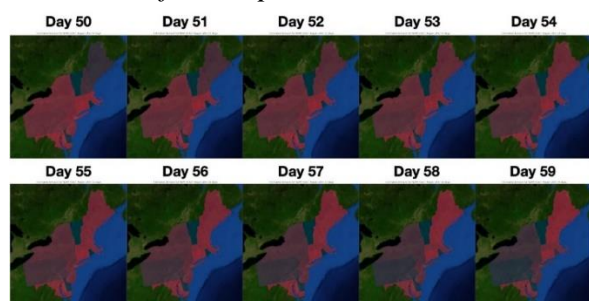
C. Estimation for Hospitalization Resources

Figure 8.   Visual Display of the IHOV Model Results

For demonstration and testing purposes, the author ran the system based on Omicron data prior to January 6, 2022. Figure 8 shows the need for hospitalization resources in each state between 50-60 days since the first case. Users of the system can input different day numbers to access the estimation for that day with a slider. Again, the author only finished the Northeast region of the United States, for it is time-consuming to enter the parameters mentioned in Methods section. Future work may expand the system to the US or even around the world.

IX.   CONCLUSION

The COVID-19 pandemic substantially impacts almost all countries in multiple aspects and can spread to populations worldwide due to its high contagiousness. Therefore, it is a serious challenge for us to quickly address some of the most basic problems with emerging viruses.

In this study, the author focused on the many issues of the current disease transmission department that were exposed in the uncontrollable COVID-19 pandemic. The author built the EPSEIRV model, designed the SI3R model to expand our understanding of mutant competition, programmed the IHOV model to project the demand for inpatient resources, and created the overall PanDict system, which informs the public about infection prediction and variant emergence, and local resource shortages when new viruses emerge. The author modified the original SEIRV model to significantly improve its accuracy by eliminating the inaccurate index, α, and introducing population density and exposure time into the system of equations.

In addition, the EPSEIRV model can be further improved by moving people from the Removed category back to the Susceptible compartment to address reinfection. Secondly, the SI3R model supports mutant competition simulation, which can be used to better understand and predict the emergence of new variants. Besides, the IHOV model uses the generated predictions to estimate the local demand for inpatient resources. Based on this estimation, the proper arrangements of limited health resources can significantly reduce the staffing and resource shortages that hospitals experienced during the Omicron outbreak.

As a result, our system can minimize inpatient resource shortages and reduce unnecessary

economic losses and human casualties when new viruses appear. This will be good for the public and the health sector to better prepare for the emergence of new variants.

X.   CODE AVAILABILITY

The relevant code is publicly available on GitHub at: https://github.com/123Bohan/LBH.git.

REFERENCES

[1] Stephanie Oum, Jennifer Kates, and Adam Wexler, "Economic Impact of COVID-19 on PEPFAR Countries," Global Health Policy, Feb 07, 2022.

[2] Kristine M. Smith,Catherine C. Machalaba,Richard Seifman... & William B. Karesh.(2019). Infectious disease and economics: The case for considering multi-sectoral impacts. One Health.

[3] Edouard Mathieu, Hannah Ritchie, Lucas Rodés-Guirao, Cameron Appel, Daniel Gavrilov, Charlie Giattino, et al. Coronavirus pandemic (covid-19). Our World Data (2020).

[4] R. M. Nayani Umesha Rajapaksha, Millawage Supun Dilara Wijesinghe, K. A. Sujith Prasanna Jayasooriya, W. M. Prasad Chathuranga Weerasinghe, B. M. Indika Gunawardana, An Extended Susceptible-Exposed-Infected-Recovered (SEIR) Model with Vaccination for Predicting the COVID-19 Pandemic in Sri Lanka. (Preprints)

[5] NCIRD & DVD. Omicron variant: What you need to know. N, CDC, 2018.

[6] Kevin, B. Fauci predicts omicron covid wave will peak in U.S. by the end of January. N, CNBC, Dec. 29, 2021.

[7] Laura, U. Expect more worrisome variants after omicron, scientists say. N, Associated Press, Jan. 15, 2022.

[8] Zappa Martina,Verdecchia Paolo & Angeli Fabio. Is the competition between variants the end of the severe acute respiratory syndrome coronavirus 2 pandemic? A journey from Wuhan to XBB.1.16. European journal of internal medicine.

[9] Topf Katherine G, Sheppard Michael, Marx Grace E, Wiegand Ryan E, LinkGelles Ruth, Binder Alison M, and Barbour Kamil E. Impact of the COVID-19 Vaccination Program on case incidence, emergency department visits, and hospital admissions among children aged 5-17 Years during the Delta and Omicron Periods-United States, December 2020 to April 2022. PloS one(12).

[10] Ao Li. Analysis on the development status and challenges of new employment patterns under the epidemic. Proceedings of 3rd International Conference on the Frontiers of Innovative Economics and Management (FIEM 2022)(pp.393-404).BCP Business & Management.

[11] Sandhu Simran K, Morozov Andrew Yu, and Farkas József Z. Modelling evolution of virulence in populations with a distributed parasite load. Journal of mathematical biology(1-2).

[12] Zhang Frank W, Meghoo Colin A, Staats Katherine L, Hayes Elizabeth Perkins, Metzner Mitch, Sobel Julia,Hultquist Eric, et al. A Spatiotemporal Tool to Project Hospital Critical Care Capacity and Mortality From COVID-19 in US Counties. American journal of public health,2021,111(6).

[13] Theodore K,David I. Law of mass action and saturation in SIR model with application to Coronavirus modelling. Infectious Disease Modelling,2021,6.

[14] Jansen Lauren, Tegomoh Bryan, Lange Kate, Showalter Kimberly, Figliomeni Jon, Abdalhamid Baha, et al. Investigation of a SARS-CoV-2 B.1.1.529 (Omicron) Variant Cluster - Nebraska, November-December 2021. MMWR. Morbidity and mortality weekly report,2021,70(5152).

[15] Klaassen Fayette, Chitwood Melanie H, Cohen Ted, Pitzer Virginia E, Russi Marcus, Swartwood Nicole A, et al. Changes in population immunity against infection and severe disease from SARS-CoV-2 Omicron variants in the United States between December 2021 and November 2022. medRxiv : the preprint server for health sciences,2022.

[16] Tian Z. COVID Mutation and Effect on Vaccine[C]//Eliwise Academy.Proceedings of the 5th International Conference on Economic Management and Green Development (ICEMGD V).Springer,2021:53-65.

[17] Anne R,Pablo G. Child Care Time, Parents' Well-Being, and Gender: Evidence from the American Time Use Survey. Journal of child and family studies,2016,25.

[18] Luwei Z,Sheng J,Shaoyao H. Spatial and Behavioral Studies of Daily Shopping Activities of Urban Residents in the Context of COVID-19[C]. A New Idea for Starting Point of the Silk Road: Urban and Rural Design for Human: Proceedings of the 14th International Conference on Environment-Behavior Studies (EBRA 2020).

[19] Krings Victoria C.,Steeden Ben,Abrams Dominic,Hogg Michael A., and Blanchard Anita L. The effects of COVID-19 on virtual working within online groups[J]. Group Processes & Intergroup Relations,2021,24(2).

[20] Ziye Lin. Analysis of the Used Car Market in the United States. Proceedings of 3rd International Conference on the Frontiers of Innovative Economics and Management (FIEM 2022)(pp.100-106).BCP Business and Management.

[21] Xiaoling Chen. Education Informationization in the Context of the Epidemic: Problems and Strategic Selection. Proceedings of International Conference on China and the World in the Context of the Globalization of COVID-19 (CWCGC)(pp.146-158).

[22] PérezSantosa Lissette, KourCardellá Vivian, TejeroSuárez Yahisel, MacíasRoig Lisandra M, PintosSaavedra Yanet, MederoDíaz Dailyn, et al. Epidemiological Characterization of Patients in the First Eight Weeks Following Detection of SARS-CoV-2 B.1.1.529 (omicron) Variant in Cuba.[J]. MEDICC review,2022,24(3-4).

[23] Breban, Romulus & Vardavas, Raffaele & Blower, Sally. (2007). Theory versus Data: How to Calculate R0? PloS one. 2(3):e282.

Design and Performance Testing of a Simulation Model for Time-Triggered Ethernet

Bidong Duan

School of Computer Science and Engineering
Xi'an Technological University
Xi'an, 710021, China
E-mail: 1145597333@qq.com

Jing Cheng

School of Computer Science and Engineering
Xi'an Technological University
Xi'an, 710021, China
E-mail: chengjing@xatu.edu.cn

Abstract—**Time-Triggered Ethernet (TTEthernet) is a new hybrid transmission network technology that introduces time-triggered, synchronization, and security mechanisms based on traditional Ethernet. It is difficult to verify the overall performance mechanism of the TTEthernet through manual calculation. Therefore, this paper models the TTEthernet End System and Switch, and simulates the overall performance of the TTEthernet Model based on the OPNET platform. Firstly, this paper introduces the key mechanisms and development status of the TTEthernet. Secondly, the simulation modeling of the TTEthernet End System and Switch are described, and the key technologies within the model are explained; The End system is an important component of the network, responsible for data generation, transmission, and processing. The Switch is responsible for data forwarding and routing, which plays a crucial role in the performance and stability of the network. Finally, the performance of the TTE network model in this article is analyzed through simulation data, verifying the timeliness, determinacy, and reliability of the model. Simulation data shows that the global throughput of the TTE network model in this article is stable at around 70Mbps, the End-to-End Delay of TT services is around 2.5ms, and the packet loss rate is almost zero, which meets the expected results. However, RC and BE services have higher end-to-end latency and packet loss rates than TT services due to their event triggered messages, but they still meet expectations.**

Keywords-Time-Triggered Ethernet; Simulation Model; Switching Architecture; OPNET

I. INTRODUCTION

A. Research Motivation and Significance

Time-Triggered Ethernet (TTEthernet) is a real-time communication protocol based on Ethernet technology. It uses time-triggered transmission to send data at predetermined intervals, ensuring the real-time and reliable delivery of data. TTEthernet can support various applications, including aerospace, military, and industrial automation. Its main features include high reliability, low latency, high bandwidth, and strong scalability.

In order to better carry out the business planning and maximum carrying capacity evaluation of various network nodes, the 503 Institute of the Fifth Academy of Aerospace Science and Technology has carried out a horizontal project called "TTEthernet Simulation and Calculation Development Tool" in recent years. The TTEthernet simulation and calculation development tool aims to provide support for product design, and is a network planning tool based on the OPNET simulation platform. The tool adopts advanced simulation algorithms and models, which can simulate the data transmission and processing process in various network environments, so as to accurately evaluate the performance and reliability of network nodes.

The First Aircraft Design and Research Institute of China Aviation Industry Corporation (AVIC 1) has developed a Time-Triggered FC Network Simulation Model based on the OPNET simulation platform in order to further improve the determinacy and reliability of aviation and aerospace networks, and meet the high-security requirements of networks. The Time-Triggered FC Network is based on the FC network and incorporates technologies such as TTEthernet and AFDX for traffic control, margin management, and time triggering, which further improves the

determinacy and reliability of the network. The time-triggered FC network simulation platform can assist system designers in the initial top-level design stage of the system to quickly simulate the entire network topology and network traffic, and verify and iterate through digital simulation to validate the ICD design.

B. Related Work

This article proposes a simulation model design for TTEthernet, elaborating in detail the core functional design of the End System Model and the Switch Model, and conducting simulation tests on the model based on the OPNET platform.

When designing the simulation of the TTEthernet Model, this article first carried out the overall model design to ensure the completeness and feasibility of the model. Then, the design ideas of the End System Model were explained in detail, including data stimulation, scheduling and transmission mechanism, and redundancy strategy. Finally, this article designed a 24-port Switch Model, and provided a detailed explanation of the various switching architectures designed in the Switch, making the Switch Model more suitable for practical application scenarios.

After completing the simulation model design, this article implemented the model simulation based on the OPNET platform and conducted simulation tests on the throughput, End-to-End Delay, and packet loss rate performance of the TTEthernet Model proposed in this article based on certain initial data. Through the summary of experimental test data, this article draws a conclusion that proves the feasibility and effectiveness of the TTEthernet simulation model design proposed in this article.

II. RESEARCH STATUS AT HOME AND ABROAD

Time-Triggered Ethernet (TTEthernet) is a network communication technology based on time synchronization, which enables high-precision data synchronization and communication. Currently, TTEthernet has been widely researched and applied both domestically and internationally. TTEthernets have outstanding advantages in real-time performance, determinism, reliability, and bandwidth protection. [1] TTEthernet has been applied in NASA's manned space shuttle project

and has attracted the attention of foreign aircraft manufacturers. China is also considering adopting TTEthernet technology in future spacecraft systems. [2]

In foreign countries, Time-Triggered Ethernet has been widely used in industrial automation, robot control, and medical equipment, aerospace and other fields. For example, the European Space Agency uses Time-Triggered Ethernet to achieve high-precision synchronization of satellite communication and navigation systems; Siemens in Germany applies Time-Triggered Ethernet to industrial automation and intelligent manufacturing; and the aerospace and military equipment industries in Europe and the United States have begun to deploy TTEthernet with good results. [4]

In China, research and application of Time-Triggered Ethernet are constantly developing. For example, the Institute of Automation of the Chinese Academy of Sciences has developed a high-precision data acquisition system based on Time-Triggered Ethernet, which can achieve microsecond-level data synchronization and acquisition. Shanghai Jiao Tong University has also conducted research on the application of Time-Triggered Ethernet in robot control and intelligent manufacturing. [7]

In general, Time-Triggered Ethernet has been widely researched and applied both domestically and internationally. In the future, with the development of industrial automation and intelligent manufacturing, the application prospects of Time-Triggered Ethernet will become even broader.

III. DESIGN OF SIMULATION MODELS

A. Overall Design

The TTEthernet overall model consists of the End System Model, Switch Model, and Link Model. The TTEthernet overall model design is shown in Figure 1.
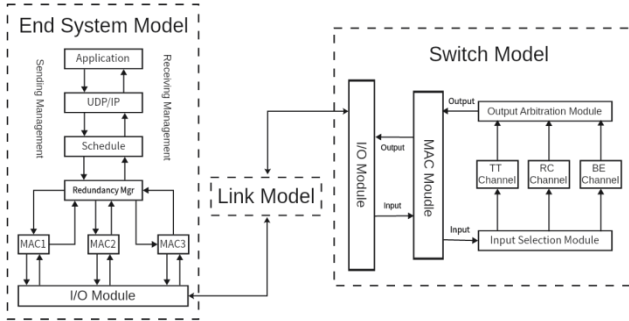
Figure 1.   TTEthernet Overall Model

The End System Model is responsible for sending and receiving processing of the three types of data (TT, RC, BE) in the TTEthernet. The Switch Model is responsible for forwarding the three types of data. The Link Model is a point-to-point full-duplex link, responsible for implementing bidirectional transmission of data frames between the End System and the Switch.

B. Design of End System Model

The End System Model of Time-Triggered Ethernet (TTEthernet) consists of six modules: Application Module, UDP/IP Module, Scheduling Module, Redundancy Management Module, End System MAC Module, and I/O Module. These modules work together to implement the various protocol contents of the TTEthernet. The TTEthernet End System Model based on OPNET is shown in Figure 2, where the arrows between modules represent the flow of three types of data and the interaction of information.
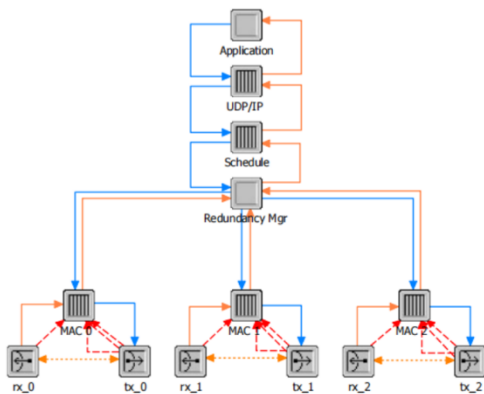

Figure 2.   TTEthernet End System Simulation Model

The frequency and conditions of message transmission are the first issues to be addressed in the TTEthernet End System simulation model. To achieve this, the association between tasks and messages must first be established for each application. The business of the application is composed of a series of messages, and the completion of tasks relies on the sending and receiving of messages. Therefore, the correspondence between tasks and messages can be described by the following equation.

$$T_k = \{t_1, t_2, \cdots, t_m\} \qquad (1)$$

The formula represents a certain task on the application of the End System, denoted as T_k, which consists of a set of m messages. Each message is defined by a five-tuple:

$$t_i = \{I_{ti}, V_{ti}, L_{ti}, P_{ti}, T_{ti}\} \qquad (2)$$

In the formula:

I_{ti} Represents the message sequence number, which is unique;

V_{ti} Represents the virtual link number of the message, which represents the virtual link that the message passes through in the TTEthernet;

L_{ti} Represents the frame length of the message and the message frame length are in bytes;

P_{ti} Represents the generation frequency or period of the message, using various function excitation methods to simulate non-periodic message events to be closer to the real network communication model;

T_{ti} Represents the message type, which is used to define the TT, RC, and BE message types.

After the TTEthernet message is encapsulated into an IPv4 data frame by the End System, it needs to enter the corresponding cache queue and wait for scheduling. The maximum carrying capacity of the cache queue is determined by the queue's packet capacity and bit capacity. Time-Triggered messages (TT) are scheduled based on the concept of time windows, which specify the start time (Tx_{start}) and end time (Tx_{end}) for the message to be sent within an integration cycle

(Tx_{period}). Therefore, if it is allowed to schedule the message at the current time (T_N), the following conditions must be met:

$$\begin{cases} Tx_{start} \leq (T_N)\mathrm{mod}(Tx_{period}) < Tx_{end} \\ L_{ti}/Pt_{rate} < Tx_{end} - (T_N)\mathrm{mod}(Tx_{period}) \end{cases} \quad (3)$$

"Pt_{rate}" Refers to bandwidth.

For the scheduling of event-triggered messages (RC and BE), it is required to be completed within the time interval between two time windows. In order to achieve bandwidth management while scheduling TT messages based on time window order, two attribute values, L_{max} and BAG, need to be set for each virtual link. In ordinary Ethernet, due to the lack of L_{max} and BAG restrictions, the network traffic sent by End Systems is relatively random, which can easily cause surge traffic, leading to congestion or even congestion of Switches, increasing the queuing time and delay of data frames, and having a high degree of uncertainty. In TTEthernets, the BAG value is applied to the scheduling of RC messages.

BAG (Bandwidth Allocation Gap): defines the minimum time interval for continuously sending RC messages on the same link. After sending a message at the sending end, if another RC message is received within the BAG time, the next message can only be sent after waiting for the BAG time.

Due to the performance differences among different scheduling strategies, they may have different impacts on the delay of data frames. In the actual scheduling process, the scheduler should try to keep the BAG and L_{max} values set for each virtual link unchanged. However, due to the introduction of the scheduler and scheduling strategies, there will be a delay time for data frames waiting for scheduling, which introduces the concept of jitter. In Time-Triggered Ethernet, jitter refers to the time interval between starting to send a data frame within the BAG value range and actually sending it. Different scheduling mechanisms may produce different time intervals. Figure 3 shows three different jitter scenarios.
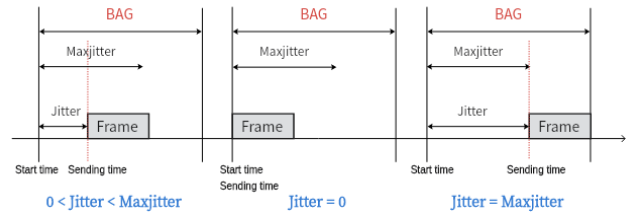
Figure 3.　Three types of jitter situations

The jitter of each End System should satisfy the following formula:

$$Jitter \leq 40 + \frac{\sum_{Set\ of\ VLs}(20+L)\times 8}{Pt_{rate}} \quad (4)$$

Due to the high reliability requirement for data transmission in TTEthernet, this model adopts a three-redundancy fault-tolerant management mechanism. The entire TTEthernet consists of three identical networks A, B, and C. Each End System contains three Ethernet interfaces A, B, and C, which are connected to the Switch ports in networks A, B, and C respectively, forming a three-redundancy network composed of networks A, B, and C. When an End System sends a data frame on a single virtual link, it duplicates the data frame into three copies and sends them to networks A, B, and C simultaneously. The data frames are transmitted independently in networks A, B, and C without affecting each other. The receiving end will receive the same data frame from networks A, B, and C on the virtual link. The three-redundancy network structure is shown in Figure 4.
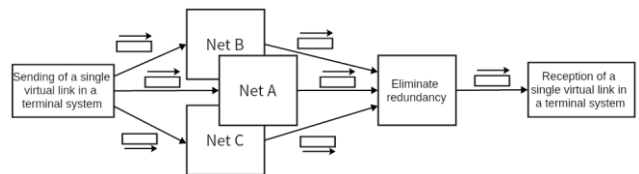
Figure 4.　Triple Redundancy Network Architecture

The redundancy processing module checks the data frames submitted by networks A, B, and C, and adopts the principle of first come, first served. By comparing the frame numbers, redundant data frames are removed to maintain the uniqueness of frame numbers, thus achieving redundancy management. In the event of a lost data frame in one network, data frames from another network

can be used to correct it, greatly enhancing the reliability of data transmission.

C. Design of Switch Model

The Switch Model of Time-Triggered Ethernet can be divided into five modules: I/O Module, Switch MAC Module, Input Selection Module, Message Channel Module, and Output Arbitration Module. The main functions of the Switch are as follows:

1) Forward data to the corresponding output port based on the configuration information of the

VL to ensure the order of data transmission for the same VL;

2) Support unicast, multicast, and broadcast based on the configuration information of the VL;

3) Support the reception, scheduling, and transmission of three types of business messages: TT (time-triggered), RC (rate-controlled), and BC (best-effort).

The TTEthernet Switch adopts different switching architectures for the three types of messages. The TTEthernet Switch simulation model based on OPNET is shown in Figure 5.
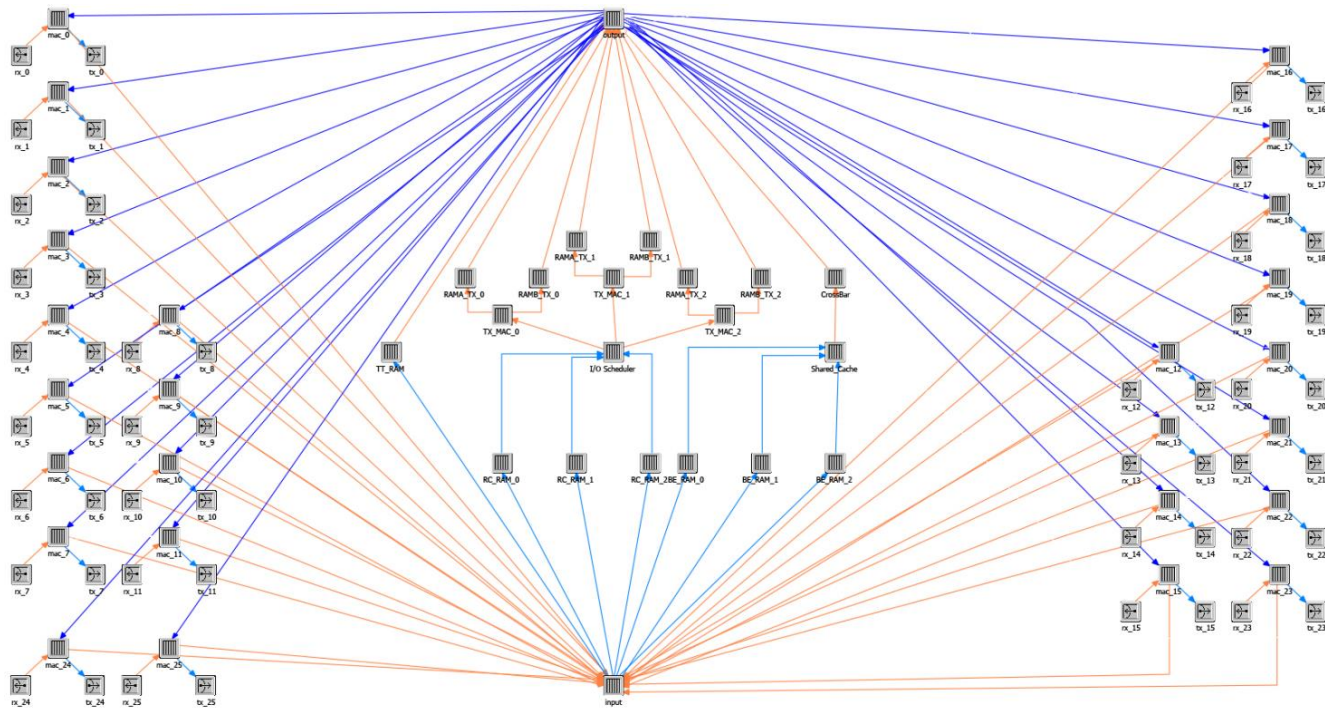
Figure 5.   TTEthernet Switch Simulation Mode

For all types of messages that arrive at the Switch, a FULL-MESH architecture is used as the exchange channel for TT messages in order to ensure real-time, deterministic, and reliable TT message delivery to the greatest extent possible. FULL-MESH is a network connection architecture, also known as a fully connected architecture, in which all nodes are directly connected, ensuring that a direct path can be found between any input port and any output port.

The RC channel is an exchange architecture consisting of a set of shared buffers and three

ping-pong buffers. Each set of ping-pong buffers consists of an input data controller and two identical RAMs. The operation structure of the ping-pong buffers is shown in Figure 6.
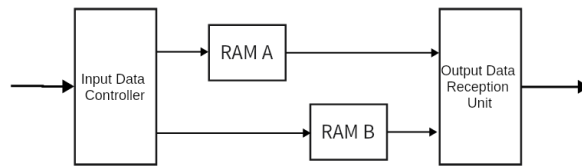
Figure 6.   Ping-Pong buffer operation structure

The input data stream is divided equally into two data buffers by the input data selector controller. In the first buffer cycle, the input data frame is stored in RAM A. In the second buffer cycle, the next data frame is stored in RAM B by switching the input data controller, while the data frame cached in the first buffer cycle of RAM A is transferred to the output data receiver unit. In the third buffer cycle, the input data frame is stored in RAM A while the data frame cached in RAM B is transferred to the output data receiver unit by switching the input data controller. This cycle continues, achieving the processing of high-speed data streams using a low-speed data preprocessing module.

The cache architecture of the BE channel adopts a shared cache combined with a CrossBar structure. CrossBar is also known as a crosspoint switch or a matrix switch, which can effectively compensate for some of the shortcomings of shared memory mode. The CrossBar switch matrix is shown in Figure 7.
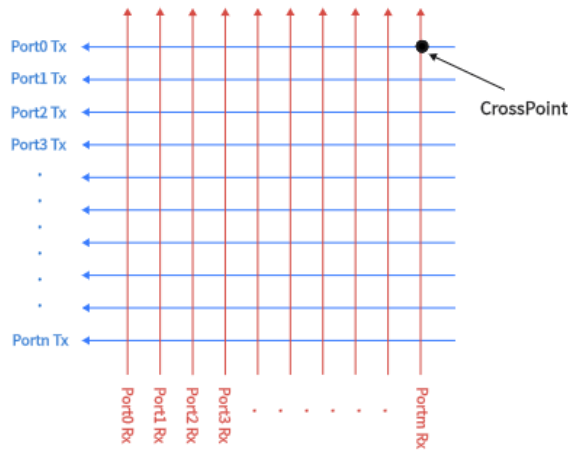
Figure 7. CrossBar Switching Matrix

The Crossbar architecture is a three-level architecture that consists of a switch matrix. Each CrossPoint is a switch, and the switch controls the forwarding of input to a specific output. The Crossbar is non-blocking internally (relatively speaking). As long as multiple crosspoints are closed simultaneously, multiple different ports can transmit data simultaneously. In this sense, we consider all Crossbars to be non-blocking internally because they can support all ports to exchange data at line speed simultaneously.

Each CrossPoint has a cache queue for buffering data frames, with a capacity equal to the size of the two longest data frames in the network. During data output, a round-robin algorithm is used to sequentially poll each CrossPoint under the same output port. When a data frame is present in the node's cache, the frame information is read and the data frame is output. The output scheduling process involves checking whether the output port is idle and whether the CrossPoint cache is readable when a data frame enters the CrossPoint cache. If the conditions are met, the round-robin scheduling algorithm is used to poll the destination port number that needs to be dequeued, and the data frame is output accordingly. After data output is complete, the output port is set to idle.

IV. SIMULATION TEST RESULTS AND ANALYSIS

The behavior between the End Systems, switches, and links in the TTEthernet simulation system implemented based on OPNET can be represented by the timing diagram shown in Figure 8.
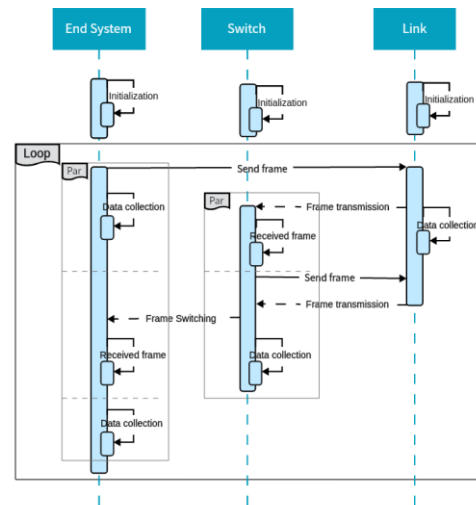
Figure 8. TTEthernet Simulation System Timing Diagram

After having sufficient initialization data support, the entire simulation network will continuously perform loop processes such as sending, forwarding, and creating and destroying data frames, data recording, error handling, etc. until the simulation is completed. After the simulation is executed, the network's statistical

module will display the simulation test results, making it easier to evaluate the performance of the entire network.

This article conducts simulation tests on the network topology shown in Figure 9.
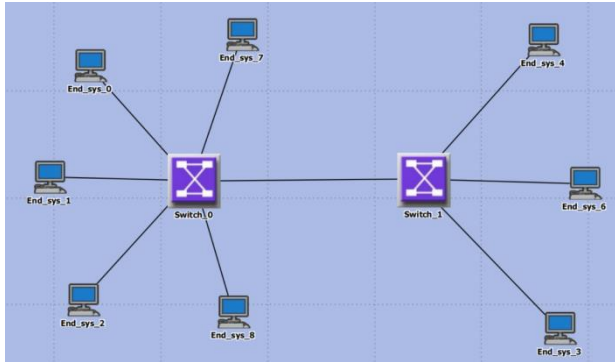
Figure 9. TTEthernet topology

The TTEthernet simulation test results require input of configuration information. Figure 10 shows some of the configuration information during the simulation test process.


Figure 10. Simulation configuration information

The initial amount of data obtained from each simulation is often very large, so the concept of time bucket is introduced to process the simulation data properly before presenting the final results. In OPNET's simulation data processing, one time bucket is often defined as one percent of the total simulation time, denoted as T_B in this article, and the following test results can be described accordingly.

A. Throughput

Assuming that the TTEthernet simulation system received n data frames within a certain time period, the throughput can be calculated using the following Equations.

$$R_t^F = \frac{(L_T + L_1)(T_1 - \lfloor T_1/T_B \rfloor \times T_B)}{T_1 \times T_B} \quad (5)$$

$$R_t^M = \sum_{j=2}^{n-1} \frac{\left(L_T + \sum_{i=1}^{j} L_i\right)(T_j - T_{j-1})}{T_j \times T_B} \quad (6)$$

$$R_t^L = \frac{\left(L_T + \sum_{k=1}^{n} L_k\right)(\lceil T_n/T_B \rceil \times T_B - T_n)}{T_n \times T_B} \quad (7)$$

$$R_t^n = R_t^F + R_t^M + R_t^L \quad (8)$$

R_t^n Represents the throughput value that the simulation system needs to record at time t; L_t represents the total amount of data received by the current simulation system; T_n represents the simulation time when the system receives the message; L_i represents the length of the data frame received at time T_i. The throughput of the TTEthernet simulation system obtained by this calculation method is shown in Figure 11, and from the test results, the throughput of the entire network is stable at around 70Mbps,indicating that the network model has good data transmission ability and can meet the needs of most application scenarios.
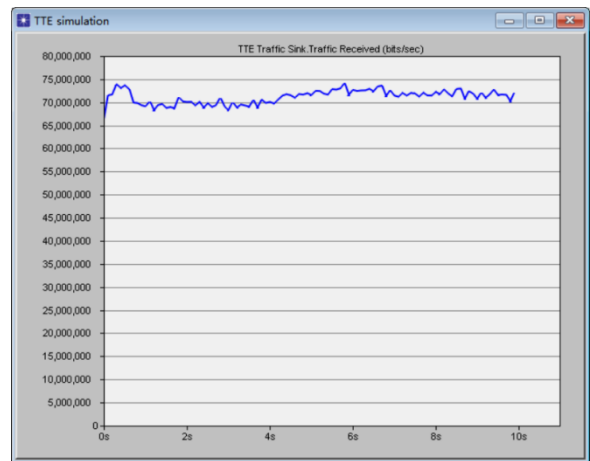
Figure 11. Throughput of TTEthernet simulation system

B. End-to-End Delay

End-to-End Delay refers to the total time it takes to send data from one network endpoint to another and receive confirmation. The key factors that affect end-to-end delay in the TTEthernet simulation system are as follows:

1) Frame encapsulation delay;

2) Cache size and the speed of data frames entering and leaving the cache;

3) Queuing delay, which refers to the time it takes for data to be stored in the buffer queue of network devices such as routers or switches waiting for processing, and is related to network congestion and buffer size;

*4)* Delay in scheduling policies executed by End Systems and switches;

5) Port transmission rate, the time it takes for the transmitter to push the message onto the link;

6) Link propagation rate, the transmission rate of messages on the cable;

7) Delay in performing data frame verification;

8) Interval for Switch polling of data frames;

9) Delay in executing redundancy policies;

10) Number of switches in the network, too many switches will increase the number of hops for data frames, and too few switches will cause internal congestion in the switches;

11) Delay in the internal cache architecture.

The TTEthernet simulation system will automatically simulate the above-mentioned delay. Therefore, after receiving a data frame, the formula for calculating the End-to-End Delay of the data frame is as follows:

$$End\text{-}to\text{-}End\ Delay = Frame.T_N - Frame.T_C \quad (9)$$

In the formula, $Frame.T_N$ represents the time when the receiving end receives the data frame, and $Frame.T_C$ represents the time when the data frame is created. Therefore, after the simulation is completed, the End-to-End Delay of the three types of messages in the TTEthernet simulation system can be obtained as shown in Figure 12.
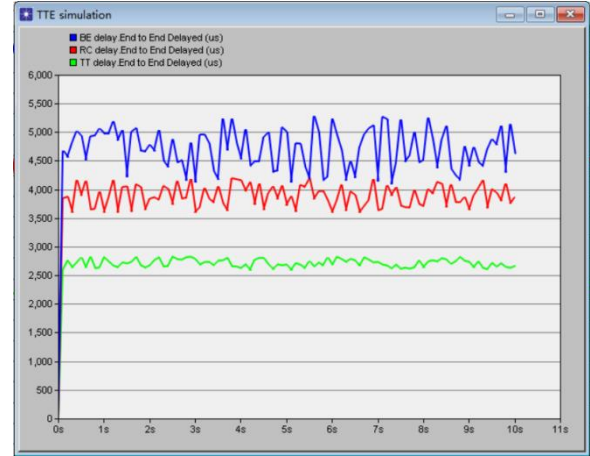
Figure 12. End-to-End Delay of three types of messages

Due to the fact that time-triggered (TT) messages are scheduled and sent based on time windows and have the highest scheduling priority, the End-to-End delay of TT messages is the smallest among the three types of messages and the fluctuation of the delay curve is also relatively small. Best-Effort (BE) messages, as messages sent with best effort, have the lowest real-time performance and reliability, resulting in the largest fluctuation of the End-to-End Delay curve, which is slightly higher than that of RC messages in terms of numerical value.

C. Packet Loss Rate

The packet loss rate refers to the ratio of the number of lost data packets to the number of packets sent during transmission. The packet loss rate is related to configuration information such as packet length, packet transmission frequency, module queue size, and time window planning. The steps to calculate the packet loss rate in OPNET are:

1) Define a variable PkCreate within the End System Model to record the total number of data frames generated by the data source;

2) Define a variable PkSend to record the total number of data frames finally sent out from the model;

3) The equation for calculating packet loss rate (P_L) is (10).

$$P_L = \frac{PkCreate - PkSend}{PkCreate} \quad (10)$$

However, during the simulation process, multiple data packets may be lost at the same time, and OPNET needs to use a time bucket mode for weighted averaging internally. Assuming that m packets are lost by a terminal system within one bucket time, the final equation for calculating the packet loss rate is (11).

$$P_{LossRate}^m = \frac{\sum_{i=1}^m P_L^i (T_i - T_{i-1})}{T_B} \qquad (11)$$

In the equation, $T_0 = \lfloor T_1 / T_B \rfloor \times T_B$.

Based on the configuration information input into the TTEthernet simulation system, the packet loss rate of the TTEthernet simulation system can be obtained as shown in Figure 13.
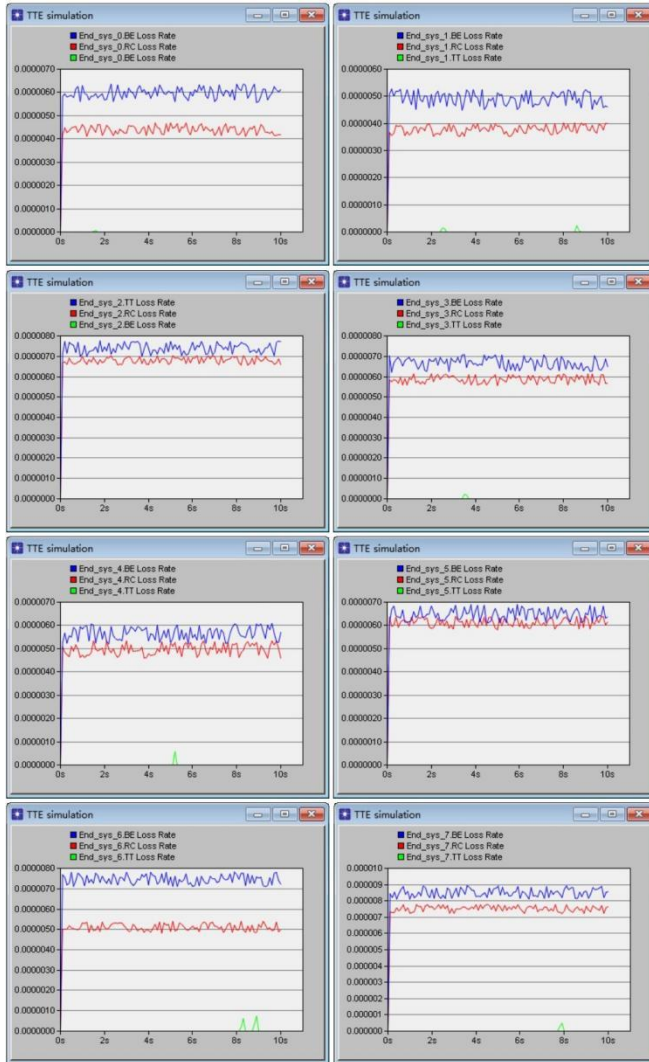
Figure 13. Packet loss rates for three types of messages

According to the simulation test results, the packet loss rate of time-triggered messages (TT messages) in the entire TTE network is almost 0, which means that the transmission of time-triggered messages is very stable and reliable. This highly reliable transmission is critical for time-triggered applications that require precise synchronization and determinism. In addition, the packet loss rate of RC messages and BE messages is also controlled below 1 in 10,000, which indicates that these two types of messages also have quite high transmission reliability and stability.

These simulation results further verify the reliability and stability of the TTE network model, and provide strong support for its practical application.

V. CONCLUSIONS

This article focuses on simulating and modeling Time-Triggered Ethernet and conducting simulation testing and analysis of network performance based on OPNET. In the End System Model, the timeliness, determinacy, and reliability of time-triggered messages are ensured through time window-based scheduling and the strategy of three redundant networks. In the Switch Model, different exchange architectures are used as message channels for different types of messages to ensure the orderliness of various messages and reduce internal congestion in the Switch. In addition, this article also simulated and modeled the TTEthernet Model based on OPNET and analyzed the overall performance of the network through experimental data.

Network simulation plays an important role in evaluating network design and optimizing network performance. Through network simulation, different network designs and solutions can be evaluated and tested before actual deployment, which can greatly save time and cost in design and deployment. It can also simulate various complex network topologies and environments, including different types of devices, protocols, and traffic volume. This allows network designers to fully understand the various possibilities and fundamental factors of network operation.

This article provides some reference suggestions for the future design of Time-Triggered Ethernet, but there are still some aspects that can be improved in the methods proposed in this article. For example, on switches with more ports, the CrossBar switching architecture may no longer be the optimal choice, and it may be considered to use CLOS architecture or other architectures to optimize the message channels of switches in the future.

REFERENCES

[1] L. Zhang, D. Goswami, R. Schneider, and S. Chakraborty, "Task- and network-level schedule co-synthesis of Ethernet-based time-triggered systems," in 2014 19th Asia and South Pacific Design Automation Conference (ASP-DAC), Singapore, Jan. 2014. doi: 10.1109/aspdac.2014.6742876.

[2] P. Tabuada, "Event-Triggered Real-Time Scheduling of Stabilizing Control Tasks," in IEEE Transactions on Automatic Control, vol. 52, no. 9, pp. 1680-1685, Sept. 2007, doi: 10.1109/TAC.2007.904277.

[3] J. Li, H. Xiong, Q. Li, F. Xiong, and J. Feng, "Run-Time Reconfiguration Strategy and Implementation of Time-Triggered Networks," Electronics, vol. 11, no. 9, p. 1477, May 2022, doi: 10.3390/electronics11091477.

[4] P. Muoka, D. Onwuchekwa, and R. Obermaisser, "Adaptive Scheduling for Time-Triggered Network-on-Chip-Based Multi-Core Architecture Using Genetic Algorithm," Electronics, vol. 11, no. 1, p. 49, Dec. 2021, doi: 10.3390/electronics11010049.

[5] L. Behera, "A fault-tolerant time-triggered scheduling algorithm of mixed-criticality systems," Computing, vol. 104, no. 3, pp. 577‒599, Mar. 2022, doi: 10.1007/s00607-021-01026-5.

[6] J. H. Goh and M. K. Ishak, "Implementing Time-triggered Communication for Embedded Ethernet Real-time Network using IEEE 1588 Time Synchronization," IEIE Transactions on Smart Processing & Computing, vol. 10, no. 5, pp. 431‒438, Oct. 2021, doi: 10.5573/ieiespc.2021.10.5.431.

[7] H. Yuan, T. Zheng, K. Zhang, and Y. Wang, "An Efficient Schedule Synthesis Method based on Constraint Programming Technology for Time-Triggered Ethernet," in 2020 5th International Conference on Computer and Communication Systems (ICCCS), Shanghai, China, May 2020. doi: 10.1109/icccs49078.2020.9118453.

[8] Z. Zheng, F. He, and H. Xiong, "Routing Optimization of Time-Triggered Ethernet Based on Genetic Algorithm," in 2020 AIAA/IEEE 39th Digital Avionics Systems Conference (DASC), San Antonio, TX, USA, Oct. 2020. doi: 10.1109/dasc50938.2020.9256594.

[9] B. Pavkovic, M. Sandic, and N. Teslic, "A genetic simulation strategy: Application to single-fault analysis of TTEthernet synchronization protocol," Journal of Systems Architecture, vol. 117, p. 102169, Aug. 2021, doi: 10.1016/j.sysarc.2021.102169.

[10] X. Ma and A. Hamdulla, "Hybrid Scheduling Technology of Time-triggered Ethernet Switches: A Review," Journal of Physics: Conference Series, vol. 1673, no. 1, p. 012024, Nov. 2020, doi: 10.1088/1742-6596/1673/1/012024.

[11] J. Lu, H. Xiong, F. He, Z. Zheng, and H. Li, "A Mixed-Critical Consistent Update Algorithm in Software Defined Time-Triggered Ethernet Using Time Window," IEEE Access, vol. 8, pp. 65554‒65565, Jan. 2020, doi: 10.1109/access.2020.2984749.

[12] A. A. Atallah, G. B. Hamad, and O. A. Mohamed, "Routing and Scheduling of Time-Triggered Traffic in Time-Sensitive Networks," IEEE Transactions on Industrial Informatics, pp. 4525‒4534, Jul. 2020, doi: 10.1109/tii.2019.2950887.

[13] X. Yang, Y. Huang, J. Shi, and Z. Cao, "A Performance Analysis Framework of Time-Triggered Ethernet Using Real-Time Calculus," Electronics, vol. 9, no. 7, p. 1090, Jul. 2020, doi: 10.3390/electronics9071090.

[14] L. Zhao, M. Ni, X. Cui, W. Wang, and J. Zhang, "The Research of Scheduling Algorithm Based on Time-Triggered Ethernet," in 2020 22nd International Conference on Advanced Communication Technology (ICACT), Phoenix Park, PyeongChang,, Korea (South), Feb. 2020. doi: 10.23919/icact48636.2020.9061364.

Why the Discovery of the Overlapped Multiplexing Principle is Bound to Cause a Revolution in Communication and Information Technology?

Daoben Li

Beijing University of Posts and Telecommunications
School of Information and Communication
Engineering
Beijing, 100876, China
E-mail: lidaoben2014@ 163. com

Han Shen

School of Computer Science and Engineering
Xi'an Technological University
Xi'an, 710021, China
E-mail: sunny_shine_zj@163.com

Abstract—This article firstly introduces the overlapped multiplexing principle discovered by Prof. Daoben Li, and the new channel capacity derived from it, which is far beyond the capacity of Shannon's channel, and then introduces the characteristics and superiority of the waveform coding theory and the brand-new communication system, OVXDM, which is the cornerstone of his work. The article exposes two paradoxes and major errors of Shannon's information theory that violate the basic principles of physics, and makes predictions about the future development of communication and information technology. It criticizes several erroneous views on the development of 6G mobile communications: 6G should move to millimeter-wave terahertz band, the only means to improve the spectral efficiency of mobile communications is ultra-large-scale MIMO, and exposes that the U.S. Starlink and StarShield satellites can realize the global Internet 6G communications when the deception, the essence of which is the seizure of space resources and maintenance of the U.S. space hegemony. He emphasizes the great advantage of overlapped multiplexing waveform coding over Shannon coding, and points out that the Internet is only a network built under the guidance of the old Shannon multi-user network theory, which is as outdated as Shannon's information theory and should be eliminated. The Internet and GPS are the kingpin espionage tools of the United States to control the global information hegemony and steal information from other countries. In order to abandon the U.S. information hegemony, our country must leave the GPS in addition to the Internet! Under the guidance of the theory of subversive overlapped multiplexing multi-user network, the author puts forward suggestions on the establishment of our country's independent ultra-large-capacity wide-area Ov information network, which is a brand-new integrated network including space, sky, ground, ground to underwater, underwater and other categories, with a capacity much higher than that of the Internet.

FOREWORD

This paper introduces the new principle of Overlapped Multiplexing (Ov) discovered by Prof. Daoben Li after more than 40 years of observation in the field of communication and information, according to which Prof. Li overthrew Shannon's channel capacity and derived a new channel capacity (Ov capacity for short), and laid the foundation of Ov redundancy-free overlapped waveform coding theory and a brand-new communication system - OVXDM (Overlapped X-domain Multiplexing). OVXDM has been repeatedly and independently simulated and verified by thousands of people in many organizations for more than 20 years, which has completely confirmed its amazing performance of overturning Shannon's theory and the correctness of Ov theory.

As we all know, the guiding theory of all present-day technologies in the field of information, such as communication, cryptography, information security, anti-jamming communication, confidential and covert communication, and multi-user network transmission, etc., is Shannon's information theory. Shannon channel capacity is recognized as one of the three most famous formulas of the 20th century, $C = B_{nai}Log(1 + P_S / P_N)$, where c is the channel capacity, i.e., the theoretical maximum transmission rate (in bits per second, bps/Hz), B_{nai} is

the system Nyquist bandwidth (in units of Hz), P_S/P_N is the received signal-to-noise ratio, P_s is the received signal power, P_N is the received noise power. $\eta = C/B_{nai}$ is the insurmountable spectral efficiency (in bits/sec/Hz, bps/Hz), the noise power spectral density is $N_0 = P_N/B_{nai}$, the received bit energy is $E_b = P_S T_b$, T_b is the bit duration, and the received normalized signal-to-noise ratio is $\dfrac{E_b}{N_0} = \dfrac{P_S}{P_N} B_{nai} T_b$. Because the Ov principle is different from Shannon's theoretical basis, not only is the Ov capacity dramatically higher than Shannon's capacity, but the face of all other information domains should change dramatically as well.

I. THERE CAN BE NO DISRUPTIVE TECHNOLOGY WITHOUT DISRUPTIVE THEORY

For example, the theory of nuclear fission and nuclear fusion produces atomic bombs, hydrogen bombs and new sources of nuclear energy, Maxwell's equations produce wireless communications, and Kao's theory produces optical fiber communications. The Ov capacity derived from the Ov principle and the non-redundant overlapping waveform multiple-access coding theory based on it will also cause a revolution in communication and information technology.

II. THE LAWS OF THE OBJECTIVE PHYSICAL WORLD ARE EQUALLY UNIVERSAL

Objective physical world laws are compatible and universal, science is to explore the study of the regularity of the objective world of learning, the core of science is mathematics, mathematics is the queen of science, is the science of science, the laws of the objective physical world are to be described by mathematical laws. For example, Einstein's general theory of relativity from the Riemann geometry, modern fiber optic communications from the Kao mathematical theory, Shannon information theory from the laws of thermodynamics of physics found proposed, Ov channel capacity is both from the thermodynamics of physics, but also from the laws of physics of the

building and transportation, they have precise mathematical form of expression.

III. TWO PARADOXES OF MODERN COMMUNICATION THEORY

Shannon information theory since it is generated from the thermodynamics of physics, should also comply with the other laws of physics, although it has guided the development of communication technology for nearly 70 years, communication technology under its guidance has indeed had a significant development, but Professor Li found that it which the two major paradoxes, which seriously hindered the development of communication technology, respectively:

- No overlap between neighboring and connected data symbols is allowed in time domain, frequency domain, airspace, or a mixture thereof, or serious "interference" will occur, deteriorating system performance.
- Shannon Channel Capacity: For a given system bandwidth B_{nai} and noise power P_N , the system capacity C (in bps , i.e., bits/second) grows at least exponentially with the received signal power P_S (the velocity of propagation of the vacuum and atmospheric dots dialed is the speed of light).

Architecture in physics points out that the basic construction of the close bite (overlap) will make the building more tough, such as China's famous Zhaozhou Bridge and the Forbidden City and other ancient buildings due to the components of the clever bite, after more than a thousand years of testing and domestic and foreign simulations to verify that they are able to withstand than the strongest earthquakes that have appeared on the earth more powerful earthquakes. Accordingly, the overlap (occlusion) between neighboring and connected data symbols in time, frequency, space and their hybrid domains of the basic building blocks (data symbols) of digital communications should not be worsened, but rather enhance the system's immunity to interference. Obviously, Shannon's information theory is contrary to the laws of construction belonging to physics.

Communications and transportation systems are essentially the same except that one transmits goods and one transmits data bits! According to the physics of transportation, the capacity of a transportation system (in tons/hour) grows at most linearly with its traction power for a given road (similar to the bandwidth and noise of a communication system) and handling speed. Shannon's information theory, however, requires that the capacity of a communication system (in bits/sec/Hz) grows at least exponentially with the received signal power. Why is there such a huge difference between two systems that are essentially the same? Clearly Shannon information theory again contradicts the laws of transportation which belong to physics.

IV. MAJOR ERRORS IN MODERN COMMUNICATION THEORY

A. Using level splitting or waveform splitting?

Shannon theory relies on different signal levels to distinguish data. It is well known that it cannot be separated from multi-level tuning to constellation diagrams, such as QAM constellation diagrams, in order for a given Nyquist bandwidth of a data symbol to Ho in K bits of information, there must be at least 2^K levels (number of constellation points) within the constellation diagrams, such as $K=4$ with $16QAM$, $K=12$ with $4096QAM$ ......, etc. Thus, in an average power constrained channel, as the desired spectral efficiency increases, the minimum distance between the constellation points (minimum interval of levels) will decrease exponentially, and as soon as the noise level exceeds half of the minimum interval of the constellation points (signal levels), the received data judgment will be wrong. This is the reason why the capacity (spectral efficiency) of the Shannon system grows exponentially with the received signal power.

Ov theory, on the other hand, relies on different signal waveforms to distinguish data. It is well known that in unusually noisy environments, one can still distinguish between very many very weak signal waveforms by utilizing the inherent characteristics of the different waveforms, which is the fundamental reason why the Ov capacity

(spectral efficiency) requires far less received signal power than the Shannon system.

B. Is redundant or non-redundant waveform coding used?

Shannon only gave theoretical capacity bounds, i.e., he only proved the existence of approximation to his capacity bounds, and did not give encodings (constructivists) to approximate his capacity bounds. Therefore, more than seventy years after Shannon's information theory, people have been constantly trying to explore various channel coding methods that approach Shannon's bound, but the results are not very effective. Shannon pointed out that the channel coding intelligence by increasing the "redundancy" to reduce the effective bit transmission rate to realize. In coded sequence, "redundancy" is the increase in parity check bits; in coded modulation, "redundancy" is the increase in constellation space. The ratio of the useful space to the coded space is the code rate r.

The ratio of the number of data bits to the number of data plus supervisory test bits in a coded sequence is the code rate r, and the additional supervisory test bits are the "residual" bits; the useful data space for coded modulation with spectral efficiency $\eta = K(bps/Hz)$ is the constellation diagram of the 2^K constellation points, the coded space is the constellation diagram of the 2^{K+l} constellation points, and the extra 2^l constellation points are the "residual", code rate . "residual" and the code rate $r = 2^{-l}$.

According to Shannon information theory, Shannon channel coding that realizes the spectral efficiency $\eta = K(bps/Hz)$ must use a constellation diagram with $2^{(K-Log_2^r)}$ constellation points whose number of constellation points, i.e., the number of output levels of the Shannon coding system, should grow with the $(K - Log_2^r)$ index!

The larger the residual, the lower the code rate r, the higher the Shannon coding gain, but the lower the effective bit rate. Such as from BCH, RS, TCM until Turbo, LDPC, Polar coding, etc. are used in this low code rate r, low bit rate coding. Unfortunately, the above coding due to the low code rate, the system spectral efficiency is very low, and are in the bit error rate 10^{-5} when

"approaching" the Shannon boundary. At lower bit error rate ($<10^{-5}$), they are all far away from the Shannon boundary, and there is an error floor, i.e., no matter how to improve the signal noise ratio, the error probability is no longer reduced. High bit rate and spectrally efficient Shannon coding will certainly never be found.

Utilizing the Ov principle, Prof. Li completely discarded Shannon's residual coding and modulation constellation diagrams, and only multiplexed waveforms without residual overlapping multiplexing of time, frequency, and spatial sequences of multiple-access waveform coding, whose immunity to interference is far superior to that of Shannon's coding. The average output power of the waveform coding system grows at most linearly with the spectral efficiency, and both theoretical and simulation results demonstrate that the threshold signal noise ratio required for the Ov system is indeed much lower than that of the Shannon system under the same conditions of spectral efficiency!

V.   OVERLAPPED MULTIPLEXING PRINCIPLE

Overlapped Multiplexing Principle is a new principle discovered by Prof. Li after more than 40 years of repeated observation and research, which was firstly published in China in November 2013 in his monograph "Waveform Coding Theory and OVTDM with High Frequency Efficiency" published by Science Press. In March 2018, IEEE Access, the world's leading journal in the field of information, published his "Overlapping Multiplexing Principle and an Improved Capacity on Additive White Gaussian Noise Channel" as a special paper on the cover of the journal and announced this principle to the world. The principle is that the overlapping of transmitted data symbols in time, frequency, space and their mixed domains is definitely not "interference" but a beneficial coding constraint. The more severe the overlap, the higher the coding gain and the better the interference immunity. Only destructive elements from outside the system are considered interference.

VI.   THE CHANNEL CAPACITY UNDER THE OVERLAPPED MULTIPLEXING PRINCIPLE IS MUCH HIGHER THAN THE SHANNON CHANNEL CAPACITY

Prof. Daoben Li firstly pointed out the error of Shannon's theory that multi-level modulation constellations must be used to improve the spectral efficiency of the system, and proved that under the guidance of the Ov principle, the optimal input data in both in-phase I and orthogonal Q channels should be ortho-anti (+, -) binary data, and that, in order to improve the spectral efficiency of the system, one should never follow Shannon's theory and use multi-level modulation signaling, but only adopt the overlap-multiplexing method with a greater number of overlapping repetitions. multiplexing. This concept is perfectly reasonable, although multiple data inputs allow more information to be loaded into each input data symbol, in a multiplexed Ov system, to ensure the same spectral efficiency, the number of overlap weights of the system with multiple data inputs will be proportionally lower compared to the binary data, and the Ov coding gain will be reduced, which is more than worth the cost. In this way, in $K \geq 2$ order overlapping multiplexed Ov systems ($K = 1$ order Ov will degrade to Shannon system), Prof. Daoben Li obtained the following three simple Ov theoretical formulas:

- The spectral efficiency of the Ov system is $\eta \triangleq C / B_{nai} = 2K, K \geq 2$;
- The normalized threshold signal-to-noise ratio of the Ov system is $E_b / N_b = 1.5K, K \geq 2$;
- The channel capacity of the Ov system is $C = 2KB_{nai}, K \geq 2$.

This is a single linear equation much simpler than the Shannon capacity formula. It can be seen that the Ov channel capacity and system spectral efficiency grows only linearly with the number of system overlap weights, K, or more rigorously, only linearly with the received bit energy.

According to the Ov principle, the Ov capacity is much higher than the Shannon capacity. The huge difference between Shannon capacity and Ov capacity can be seen in the following three figures. The theoretical and practical performance simulation results for the direct implementation of Ov principle OVXDM are also given in the figures.

The horizontal coordinate of the graph is the normalized signal-to-noise ratio in decibels (dB), $10Log\frac{E_b}{N_0}=10Log(\frac{P_S}{P_N}BT)$; the vertical coordinate is the spectral efficiency of the Ov and Shannon systems $\eta(bps/Hz)$, i.e., bits/sec/Hz (in Nyquist bandwidth).
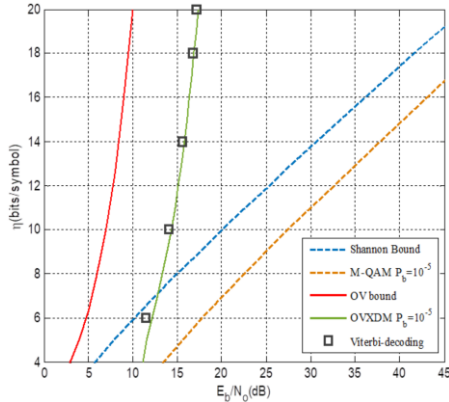
Figure 1. Simulation results of Shannon bound, Ov bound, QAM, OVXDM theory and optimal algorithm ($\eta \le 20bps/Hz$ Nyquist bandwidth)
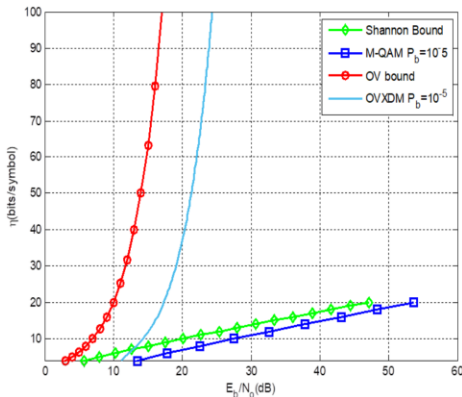
Figure 2. Comparative results of Shannon boundaries, Ov boundaries, QAM, OVXDM ($\eta \le 100bps/Hz$ Nyquist bandwidth)
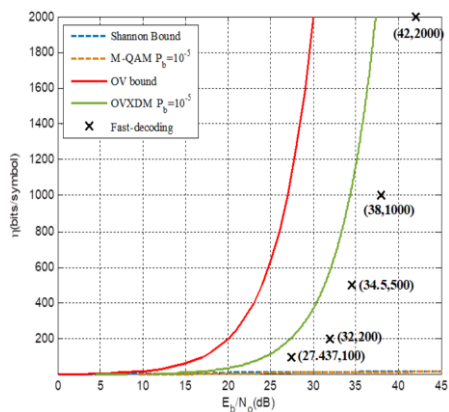
Figure 3. Comparative results of simulation of Shannon bound, Ov bound, QAM, and OVXDM fast algorithms ($\eta \le 2000bps/Hz$ Nyquist bandwidth)

As can be seen from these figures, to achieve $\eta = 16bps/Hz$, the normalized SNR of Ov is only $1/1049$ in the Shannon sector; to achieve $\eta = 2000bps/Hz$, the normalized SNR of Ov is only $1/10^{596.4}$ in the Shannon sector.

For the Shannon system to also implement $\eta = 16bps/Hz$ and $\eta = 2000bps/Hz$, it would have to use the constellation maps of the $\ge 2^{16} = 65536$ and $\ge 2^{2000}$ constellation points (the upper bound of the number of atoms of the Earth's matter at $\le 2^{250}$), and the normalized SNRs would need to be at least $\ge 10Log\frac{2^{16}-1}{16} \cong 41dB$ and $\ge 10Log\frac{2^{2000}-1}{200} \cong 5967dB$, respectively. That is, the normalized SNR of the Shannon system must be higher than $10^{4.1}(41dB)$ at $\eta = 16bps/Hz$ and higher than $10^{596.7}(5967dB)$ at $\eta = 2000bps/Hz$, while the maximum physically achievable normalized SNR is about $10^{4.3}(4.3dB)$!

The Ov system can provide spectral efficiency far beyond the Shannon bound under realizable SNR conditions! The threshold SNR of its Ov capacity bound at $\eta = 2000bps/Hz$ is only $30dB(10^3)$; the threshold SNR of the non-optimal OVXDM regime is only $37dB(10^{3.7})$; a fast decoding algorithm simulation result is $42dB(10^{4.2})$, and the threshold SNR of the $\eta = 455bps/Hz$ design is $16.1dB(40.6)$, both of which are within the realizable range!

According to the conventional wisdom, the capacity of mobile communications is increased by an order of magnitude with each new generation, and there is no doubt that Ov's capacity has been increased by more than two orders of magnitude compared to today's 5G, so it is not an overstatement to say that Ov is a post-7G technology.

Information theory is from physics, should comply with all the basic principles of physics, Professor Li in his IEEE article criticized the Shannon information theory and the laws of physics in the transport and construction is

contrary to the principle of conservation of energy is who can not be contrary to the bit of energy can never come out of thin air. If the received bit energy is not up to the standard, and then the good code is also a clever woman can't cook without rice, Shannon has a residual code will only be the icing on the cake, can't send charcoal in the snow, Ov out of control spectral waveform coding can be the icing on the cake, but also to send charcoal in the snow, once found that the received bit energy is not enough, it will automatically increase the code in the carrier frequency and antenna number, in order to increase the total transmit power.

Why is the difference in channel capacity between Shannon theory and Ov theory so dramatic? This is because the noise spectral density N_0 is not controlled by coding, and when the channel capacity grows with spectral efficiency, Shannon theory requires exponentially growing bit energy, while Ov theory only requires linearly growing bit energy. Obviously, Ov theory, in which the channel capacity grows linearly with bit energy, is more in line with physics than Shannon theory, in which the channel capacity grows exponentially with bit energy. In the white Gaussian noise interference environment, the received bit energy is the only index that determines the system performance, although the attained bit energy of Ov capacity is much smaller than that of Shannon's, but no coding can increase the bit energy out of nothing, and Ov is no exception. Communication cannot be separated from the channel coding, in the received signal power is certain, Shannon system of received bit energy is increased by increasing redundancy, reducing the effective bit transmission rate increases, resulting in the Shannon coding gain is higher, the system spectral efficiency will always be one hundred percent, and the higher the spectral efficiency, the higher the Ov coding gain on the contrary.

The Ov principle, which strictly adheres to the fundamental laws of physics, completely subverts Shannon's theory, which states that the spectral efficiency and capacity of the system only grows linearly with the energy of the received bits, and never exponentially with the energy of the received bits as stated in Shannon's theory, thus pointing out a bright prospect for the development of communications. OVXDM (Overlapped X Domain Multiplexing) is the simplest and most direct application of the Ov principle of transmission system, but also the simplest coding efficiency of 100 percent of the non-redundant waveform coding.

Prof. Li has not only derived the Ov capacity bound, but also found the universal overlapping time, frequency, space sequence multiple access waveform compilation code method that can approach the Ov bound under any spectral efficiency, and found that its decoding complexity is very low, so low that it can be detected bit by bit in a surprisingly low way! The decoding complexity of the optimal non-coded OVXDM also increases exponentially with the spectral efficiency, which means that the decoding complexity of the Ov coding system is extremely reduced compared to that before coding, which shows that the power of overlapping time, frequency, and spatial sequences of multiple-access waveform coding is huge! Excellent Ov sequence multiple access waveform coding should have the following basic characteristics:

- The coded Ov system should exist a steeply falling threshold SNR, which is controlled by the selection of multiplexed waveforms and the length of the Ov intrinsic coding constraints, when the received SNR is lower than the threshold, the error probability of the coded Ov system not only does not improve but worsens, and once the received SNR is higher than the threshold, the error probability will be a sharp and steep decline without a plateau approaching zero;
- The steepness of the error probability of the coded Ov system is controlled by the length of the Ov coding constraints, and the longer the coding constraints the steeper the steeper the drop;
- The receive threshold SNR at which the error probability of the coded Ov system is equal to a particular value such as 10^{-5} is close to the Ov bound;

- the coding Ov system does not exist error floor, that is, the current further increase in the reception of SNR, the error probability will only be further reduced until zero, there will be no irreducible error probability;
- The power spectral characteristics of the coded Ov system are gradually approximated to the ideal rectangle as the coding constraint length increases;
- Coding Ov systems are encoded in a universal way and are used uniformly for any spectral efficiency;
- The decoding complexity of the coded Ov system should not be high, and it is desirable that it can be done on a bit-by-bit basis.

VII. WHAT IS OVXDM?

OVXDM (Overlapped X Domain Multiplexing) is one of the simplest technical means of realizing the principle of overlapped multiplexing in a communication system, e.g., Time Domain $X = T$, Frequency Domain $X = F$, Hybrid Domain $X = H$, etc.
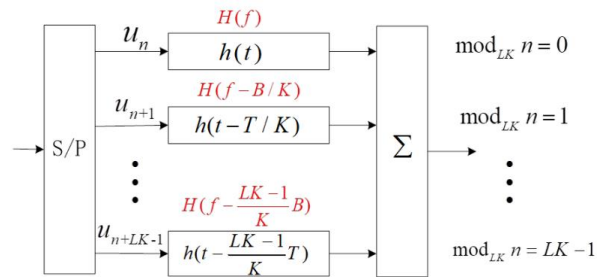
$$H(f) = 0, \forall f \notin [f_C - B/2, f_C + B/2), \ h(t) = 0, \forall t \notin [0, T)$$

Figure 4.   OVXDM system model

OVXDM belongs to a new waveform coding, which is a direct and simple application of the OV principle, but is not optimal overlap multiplexing, and is about 7 dB away from the OV boundary. OVXDM does destroy the one-to-one correspondence between the input data and the output symbols, but retains the one-to-one correspondence between the input data sequences and the overlap-multiplexed output waveform sequences! This will lead to the necessity of sequence decoding for OVXDM, and since the complexity of optimal sequence decoding grows at

an exponential rate with the spectral efficiency, fast sequence decoding algorithms with a loss of performance are generally used when the system's spectral efficiency is high (Fig. 3), whereas after the invention of the three-dimensional overlap-multiplexed waveform coding in time, frequency, and space invented by Prof. Li, the decoding complexity can be reduced to an amazingly low bit-by-bit process instead.

The output power of OVDXM grows not exponentially with the spectral efficiency (number of overlapping reps) of the system as Shannon pointed out, but only at a linear rate, which is the reason why the required transmit power of OVXDM is much smaller than that of existing systems. In addition OVDXM belongs to the new waveform coding, which is known to be able to distinguish the desired weak signals based on the characteristics of the waveforms even in strong background noise environments, which is another reason why OVXDM requires only a small transmit power.

OVDXM's strong anti-jamming capability reflects the truth that unity is strength, and the bigger the team, the stronger it is. Existing communication systems are simply scattered compared to it, and cannot withstand even a small blow (interference).

VIII. WHY THE DISCOVERY OF THE PRINCIPLE OF OVERLAP MULTIPLEXING IS BOUND TO LEAD TO A REVOLUTION IN COMMUNICATION AND INFORMATION TECHNOLOGY?

1) There are five main requirements for wireless communication systems:

Large coverage (propagation distance as far as possible); high spectral efficiency (the smaller the occupied spectral resources, the better); high power efficiency (the smaller the occupied energy resources, the better); support for high-speed mobility; high confidentiality and security; high reliability.

2) With the arrival of the information society, people's demand for information is explosive, and the demand for communication capacity is also explosive growth, has grown from Kbps (kilobits per second) to Gbps (gigabits per second) to Tbps

(terabits per second). And the achievable SNR is limited by environmental conditions can not be increased indefinitely, half should be satisfied $E_b / N_0 < 43dB$. Then, according to Shannon's boundaries, increasing the system capacity C can only be achieved by expanding the system bandwidth B and thus increasing the carrier frequency f_c . Also according to Maxwell's equation, the propagation loss of radio waves in free space decays with the square rate of the product of the carrier frequency f_c and the transmission distance r $(f_c r)^{-2}$. If the carrier frequency of the system is increased from $f_c = 1GHz$ to $f_c = 100GHz$, the transmission loss will increase by a factor of 10,000 $(40dB)$ at the same distance r ! In addition, as the carrier frequency f_c increases, the ground Doppler frequency spreads more and more, in addition to the coverage area is getting smaller and smaller, and the moving speed that the ground wireless system can support will be lower and lower. Nowadays, the development of 2G, 3G, 4G and 5G ...... is in the trend of deterioration by G. The reality requires that the capacity of the communication system is getting higher and higher. The reality requires that the capacity of the communication system is getting higher and higher, but the coverage of the Shannon system is getting smaller and smaller, supporting the mobile speed is getting lower and lower, and the power consumption is getting bigger and bigger with the bandwidth widening. Power consumption is large in addition to the carrier frequency f_c increase, bandwidth expansion caused by the device itself, mainly because of the modern communication system are required to linear amplifier, there must be power back, power amplifier conversion efficiency itself is low, the higher the carrier frequency f_c , the wider the bandwidth, the power amplifier power consumption and cost is also higher.

3) The first generation of mobile communications (1G) was analog, using a carrier frequency of a few hundred MHz, which was optimal for terrestrial propagation, and occupying a bandwidth of 30 KHz. Despite the backwardness of the technology, it was able to cover a range of 5-10 kilometers and support speeds of several hundred kilometers per hour. Subsequent developments in mobile communication systems have been relatively advanced digital technologies, with mobile communication systems being updated about every 10 years from the second generation (2G) onwards, with 5G now being commercially available and 6G already under development.

4) With the explosive growth of the demand for information, mobile communication is constantly upgraded, the capacity provided by the mobile communication system, i.e., the highest transmission rate, every new generation than the previous generation of about an order of magnitude; occupies the bandwidth proportionally widened by an order of magnitude; bandwidth expansion of the consequences is the carrier frequency must be increased with it. The consequence of the carrier frequency increase is one generation more than one generation is more unsuitable for terrestrial mobile communication, the scope of the coverage of one generation more than one generation shrinks, 2G can still cover about 2-3Km. to 5G when there are only 200-300m left; support mobile speed is more and more generation by generation reduction, from 2G 200-300 km / h generation by generation shrinks to the basic requirements of the 5G does not support the mobile; base station and cell phone is more and more generation by generation atypical, such as the 5G Base station is power consumption is about 4G 3-4 times, coverage radius is only 4G 1/3-1/4. this is an indisputable fact, no need to repeat. According to the development of this trend, the future of mobile communications systems should be to carrier frequency higher, less suitable for mobile communications millimeter wave and terahertz band into. Consequences are bound to be the base station coverage will only be smaller, more difficult to support mobile state communications, cell phones and base stations will only be greater power consumption, so the development prospects are not complimentary. Unfortunately, at present, domestic and foreign mobile communications will inevitably millimeter-wave and terahertz and even laser frequency bands

into the mainstream trend seems to have been lamentable and sad!

5) Overlap multiplexing principle can be used to significantly improve the spectral efficiency in addition to the time domain, frequency domain, air domain three-dimensional coding can also be used in power synthesis to improve power efficiency, that is, in the Ov system, you can use a number of small power amplifiers to synthesize a high-power output, and non-Ov of today's Shannon system is absolutely not possible to do this.

IX. CRITICIZING SEVERAL ERRONEOUS VIEWS OF 6G R&D

A. *Using ultra-large-scale MIMO*

Cover, recipient of the Shannon Centennial Award for Distinguished Contributions, finds that the capacity and spectral efficiency of a system of independently parallel Gaussian channels is equal to the sum of the independent parallel subchannels in a Gaussian noise interference environment. The system can have extremely high total capacity and spectral efficiency, and the performance is determined by the number of independent parallel channels and the total received signal-to-noise ratio.

An independent parallel Gaussian channel should have the following two basic characteristics:

- Each sub-channel has independent transmission data independent of Gaussian noise;
- All subchannels occupy the same time-frequency space.

It must also have the following four characteristics:

- The total received signal-to-noise ratio is equal to the sum of the received signal-to-noise ratios of the sub-channels;
- The total system capacity and spectral efficiency is equal to the sum of the sub-channels;
- The total system capacity and spectral efficiency grow linearly with the total received signal-to-noise ratio;

- The system has very high capacity and spectral efficiency.

A Multiple Input Multiple Output (MIMO) system in a rich scattering channel is a naturally occurring independent parallel Gaussian channel transmission system, the principle of which will not be repeated. The number of independent parallel channels is equal to the smallest of the number of independent antennas at the transmitter and receiver, i.e., $Min(T_T, T_R)$, where T_T is the number of independent antennas at the transmitter end (the total transmitter energy increases linearly with T_T) and T_R is the number of independent antennas at the receiver end, and the extra antennas will be designed to provide graded gain to improve the system performance. Apparently, by increasing $Min(T_T, T_R)$, the total system capacity and spectral efficiency can be increased "without limit", but can this really be the case?

First of all, MIMO must rely on the rich scattering propagation environment, can only work in urban environments of high-density complexes and indoor and other rich scattering environments, for the poor scattering or even no scattering flat open environment, such as large areas of farmland, open plains and grasslands, the sea, airplanes and airplanes, airplanes and the ground, especially satellites, deep space, unmanned aerial vehicles, and other channels whose effectiveness will be lost or greatly reduced.

Secondly, MIMO must take up a lot of space resources, which seems to be less of a problem for mobile base stations, but what about cell phones? How many antennas can be placed on a small cell phone to meet the independence requirements? Some people say that we can consider cooperative communication, so that multiple cell phones work together to realize the receiving end of the multiple antennas. Is it possible to realize "cooperative" communication with multiple cellular phones? What if there are not many cell phones around? And how much extra resources does it take to get them to work together? Last but not least, people nowadays attach great importance to personal privacy, so why can't they refuse to provide service to others when they don't need to

communicate with each other? Is there any danger that one's right to privacy will be compromised?

Finally, a MIMO system must have precisely known $T_T T_R$ fading channel characteristics, which will force the system to provide at least $T_T T_R$ "orthogonal" guides for measuring channel characteristics, consuming a huge amount of system resources that increase with the square law of MIMO size.

Is there an independent parallel Gaussian channel that requires only a single antenna for transmission and reception without the disadvantages of MIMO mentioned above? OVXDM, guided by the principle of overlap multiplexing, is the solution, eliminating the need for numerous frequency guides and providing extremely high capacity and spectral efficiency. Since OVXDM implements Gaussianized overlap multiplexing on its parallel input data symbols, and the independence of the shifted Gaussian noise itself, OVXDM has all the two core features and four features mentioned above for independent parallel Gaussian channel, and OVXDM's threshold SNR only grows linearly with the channel capacity and the spectral efficiency, and its system capacity and the spectral efficiency grows linearly with the received SNR, all of which are consistent with MIMO. growth, all of which are known with MIMO. The author fully demonstrates that OVXDM is indeed an independent parallel Gaussian channel transmission system under Gaussian white noise interference environment.The independence of MIMO subchannels is formed by the independent complex Gaussian fading of the subchannels, whereas the independent Gaussianity of the OVXDM subchannels is formed by the independence of the subchannels' Gaussian noises and the overlapping multiplexing of Gaussianization of their parallel independent data symbols. It is valuable that it is not limited by propagation conditions and can work in any channel, both fading and non-fading channels, and the above limitations for practical MIMO systems will disappear!

B. *Future mobile communication intelligence to millimeter wave and terahertz band development.*

This seems to have become the consensus of the US-led Western bloc and domestic forces following the West, who believe that the potential of the Shannon theory has been nearly exhausted, and that in addition to MIMO, moving to higher frequency bands and further expanding the system bandwidth is the way out (see their 6G white paper).

The transmission distance of mobile communication should be as large as possible, and the bypass penetration ability should be very strong. Millimeter-wave terahertz and even laser band transmission loss is very great, no penetration ability, no bypass ability, atmospheric composition, leaves, dust, haze, water vapor, etc., its absorption loss is very large, blindly tracking the West, refused to resist new theories and new technologies to the high frequency band forward will only lead the country's mobile communications to extinction.

Only in the Ov principle of waveform coding theory, under the guidance of a substantial increase in the narrow bandwidth suitable for mobile communications, lower frequency band spectral efficiency, increase the capacity of the Ov system does not need to widen the bandwidth, higher carrier frequency, all the Shannon theory under the guidance of the system is impossible to solve the contradictions in the Ov system can be solved.

C. *"Low-orbit satellite systems such as Starlink and Starshield".*

They are a cover for maintaining space hegemony, espionage, military use and seizure of orbital and frequency resources under the guise of claiming to be able to provide global wireless Internet services using tens of thousands of low-orbiting satellites. A measure of wireless Internet quality is the maximum number of gigabits per second (Gbps/Km2) per square kilometer. 4G, for example, has a carrier frequency of a few GHz (5Ghz as an example) covering about 1Km (1Km as an example). Star Chain, Star Shield satellite

from the ground at least 330Km, otherwise it will fall down quickly, the transmission distance is at least 330 times that of 4G, the free space loss in the same frequency band is at least 100,000 times higher than that of 4G ($\geq 50dB$). For this reason, the star chain, star shield satellite two sections have to use high gain antennas, which in turn proportionally reduce its coverage, mobile interconnection indicators Gbps/Km2 unchanged. Transmission loss is extremely large, mobile, mobile interconnection index Gbps/Km2 is far lower than the ground mobile network is the root cause of its inability to provide global 6G wireless interconnection services. As of August 1, 2023, China has built nearly 4 million terrestrial 5G base stations, has not yet covered ten percent of the country, a few tens of thousands of small microsatellites away from the earth can provide global 6G Internet services? A fool's errand, right? The Americans claimed success in its transceiver two sections are using directional antennas in the laboratory, a little specialized knowledge of the people understand that the success of individual cases can not confirm its inability to provide 6G services to as many as billions of users around the world in essence, can not cover up the pollution of space, the creation of a huge amount of space debris, and military, espionage, seize the frequency, the space orbit resources, the maintenance of hegemony in space of the wolf's ambitions.

X. THE IDEA OF ESTABLISHING CHINA'S ULTRA-HIGH-CAPACITY SPACE, AIR, GROUND, SURFACE-TO-SURFACE AND UNDERWATER NETWORK INTEGRATED WIDE-AREA COMPREHENSIVE OV NETWORK.

The biggest advantage of Ov is to improve the system capacity and spectrum efficiency under the condition of physically realizable SNR, which has nothing to do with the frequency band used! For this reason, we can use Ov technology, synchronous research and development in different networks, and gradually greatly improve the capacity of the ground wireless backbone network, fiber optic backbone network, step by step to build China's unique wide-area air and space integrated Ov core backbone network.

A. Terrestrial fiber optic cable & wireless backbone.

It is the economic traversal means of 1G-5G for users in large densely populated areas, but it can not cover all environments, especially it can not provide services in some special and harsh environments, such as vast oceans, high mountainous areas, underwater, ground to underwater, bridges and tunnels, and underground and other special environments. In the future, Ov technology should be used to transform it into an ultra-high-capacity network.

B. Formation of China's unique ultra-high-capacity space Ov backbone network.

The space satellite network can provide global services especially in some special environments, for this reason, it is necessary that the ultra-high-capacity satellite backbone network should be combined with the ultra-high-capacity terrestrial fiber optic cable + wireless backbone network, stratospheric backbone network, unmanned aerial vehicle (UAV) network, ground-to-water underwater network, underwater communication network and so on to form a wide-area integrated ultra-high-capacity Ov-info network in the sky, in the air, on the ground, and under the water.

Millimeter wave, terahertz and even laser should be used for links between most satellite network nodes (including stratospheric or terrestrial fiber-optic cable + wireless network nodes, hereinafter the same) that do not require wide-area coverage. Their wavelengths are extremely short, available very small size antennas to provide star-to-star, star-to-ground or ground base station between the very narrow beam high antenna gain point-to-point links to make up for their transmission loss of large coverage of the small shortcomings of the satellite network of the core node is responsible for linking with the stratospheric or terrestrial fiber optic cable + wireless network, the stratosphere or terrestrial fiber optic cable + wireless network nodes are exactly the same. Millimeter-wave, terahertz, and lasers have extremely wide available bandwidths and can provide very large capacity. Satellites, stratospheric, terrestrial fiber optic + wireless, terrestrial-to-submarine, and underwater can

complement each other to form a powerful integrated wide-area Ov information network. They (including non-wireless terrestrial and underwater fiber-optic cable networks) should be ultra-large-capacity networks using Ov technology, and satellite networks and stratospheric and terrestrial Ov networks can complement each other to form a powerful integrated Ov information network in the air and the sky.

As for the topology of the network, it should not follow Musk's simple chain, but should be the best lattice structure. Due to Musk one-sided pursuit of low orbit, low cost, have to use small micro-satellite, low orbit will make its satellite life is very short, must constantly launch new stars to replenish, small micro-satellite solar panels and antenna size is not likely to be large, the transmitter power is not likely to be high, transmitter antenna gain will not be too high, resulting in the user must be configured with high gain antenna. Coupled with the relative high-speed movement of satellites, and ground communications can only be high-speed chain switching between the stars, switching and consume a lot of resources, and low-cost small micro-satellite and have to use relatively backward and simple signal processing and handover switching technology, the star processing capacity is not likely to be high, and can not be realized on-demand jumping between the satellites to interconnection and interoperability.

Therefore, our space network should be composed of satellite Ov-networks with ultra-high capacity guided by the principle of overlap multiplexing, which may be deployed in low, medium, and high orbits, respectively, as needed, and in the next section are my suggestions for other compositions of an integrated Ov-network of heaven, earth, and space.

C. *Deployment of the Ov ultra-high-capacity stratospheric airship communications monitoring network.*

Stratosphere is 35Km-55Km from the ground in the atmosphere, the temperature is basically constant (-55 ℃ or so, also known as the stratosphere), the air velocity is stable and very slow, can make the airships for a long time

relatively fixed in the high altitude, its altitude will not be higher than the orbiting satellites of the 1/10, the ground communication transmission loss will not be higher than the low-orbit satellites of the 1/100 (20dB), which applies to a variety of frequency bands. Airship cost is very low, the volume can be very large, especially tethered airships, and the ground with fiber optic cables and cable links, it is easy to deploy ultra-high-power, large size antennae, ultra-high-capacity stratospheric communication and detection network. Use it to implement the ground detection, can get far more than the satellite detection of the fineness of the image, as a mobile communication base station, preliminary estimates in the Ov system, only need to configure no more than 3G base station airships can be realized in all of the country and territorial sea coverage. Due to the different networking methods with the ground base station, the base station is all high gain downward narrow beam, not the ground base station low gain horizontal wide beam, the signal level in the coverage area is more uniform relative to the ground base station, basically can not consider the interference between base stations, antenna gain can be much higher than the ground base station, cell phones do not need additional configuration of the directional antenna, the automobile, high-speed railroads, airplanes, missiles, sea vessels, etc., including the quality of the users provide Far beyond 5G, far beyond the star chain, star shield of the Internet and special services, stratospheric airship base station can completely replace the traditional ground mobile base station, and floods and earthquakes and other natural disasters will not affect its work, can keep the communication has a higher reliability. In addition, with little additional cost, it can jam or block out the Musk Starlink and local satellites located above it. Because it is higher than all airborne vehicles, it has virtually no effect on their flights, and can be deployed intensively over key areas during war to intercept and provide real-time warning of attacks from space.

D. *Deployment of terrestrial, air-to-underwater Ov ultra-long-wave communications networks.*

Although the existing ultra-long-wave communication system guided by Shannon's

theory can realize such communication, its capacity is still very low, and with the adoption of the Ov principle system, it is entirely possible to increase its capacity by one or two orders of magnitude over the existing system.

E. Deployment of the underwater mobile sonar Ov communication network.

Although the capacity of existing sonar communication systems under Shannon's theory is still very low and the transmission range is very limited, it is entirely possible to increase its transmission range by one or two orders of magnitude and its capacity by one or two orders of magnitude over the existing system with the adoption of the Ov principle system.

F. Deployment of the Ov ultra-high-capacity ionospheric scattering communications network.

The ionosphere is an atmospheric layer from 50Km to 100Km from the ground, and because the atmosphere in this layer is ionized by solar radiation, it has a scattering effect on electromagnetic waves of short-wave frequency, which can realize long-range communication over several thousand Km. Although the capacity of the existing ionospheric scattering communication system under the guidance of Shannon's theory is very low, after adopting the system of Ov principle, it is completely possible to enhance its capacity by one or two orders of magnitude compared with the existing system.

G. Deployment of the Ov ultra-high-capacity tropospheric scattering communications network.

The troposphere is an atmospheric layer from 8Km to 18Km from the ground, and due to the inhomogeneity of the convective air mass, it scatters electromagnetic waves in the microwave band, allowing long-distance communications over thousands of Km. Although the capacity of the existing tropospheric scattering communication system guided by Shannon's theory is not high enough, it is entirely possible to increase its capacity by one or two orders of

magnitude over the existing system with the adoption of the system based on the Ov principle.

H. Deployment of the Ov UAS emergency communications network.

The low cost of drones and the fact that they can fly at altitudes ranging from near the ground up to the stratosphere allow for the establishment of emergency high-capacity communication networks anywhere and at any time.

F, G, H three to ensure that China's wartime and emergency communications is essential. The above networks are all established under the guidance of the Ov principle, the final formation of a comprehensive wide-area Ov information network is able to provide information services to the global network, a variety of networks are indispensable.

XI. SCENARIOS FOR THE INTEGRATION OF SPACE, AIR AND GROUND INTO THE WIDE-AREA OV INFORMATION NETWORK AND INTERNATIONAL CONNECTIVITY

The world cannot be separated from the Internet without a moment's notice, and there can be no national security without information security! The Internet is the United States according to the Shannon multi-user information network theory established in the 1970s, and then constantly updated and upgraded, but a thousand changes, the core of the ability to control more and more strong, in order to achieve global information hegemony. The United States long-term efforts and even free promotion of the Internet, the same as GPS, the international community generally fooled into using the Internet, so that many people mistakenly believe that the Internet is the Internet. In fact, the Internet is only a network of Shannon's Multi-User Information Network (MUIN), which, like Shannon's theory, should be eliminated. The United States in order to maintain its information hegemony, in addition to controlling the GPS is also firmly held the Internet's "main root", although the hypocrisy of allowing countries to have some of the network "root", but can never touch the "main root! Although it is hypocritical to allow countries to

have some network "root", it can never touch the "main root", but only the "mirror root". So that the United States can be free to steal the secrets of other countries, to master the global information hegemony, the Internet and GPS is the United States to control the global information hegemony of the killer mace. You enter the GPS, your whereabouts can not be mastered? You enter the Internet, your information secrets can exist? In order to break the U.S. hegemony, our country should not only stay away from GPS, but also firmly abandon the Internet, including its improved version of IPv6! The construction of a wide-area Ov information network with independent intellectual property rights under the theory of revolutionary Ov multi-user network. Initially, only a number of geostationary orbit satellites and fiber optic cable nodes to achieve international interconnection and interoperability with the system swap. the construction of Ov network should take the BeiDou, mobile communications and high-definition point of time to gradually update and iterative way, the initial coexistence of old and new systems, and ultimately, because of the absolute advantage of the Ov will soon be widely accepted, so as to fully replace the old system, and promote the global.

XII. OUTLOOK

Using the overlapped multiplexing theory and its guidance of time domain, frequency domain, air domain overlap sequence multiple access waveform coding technology, only need to use the transformation of the existing system's basic architecture, equipment in addition to the baseband part of the other parts can be largely retained only need to do the corresponding changes to them, the system performance can be far better than the plan of the 6G, to meet the needs of the future 7G and beyond. Especially the stratospheric base station communication can realize the huge saving of frequency and energy resources and the green communication with higher security, and the safe and reliable national information network investment and will be a huge saving. Chips developed based on the new theory will certainly promote the whole communication and information system, information network upgrading, which will produce the next generation of new green, safe, secure and reliable information system.

Overlap multiplexing principle is discovered by Chinese people, overlap multiplexing waveform coding theory is the foundation of Chinese people, time domain, frequency domain, space domain three-dimensional overlap sequence multiple access waveform coding theory and technology is also the foundation of the Chinese people and the invention of the future of mobile communications, satellite communications, underwater communications, ground to underwater, and even wide-area information network capacity has a huge increase in the huge savings in resources. At the same time, information security, information security, electronic countermeasures, electronic concealment, wide-area information networks and other related fields are bound to change, and will certainly affect the information industry field upgrading. The national economy, especially the defense industry will bring significant social and huge emergency benefits.

UAV Path Planning Based on Deep Reinforcement Learning

Yifan Guo

School of Computer Science & Engineering

Xi'an Technological University

Xi'an, China

E-mail: 958782423@qq.com

Zhiping Liu

School of Computer Science & Engineering

Xi'an Technological University

Xi'an, China

E-mail: leopard@xatu.edu.cn

Abstract—**Path planning is one of the very important aspects of UAV navigation control, which refers to the UAV searching for an optimal or near-optimal route from the starting point to the end point according to the performance indexes such as time, distance, et al. The path planning problem has a long history and has more abundant algorithms. The path planning problem has a long history and a rich set of algorithms, but most of the current algorithms require a known environment, however, in most cases, the environment model is difficult to describe and obtain, and the algorithms perform less satisfactorily. To address the above problems, this paper proposes a UAV path planning method based on deep reinforcement learning algorithm. Based on the OpenAI-GYM architecture, a 3D map environment model is constructed, with the map grid as the state set and 26 actions as the action set, which does not need an environment model and relies on its own interaction with the environment to complete the path planning task. The algorithm is based on stochastic process theory, modeling the path planning problem as a Markov Decision Process (MDP), fitting the UAV path planning decision function and state-action function, and designing the DQN algorithm model according to the state space, action space and network structure. The algorithm enables the intelligences to carry out strategy iteration efficiently. Through simulation, the DQN algorithm is verified to avoid obstacles and complete the path planning task in only about 160 rounds, which validates the effectiveness of the proposed path planning algorithm.**

Keywords-Component; UAV; Path Planning; DQN; Deep Reinforcement Learning

I. INTRODUCTION

In recent years, unmanned aerial vehicles (UAVs) have been used in a wide variety of fields and nowadays, UAVs are always used to collect data for humans in dangerous places. Quadrotor UAVs, as a type of UAV, have a wide range of applications (due to their hovering capabilities and low condition takeoff and landing capabilities) such as search and rescue, aerial photography, environmental monitoring, industrial inspection, et al [1]. Regardless of the mission, autonomous path planning is always the key to accomplish the task.

Traditional path planning methods are relatively mature, such as Dijkstra's method, A* algorithm, D* algorithm, and artificial potential field method, et al [2]. These methods have been widely used in some scenarios, but as the difficulty of the task to be performed increases, especially in unknown environments, the path planning problem becomes more complex and increases the uncertainty, from the existing path planning methods, each method has its own advantages and shortcomings, and none of them has the ability to learn, and also does not have the ability to cope with the changes in the environment and the uncertainty.

In recent years, artificial intelligence and machine learning (ML) have been widely used in the field of robotics, and reinforcement learning (RL) is even more with the improvement of algorithms and theories, with the ability to apply its latest theoretical achievements to the actual control of robotic systems. Based on the theoretical foundation of reinforcement learning, this paper proposes a deep reinforcement learning (DRL)-based UAV path planning method different from the traditional method, which can make the UAV obtain human-like learning ability, and in

the task with high difficulty coefficient, unknown environment, complex and uncertain factors, it can cope with unexpected situations and complex terrain to a considerable extent and complete the task. A 3D map environment model is constructed based on the OpenAI-GYM architecture, with the map grid as the state set and 26 actions as the action set, which does not need an environment model and relies on its own interaction with the environment to accomplish the path planning task. The algorithm is based on stochastic process theory, modeling the path planning problem as a MDP, fitting the UAV path planning decision function and state-action function, and designing a DQN algorithm model based on the state space, action space and network structure. The algorithm enables the intelligences to carry out strategy iteration efficiently. Simulation experiments demonstrate that the DQN algorithm can avoid obstacles and realize the path planning task in only a small number of rounds, proving the effectiveness of the proposed algorithm.

II. RELATED WORKS

The path planning problem has a long history, and scholars at home and abroad have made a large number of research results. Path planning is one of the very important aspects of UAV navigation control, which means that the UAV searches for an optimal or near-optimal route from the starting point to the end point according to time, distance, and other performance metrics. Its essence can be treated as a conditional optimization problem, and the optimization index will be different in the face of different demands. For different task requirements, scholars have proposed a large number of methods from different angles and different fields.

Traditional path planning methods are relatively mature and have been widely used, with the continuous completion of reinforcement learning theory and the vigorous development of methods, many traditional problems can be solved under the framework of reinforcement learning, and the path planning problem is one of them [3]. RL, as an important research direction in the areas of ML, optimizes action strategies based on the interaction between an intelligent body and its

environment, and scholars have been paying more and more attention to this direction in recent years. Different from traditional methods, reinforcement learning enables agents to learn optimal strategies autonomously and maximize cumulative rewards through trial-and-error interactions with the environment [4]. As for deep reinforcement learning, which is the use of deep neural networks to solve the problem model of reinforcement learning, the integration of the two techniques can solve the problems of high storage capacity requirements for high-dimensional state and action space and complex model training, which were difficult to deal with in the past. Deep reinforcement learning is a technique that empowers intelligences to learn by themselves, so this method is very suitable for tackling the path planning problem of UAVs.

In terms of solving the path planning problem, Faust et al [5] used preference estimation to realize the path planning of robots in moving obstacle environments while solving the "dimensional catastrophe" problem, and Jaradat et al [6] proposed a new method to define the state space based on the Q-learning algorithm to reduce the number of states in dynamic environments, which effectively reduces the number of dimensions of Q-tables and improves the system learning efficiency. Method to reduce the number of states in a dynamic environment, which effectively reduces the dimension of the Q-table, accelerates the convergence speed, and improves the learning efficiency of the system. Shammah et al [7] combined deep learning with reinforcement learning methods and applied the policy gradient method, which successfully solved the path planning problem in automated driving, and improved the efficiency of the path planning problem. Wang et al [8] combined the Q-learning algorithm with Sarsa's algorithm and proposed a reverse Q-learning algorithm, which can improve the convergence speed and learning efficiency of the system. Bianchi et al [9] proposed an accelerated Q-learning algorithm based on a heuristic strategy, i.e., a heuristic function is used to help decision-making during action selection, and experiments show that a simple heuristic function can improve the convergence speed and

computational overhead of the reinforcement learning algorithm.

III. RELATED THEORETICAL STUDIES

A. *Definition of path planning*

Trajectory planning is one of the very important technical aspects of UAV navigation control. It is a trajectory from the start point to the end point that can avoid obstacles and is short enough based on the map environment information within the mission area and satisfies the aircraft's own physical performance constraints [10].

There are two methods for UAVs to perform path planning. The first is pre-flight planning; this method also needs to scan the surrounding environment and establish the initial model in advance when considering the mission target point, and to fully consider the impact of factors such as surrounding obstacles and weather on the trajectory. The second is real-time planning of the flight path. When using this method for planning, although there are fewer integrated factors to consider, satisfying the real-time nature of the path, it is necessary for the aircraft load to have a powerful chip to process the surrounding environment and update the path at any time. Therefore it will greatly increase the cost of flight cost. In this paper, the first UAV trajectory design method using pre-flight planning is chosen. At present, the theoretical technology about the trajectory planning in the two-dimensional plane is relatively mature and there are many related literature, but many of these algorithms degree cannot meet the requirements of three-dimensional space and do not have the actual flight. Because path planning in three-dimensional space is closer to real-life applications, the problem will definitely become a focus of research in the future, but when the space is expanded to three-dimensional space, it is necessary to consider not only the theoretical planning algorithm of the trajectory, but also involves GPS, sensor technology, et al. The requirements for path planning for UAVs are as follows:

- Flight paths that achieve mission requirements.

- The trajectory is a continuous curve or line from the starting point of the aircraft to the target point.

- Try to ensure that the path of the UAV is optimal, that is, to achieve the purpose of the algorithm to plan the path with the least amount of time or the shortest designed path.

B. *Markov Decision Process*

In DRL, the main core still lies in the foundation of RL, through the ability of deep learning to extract features and complex mapping of functions, some pain points in reinforcement learning will be solved. In reinforcement learning, it is mainly expected that an intelligence learns a behavioral strategy and is able to output a behavior corresponding to the current environmental information:

$$a = \pi(s) \tag{1}$$

Where a is the action and s is the state of the intelligent body in the environment. Depending on the environment, the actions and states may be discrete or continuous.

The problem of reinforcement learning can be modeled as a MDP, which is characterized by a system in which the state at the next moment is related to the current state only and is independent of the previous state, and by a MDP in which the state at the next moment is determined by the current state and the action at the current moment. The MDP can be defined by a five-tuple $< S, A, R, P, \gamma >$. The tuple $< S, A, R, P, \gamma >$ consists of the set of states S, the set of actions A, the reward function $R(s, a)$, the transfer function $P(s' \mid s, a)$, and the discount factor $\gamma \in [0,1]$. In each state $s \in S$, the intelligence takes an action $a \in A$. After performing the action a in the environment, the intelligence receives the reward $R(s, a)$ and arrives at the new state s', determined by the probability distribution $P(s' \mid s, a)$ [11].

Solutions to dynamic programming problems with finite states and action spaces can be obtained by a variety of methods, especially with a given

transfer probability. However, in most MDPs, transfer probabilities or reward functions are not available. In this case, the intelligence needs to interact with the environment to obtain some internal information to solve the MDP, which is achieved by reinforcement learning methods. The core problem to be solved by the Markov decision process is the strategy of choosing an action, which is mathematically represented using the π function as follows:

$$\pi(a|s_0) = P(a_t = a | s_t = s_0) \qquad (2)$$

C. Reinforcement learning algorithms

RL, also known as augmented learning, is a branch of ML [12]. The method differs from the common supervised learning and from unsupervised learning. RL is trained without explicit supervised data, i.e., the environment does not give explicit feedback that the action made by the intelligence at the current moment must be correct or incorrect; the environment simply helps the intelligence to learn by giving it a reward signal. Alternatively, instead of directly determining whether a state or action is good or bad, the environment assists the learning by giving a reward for a state or action. In the case of Go, for example, the current move is not directly judged as a correct or incorrect move, but a reward feedback is generated at the end of the whole game [13].

While the training data used in the traditional supervised and unsupervised learning training process are independent of each other, in RL the data are time-series related. The state generated by an intelligent body at each interaction with the environment influences the next move and the subsequent state.

RL is based on the principle that if an action taken by an intelligence in a state returns a positive reward to the environment, the tendency of the intelligence to take that action in that state will increase in the future. The basic model of RL, which views learning as a process in which an intelligence explores the learning environment, is shown in Figure 1. In RL, the intelligence selects an action a based on the current policy and passes it to the environment by observing the

environment at the current moment, and the new state is generated based on the state transfer matrix after the action is executed in the environment. At the same time, the environment also transmits a reward signal r to the intelligent body, which adjusts its strategy by using the reward signal r to generate the next action according to its strategy and the current state of the environment [14].
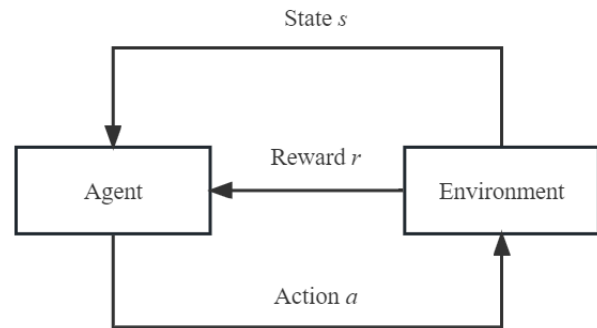

Figure 1. Reinforcement learning model

Reward r, is a scalar quantity that reflects the performance of the action produced by the intelligence in the environment performance in the environment, and the aim of the intelligence is to maximize the cumulative reward. RL is based on this hypothesis: the goal of all the goal of all problems can be expressed as maximizing the cumulative reward.

The intelligence and the environment, the RL problem can be described from both the perspective of the intelligence and the environment. At moment t, the perspective of the intelligent body is that it observes the state s_t of the environment, needs to make an action a_t at based on this state, and gets a reward signal r_t returned by the environment after executing this action in the environment. The perspective of the environment is that it receives the action a_t of the intelligent body to update the environment information, generates a new state, and gives a reward signal r_t back to the intelligent body.

State s, which can be divided into environment state, intelligences state, and information state. The environment state, which is the detailed description of the environment, including the data

of the next observation needed by the intelligence and the data of the reward signal r_t generated, et al., is usually not fully visible to the intelligence, that is, the intelligence sometimes does not know all the detailed data of the environment state, and even if sometimes the environment state is fully visible to the individual, these data may contain some data that are not needed by the intelligence. The intelligences state, which is the internal structure and parameters of the intelligence, includes all the data that the intelligence uses to determine future actions, such as network parameters, policy information, et al. The information state is all the useful data in the history, also known as Markov state.

From the above description it is shown that the state space S, action space A, the reward function R and the state transfer probability matrix P need to be designed in the RL algorithm. The state space is a characterization of the environment other than the intelligent body and is the basis of information provided to the intelligent body for selecting actions. The action space describes the decision details of the intelligent body. The reward function is the benefit of performing an action in a certain state, which is the evaluation of the goodness of the performed action, and is the most central part of RL. A good reward function often helps RL algorithms converge quickly and achieve good results and learn the best strategies.

D. Deep Reinforcement Learning

Deep reinforcement learning (DRL) was proposed because RL deals with problems with small sample spaces and discrete actions, while it does not work well for the kind of problems with huge state spaces and continuous actions [15]. Therefore, it is difficult to find good strategies in large state spaces using RL. DRL introduces neural networks in deep learning based on RL, combining both the technique of giving rewards based on actions in RL and the idea of using neural networks to learn feature representations by processing some high-dimensional state data through neural networks, training deep neural networks and learning the underlying features of the input data to approximate any nonlinear function. Its powerful representation capability

allows another breakthrough in the integration of RL with deep neural networks.
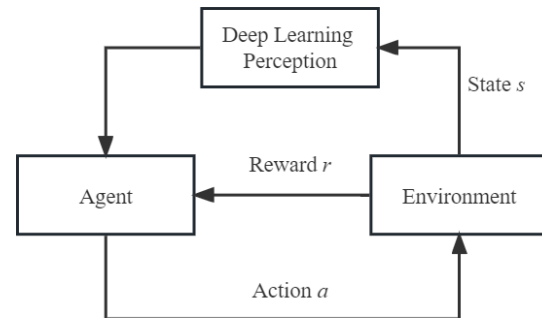
The basic model of DRL is shown in Figure 2.

Figure 2.   Basic model of deep reinforcement learning

IV. METHODS AND MATERIAL

The DQN algorithm is based on deep learning and Q-learning algorithms, i.e., it combines the advantages of both the feature-awareness capability of deep learning and the trial-and-error-learning capability of Q-learning algorithms. Based on the Q-learning algorithm, in order to overcome the shortcomings of using Q-tables that occupy a large amount of space and the inefficiency of updating in a high-dimensional state space, DQN is able to compute the action value function $Q(s,a)$ in a huge state and action space, and the DQN algorithm uses $Q(s,a,\theta)$ to approximate the optimal action value function as follows:

$$Q(s,a,\theta)=Q(s,a) \qquad (3)$$

Where $Q(s,a,\theta)$ is a deep neural network (DNN) with parameters θ, called Q-network.

When using the temporal difference (TD) method, $Q(s,a,\theta)$ is used to approximate $E\left[r+\gamma \max_{a'} Q(s',a',\theta)\right]$, and in the DQN algorithm, the set of loss functions of Eq. (4) is used as the optimization objective of the current network, and the gradient descent method is used to solve for its weights θ.

$$L(\theta) = E\left[\left(r + \gamma \max_{a'} Q(s', a', \theta) - Q(s, a, \theta)\right)^2\right] \quad (4)$$

However, the current Q value and the target Q value in Eq. (5) both use parameters of the same shape θ and are updated simultaneously, making the model training unstable and difficult to converge. To solve this situation, the DQN algorithm uses the old network parameter θ' to evaluate the state Q value at the next time step, and updates the parameter θ' every certain time step, providing a clearer reference target to the current Q network to be fitted in this way, and adjusting the optimization target to that shown in Equation (5).

$$L(\theta) = E\left[\left(r + \gamma \max_{a'} Q(s', a', \theta') - Q(s, a, \theta)\right)^2\right] \quad (5)$$

Therefore, the DQN algorithm contains two neural networks. As shown in Figure 3, the current network $Q(s, a, \theta)$ is used to evaluate the value function of the current state and action, and the target network $Q(s, a)$ is used to compute the temporal difference target. The algorithm updates the parameters θ for N rounds and then replicates them directly to θ'.
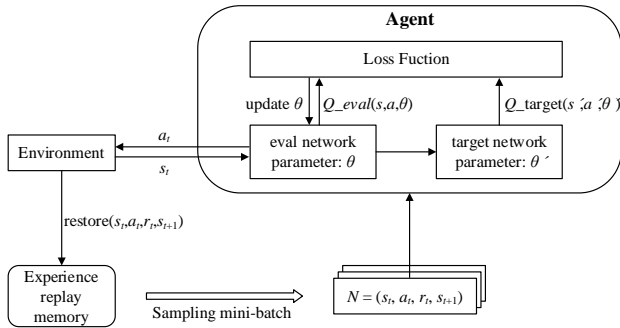

Figure 3.　DQN algorithm structure diagram

In the training process of deep learning, it is usually required that the training data must satisfy the nature of independent identical distribution, and if the correlated data of RL is trained directly, it will lead to the difficulty of convergence of the model or the continuous riot of loss values. Based on this, the DQN algorithm proposes an experience replay mechanism, where the algorithm saves the current moment's state s_t , the action a_t generated by the intelligence, and the new state

body s_{t+1} and reward r_t generated by the environment performing the action in the form of a tuple (s_t, a_t, r_t, a_{t+1}) into the experience pool, and randomly draws a specific batch of experience data from the experience pool for training during training, effectively removing the correlation and dependence between samples.

The detailed process of the DQN algorithm is shown in Algorithm 1. It can be seen that the algorithm mainly consists of two loop operations, the first loop is responsible for the replay of the empirical trajectory, which is executed M times; the second loop is responsible for iteratively traversing the empirical trajectory with time steps, T being the termination time step, while updating the parameters of the prediction model using the gradient descent method based on small batch sample data. In the second loop, the algorithm copies the model parameters p of the current network to the target network k at every C steps to achieve the update of the target network model parameters. Accordingly, the algorithm performs continuous loop computation to continuously update the network parameters and learn the update strategy from historical experience until convergence to a relatively stable state.

Algorithm 1 DQN.

Input: replay memory D, initial current network parameters θ , initial target network parameters θ', Update Frequency C.

1.　**for** episode = 1 to M **do**

2.　　Initialize the state s_0

3.　　**for** t = 1 to T **do**

4.　　　Select $a_t = \max_a Q(s_t, a, \theta)$

5.　　　Execute the action a

6.　　　Get the next state s_{t+1}

7.　　　Get the reward value r

8.　　　Store D $= (s_t, a_t, r_t, s_{t+1}, is\_end_t)$

9.　　　Sampling mini-batch in D

10.　　Calculate y_j

11.　　**if** is_end_t = true **then** $y_j = r_j$

12.　　**else** $y_j = r_j + \gamma \max_{a'} Q^*(s_{j+1}, a_j, \theta')$

13.　　**end if**

14.　　Update $\theta = \dfrac{1}{m}\sum\limits_{j=1}^{m}\left(y_j - Q\left(s_j, a_j, \theta\right)\right)^2$

15.　　Update $s_t = s_{t+1}$

16.　　Every C step copy θ to θ'

17.　**end for**

18. **end for**

V. RESULTS AND DISCUSSION

In the path planning process, the DQN algorithm is studied and analyzed using the raster method to define the environment model. The simulation study in this paper is conducted in a 3D simulation environment, and to ensure the planning accuracy and at the same time ensure the safety of the UAV's body, the raster size is set to be exactly the same as the length of the UAV's outer contour side, and the following assumption is made: when the quadrotor UAV performs diagonal motion, its collision with the obstacle boundary is not considered. The path planning results using the DQN method are shown in Figure 4.
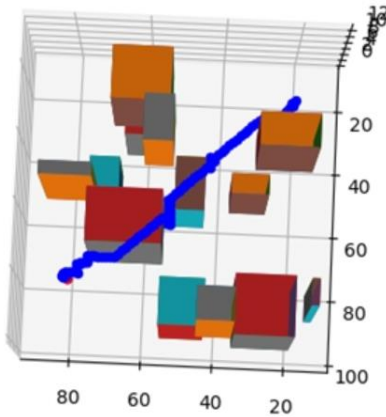

Figure 4. DQN algorithm learning results

The number of neurons in the input layer of the deep neural networks (DNN) is consistent with the size of the state of each time slot, and the number of neurons in the output layer of the network is consistent with the size of the action space. The parameters used in the DQN algorithm in this chapter are shown in Table 1. As can be seen in Figure 5, after 160 experiments, the DQN method was able to solve the path from the starting point

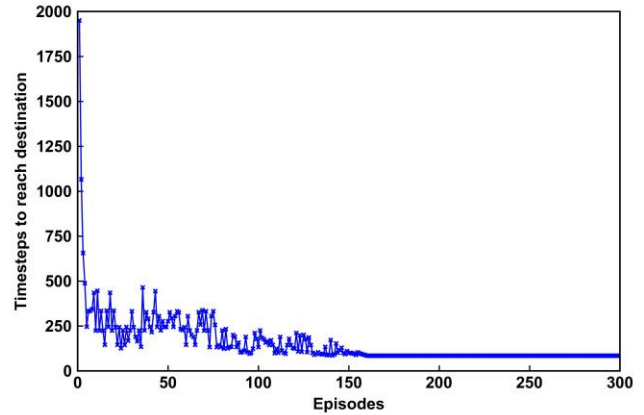to the end point and successfully bypassed all obstacles with a time step of 84.

Figure 5. DQN algorithm learning results

TABLE I. DQN SIMULATION PARAMETERS

Parameters	Value
Size of the replay memory pool D	5000
Size of Mini-batch	64
Discount Factor γ	0.9
Initial exploration rate ε	0.9
Learning Rate	0.0002
Neural network activation function	ReLU

VI. CONCLUSIONS

In recent years, ML has been widely used in the field of robotics, and with the improvement of RL algorithms and theories, it has the possibility of being applied to robotic systems. Distinguished from traditional methods, RL theory applied to the field of robot path planning, can enable the robot to obtain human-like learning ability, in the higher difficulty coefficient, the environment is unknown, complex and uncertain factors in the task, to a considerable extent, can cope with the unexpected situation and complex terrain, to complete the task. And DRL that combines DNN to solve the problem model of RL, after the fusion of the two technologies can cover the traditional algorithms are difficult to deal with the high-dimensional state and action space under the high storage capacity requirements, the model training complexity and other issues. DRL is a technology that empowers intelligences with self-learning capabilities, so such methods are very suitable for solving the problems faced by traditional UAV path planning algorithms. Therefore, a UAV path planning

method based on DQN algorithm is proposed in this paper.

This paper systematically introduces the model, principle and its main components of the RL method, and also includes the Markov decision process, an important description method of the RL method. The path planning task is realized based on the deep reinforcement learning method. Based on the OpenAI-GYM architecture, the 3D environment is described by the raster method and a raster-based map is built. The DQN algorithm is used to solve the optimal policy by taking each raster as a state, the movements in 26 directions as action sets, and the action value function composed of state-action pairs as the objective function. Through simulation, the DQN algorithm is verified to avoid obstacles and complete the path planning task in only about 160 rounds, which validates the effectiveness of the proposed path planning algorithm.

In this paper, although the DQN method is used to realize the path planning task, but there are still some problems and shortcomings when applied to the actual system. The maps in this paper are discrete maps based on grids, which means that the state space and action space are discrete and finite, and the discrete states and actions determine the upper limit of the shortest paths planned, i.e., they cannot be moved at any angle within the map, and the absolute shortest paths cannot be obtained. At the same time, after simulation experiments, it appears that the sample efficiency of this model algorithm is poor, and the next step is to improve the sample efficiency by combining the off-policy method.

REFERENCES

[1] Cui Z, Wang Y. UAV Path Planning Based on Multi-Layer Reinforcement Learning Technique [J]. IEEE Access, 2021: 59486-59497.

[2] Qadir Z, Zafar M H, MOOSAVI S K R, et al. Autonomous UAV path planning optimization using Metaheuristic approach for pre-disaster assessment [J]. IEEE Internet of Things Journal, 2022: 12505-12514.

[3] Wu R, Gu F, Liu H L, et al. UAV Path Planning Based on Multicritic-Delayed Deep Deterministic Policy Gradient [J]. Wireless Communications and Mobile Computing, 2022: 1-12.

[4] Yan C, Xiang X, Wang C. Towards Real-Time Path Planning through Deep Reinforcement Learning for a UAV in Dynamic Environments [J]. Journal of Intelligent & Robotic Systems, 2020: 297-309.

[5] Faust A, Chiang H T, Rackley N, et al. Avoiding moving obstacles with stochastic hybrid dynamics using PEARL: PrEference Appraisal Reinforcement Learning [C]//2016 IEEE International Conference on Robotics and Automation (ICRA), Stockholm, Sweden. 2016.

[6] Jaradat M A K, Al-Rousan M, Quadan L. Reinforcement based mobile robot naviga tion in dynamic environment [J]. Robotics and Computer Integrated Manufacturing, 2011, 27(1): 135–149.

[7] Shalev-Shwartz S, Shammah S, Shashua A. Safe, Multi-Agent, Reinforcement Learning for Autonomous Driving [J]. arXiv:1610.03295v1, 2016.

[8] Wang Y H, Li T H S, Lin C J. Backward Q-learning: The combination of Sarsa algorithm and Q-learning [J]. Engineering Applications of Artificial Intelligence, 2013, 26(9): 2184–2193.

[9] Bianchi R A, Martins M F, Ribeiro C H, et al. Heuristically-accelerated multiagent reinforcement learning.[J]. IEEE Transactions on Cybernetics, 2014, 44(2): 252–265.

[10] Roberge V, Tarbouchi M, Labonte G. Comparison of Parallel Genetic Algorithm and Particle Swarm Optimization for Real-Time UAV Path Planning [J]. IEEE Transactions on Industrial Informatics, 2013: 132-141.

[11] Smolyanskiy N, Kamenev A, Smith J, et al. Toward low-flying autonomous MAV trail navigation using deep neural networks for environmental awareness [C]//2017 IEEE/RSJ International Conference on Intelligent Robots and Systems (IROS), Vancouver, BC. 2017.

[12] Walker O, Vanegas F, Gonzalez F, et al. A Deep Reinforcement Learning Framework for UAV Navigation in Indoor Environments [C]//2019 IEEE Aerospace Conference, Big Sky, MT, USA. 2019.

[13] Walker O, Vanegas F, Gonzalez F, et al. A Deep Reinforcement Learning Framework for UAV Navigation in Indoor Environments [C]//2019 IEEE Aerospace Conference, Big Sky, MT, USA. 2019.

[14] Mnih V, Kavukcuoglu K, Silver D, et al. Human-level control through deep reinforcement learning [J]. Nature, 2015: 529-533.

[15] Chen P, Pei J, Lu W, et al. A Deep Reinforcement Learning Based Method for Real-Time Path Planning and Dynamic Obstacle Avoidance [J]. Neurocomputing, 2022, 497: 64-75.

Survey on the LAN MCS Gap Analysis (LMGA)

Jianguo Wang
ISO/IEC JTC 1/SC 6/WG 1 expert
Xi'an Technological University
Xi'an, Shaanxi, China
E-mail: wangjianguo@xatu.edu.cn

Zhongsheng Wang
ISO/IEC JTC 1/SC 6/WG 1 expert
Xi'an Technological University
Xi'an, Shaanxi, China
E-mail: wzhsh1681@163.com

Ao Li
School of Computer Science and Engineering
Xi'an Technological University
Xi'an, 710021, China
E-mail: 245843115@qq.com

Kingston Zhang
State and Provincial Joint Engineering Lab. of
Advanced Network, Monitoring and Control, China.
Xi'an Technological University
Xi'an, Shaanxi, China
E-mail: kingston_zhang1999@126.com

Abstract—**This survey paper can fill a literature gap in LAN/Ethernet modulation and coding scheme. During the past several decades, even though there were many technical papers on MCS technologies in the IEEE 802.3 Ethernet standard development process, those papers are only technical discussions for specific technical proposals and analysis for special application scenarios. There is no paper providing a historical overview of IEEE LAN/Ethernet MCS system. This paper is proposing to establish a research project to cover MCS deficiency gap analysis in the application field of LAN (Ethernet) communications systems. Research on LMGA is a mission to collect information on LAN MCS technologies, conduct analysis on the gaps between MCS practices and market needs so that in the future MCS Innovation development stages including technical requirements and proposal selections，LAN MCS gaps can be filled and to facilitate quick application and adoption into the field for new MCS technologies.**

Keywords-Ethernet Modulation Schemes; Spectral Efficiency; Power Efficiency; Coding Deficiency LAN; MCS

I. INTRODUCTION

On 13 December 2022, ISO/IEC SC 6 Secretariat circulated 6N17882 Liaison of IEEE 802.3 Working Group to share IEEE 802.3-2022 standard under the PSDO agreement. The paper contains 7026 pages of technical specifications of LAN (Ethernet) standard.[1] As the title of 6N17882 indicates, it is not a formal submission for 60-day ballot under the PSDO paper, but to share the paper with ISO/IEC SC 6 for information and comments. Therefore, members of ISO/IEC SC 6 committee are expected to provide comments for consideration of IEEE 802.3 Working Group. [2] As a working group of ISO/IEC 6, AG 4 and its members are entitled to make comments on 6N17882.

At about the same time as IEEE's submission of 802.3-2022, ISO/IEC SC 6/AG 4 on MCS Innovation posted a paper (AG 4/N 22) entitled "Execution Plan for Industry Survey on MCS Deficiencies". [3] The paper is a follow up to AG 4/N10, a contribution from Chinese Hong Kong expert YIM Wai Ning proposing an Industry Survey on MCS Deficiencies. AG 4/N 22 listed ten application fields including WLAN, Mobile Communications, UAS/UAAN, Ultra-Short-Wave Radio, WIA-FA, Maritime Satellite, TETRA, Beidou, HDTV. [4] From the list, notably missing is LAN/Ethernet application field. The circulation of 6N17882 provides a good opportunity for AG 4 to consider including LAN MCS Gap Analysis （LMGA） into the scope of industry survey.

The subject of LMGA emerged in AG 4 in the very beginning of this year. [5] On 6 Jan., 2023, Convenor Zhang wrote to IEEE 802 Liaison Officer Andrew Myles and IEEE 802.3 Chair

David Law, informing them that the idea of studying LMGA has emerged in ISO/IEC SC 6/AG 4 and inviting IEEE participation in AG 4 meetings (AG 4 N30). IEEE responded positively by registering two representatives in AG 4 Global Directory (AG 4 N42).

In the 3rd AG 4 meeting, there were brief discussions between Convenor and IEEE representative Dr. George Zimmerman regarding the issue the interest of AG 4 on LMGA and how can IEEE help on the task. [6] The interest and need for an LMGA was confirmed and the remaining question was how to proceed. Convenor Zhang promised to provide a question list as a base to work on.

After the conclusion of ISO/IEC SC 6 Plenary Meeting on 24 March 2023 and with the extension of AG 4 to the 2nd term, Convenor Zhang spent some time to work out this paper to fulfill his promises.[7]

This paper contains analysis and comments on IEEE 802.3-2022 as contained in 6N17882.

II.   METHOD AND TECHNIQUE

A. Overview of LAN Techology

Local Area Network (LAN, also known as Ethernet) is a network technology connecting computer systems through wired communication channels such as copper wires and fibre optical cables but with limited range not exceeding 40 kilometers. [8] The technology is mainly developed by IEEE 802.3 group and adopted into International Standards system through bilateral PSDO agreement with ISO. [9] Another local area network technology is connecting systems through emission of electromagnetic waves. It is called Wireless Local Area Network (WLAN) and is also mainly developed by IEEE and enters international standard through ISO.

Local Area Networks, in the beginning known as carrier sense multiple accesses with collision detection (CSMA/CD) access method and physical layer specifications was approved as an IEEE standard by the IEEE Standards Board in 1983 and subsequently published in 1985 as IEEE Std

802.3-1985. In 2012, the title of the standard was changed to Standard for Ethernet.

Communication speed is the major base to categorize IEEE LAN/Ethernet Standards. [10] The First version of LAN standard in 1985 had a 2.94 Mb/s data rate. IEEE Std 802.3u™ added 100 Mb/s operation (also called Fast Ethernet), IEEE Std 802.3z™ added 1000 Mb/s operation (also called Gigabit Ethernet), IEEE Std 802.3ae™ added 10 Gb/s operation (also called 10 Gigabit Ethernet), IEEE Std 802.3ah™ specified access network Ethernet (also called Ethernet in the First Mile) and IEEE Std 802.3ba added 40 Gb/s operation (also called 40 Gigabit Ethernet) and 100 Gb/s operation (also called 100 Gigabit Ethernet). [11] These major additions are all now included in and are superseded by IEEE Std 802.3-2022 and are not maintained as separate papers. Now, IEEE is working on Ethernet technologies capable of delivering 800 Gbps, 1 Tbps and beyond.

Comparing WLAN and LAN, there are some commonalities but also striking differences in the perspective of MCS Gap Analysis. The differences are summarized in the following table.

TABLE I.   COMPARING WLAN AND LAN

Parameters	WLAN	LAN/Ethernet
Connection Method	Wireless	Wired
Communication Medium	Air	Copper, Fiber, etc.
Latency	Low	High
Mobility and Rooming	higher	limited
speed	Gigabits	Higher speed over 400G
Need for MCS	required	required
access	Proximity required	Physical access required
Sharing	Shared	dedicated
interference	high	Much less
Fluctuation vulnerability	high	Much less
Reliability	Much Less	high
coverage	100 meters	Meters to kilometers

With these differences, a lot of MCS related questions need to be answered:

- How the different application scenarios and conditions affect MCS systems in these two application fields?
- Does LAN/Ethernet face similar or same MCS challenges of WLAN?
- How much impact does MCS systems have on the development and performances of these two fields?
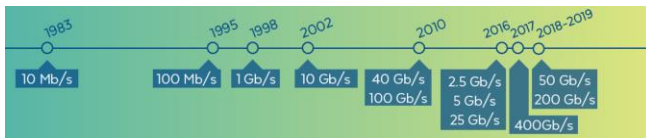- Which one has higher efficiency MCS schemes and why?

Figure 1.   Date Rate Explosion

From the above brief summary, it shows a remarkable trend that over forty years since its start, the data rate of Ethernet has been increased from 10 Mb/s to over 400 Gb/s, which is 40,000 times.

Unlike Wireless LAN and Mobile Communications which transmits radio waves through the air, Ethernet transmits information signals through wired cables. Because of the physical, economic and other considerations in different application scenarios, Ethernet uses different cables and transmission protocols.

The evolution of Ethernet technology indicates that the increase of speed over the past three decades was primary due to the exploration of cabling technology like using different categories of twist pairs, using higher frequencies and optical transmission technologies.

However, due to physical constraints, cable transmission also has maximum performance limits. Has Ethernet reached those limits? How far is from the limits? These questions are relevant to MCS gap analysis.

B.   MCS and LAN/Ethernet Technology

In IEEE standard systems, there is no uniformed rule for the abbreviation of MCS. [12]

It different standards it refers to different technologies.

In IEEE 802.16 for example, MCS is short form for "modulation and coding scheme". In IEEE 802.11 WLAN standards, MCS is not included in the abbreviation list, but in the text it is clearly indicated that MCS refers to modulation and coding scheme.

In IEEE 802.3, MCS is not listed in the abbreviations tables. [13] In 802.3:2022, MCS is not used to define "Modulation and Coding Scheme"，but as "MAC Control Services".

Figure 2.   MAC Control Services

To avoid confusion with modulation and coding scheme, whenever the abbreviation of MCS appears in Ethernet standards, the full term "MAC control service" is included.

It is therefore necessary to restate that in AG 4 produced paper and in our discussion on LAN MCS deficiencies, MCS has always been defined as the abbreviation of "Modulation and Coding Scheme."

During the discussion on WLAN MCS deficiency before the founding of AG 4, there were questions about the MCS related descriptors such as HT, HE-MCS, VHT and UHT in IEEE 802.11 standards. [14] This issue does not arise in Ethernet standards because of the following factors:

- Ethernet categorizes its technology into different speeds (throughput) such as 10M,100M, 10G, 100G, and 400G
- Each category has names with relevant prefixes such as 10MBASE, 10GBASE, etc.
- First suffixes are attached to the names to show media types.
- The evolutions of Ethernet are along the line of speed increases over the years.

- The most fundamental driving force behind the speed increase is the fast development of fibre-optical transmission capabilities.
- MCS technology does not have as much impact in Ethernet development as in WLAN and Mobile communications.
- Therefore, IEEE 802.3 neither use MCS to define its technologies no assign descriptors to MCS systems in the Ethernet standards.

IEEE 802.3 standard adopts a rate based classification system for its programs and standards. [15] In this system, from the titles of the groups, their missions and objectives are clearly indicated. The following list is from IEEE website:
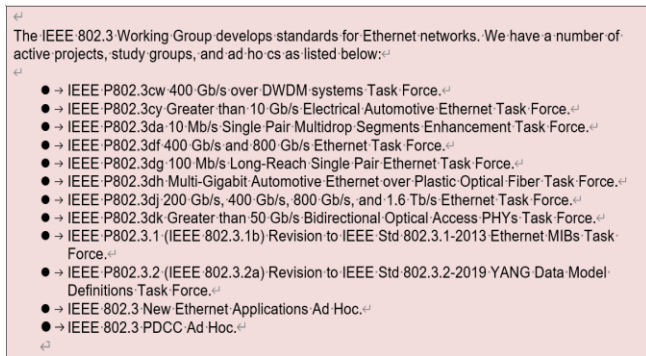

Figure 3.   Rate Based Classification

C. Ethernet Modulation Schemes

There are two major types of modulation schemes in IEEE Ethernet standards, PAM and QAM. [16] PAM modulation was the major scheme in LAN standards and QAM modulation is introduced into Ethernet only for about five years and in limited application scenarios. In efficiency, PAM modulation belongs to the lower end and QAM modulation is considered as the choice for higher order solutions.

PAM modulation and Ethernet are considered as a perfect match. Most forms of Ethernet use pulse amplitude modulation (PAM) constellations. In PAM signal modulation, information is encoded in the amplitude of a series of signal pulses. [17] The advantages of PAM include simplicity of receiver and transmitter design and easy transmission over a pair of wires.

The following table shows Ethernet PAM modulation types and application scenarios:

TABLE II.   PAM MODULATION

Modulation	Application
PAM 3	100BASE-T1 100BASE-T4 1000BASE-T1
PAM 4	400G
PAM 5	10BASE-T 100BASE-T2 1000BASE-T
PAM 16	2.5GBASE-T 5GBASE-T 10GBASE-T 25GBASE-T 50GBASE-T

- PAM 3 and PAM 5 modulation schemes are implemented in sub-G rates applications.
- Higher order PAM 16 is used for gigabit systems.
- There is a tendency to move back to lower order modulation (PAM 4) in standards providing over 100 Gb/s Ethernet systems.
- Emphasis on reliability in some other advanced communication fields is also reflected in Ethernet.

In IEEE Std 802.3™-2015, there was only one reference to QAM in 62.3.1 PMD Overview: "The bytes within the frame are encoded to a set of QAM constellation points that are used to modulate the carriers of the DMT symbol. [18] The time-domain symbol is cyclically extended and then windowed to reduce side lobe energy." And, QAM was not even included in the abbreviation list.

On 22 Nov. 2016, IEEE approved 802.3bn-2016 Physical Layer Specifications and Management Parameters for Ethernet Passive Optical Networks Protocol over Coax (EPoC）.The new amendment contains 169 references to QAM.

Three years later when IEEE released IEEE Std 802.3™-2018, QAM was cited 209 times. In IEEE Std 802.3™-2022, QAM was cited 202 times.

TABLE III.   M-QAM APPLICATION

Modulation	Standard
M-QAM	10GPASS-XR 1000BASE-RHx Management Data Input/Output (MDIO) Interface EPoC (802.3bn-2016)

- 10GPASS-XR is a collection of IEEE 802.3 EPON Protocol over Coax (EPoC) Physical Layer specifications for up to 10 Gb/s downstream and up to 1.6 Gb/s upstream point-to-multipoint link over a coax cable distribution network.
- 1000BASE-H comprises a Physical Coding Sublayer (PCS) and a Physical Medium Attachment (PMA) sublayer that supports Physical Medium Dependent (PMD) sublayers for operation at 1000 Mb/s over duplex plastic optical fiber (POF) as the transmission medium. The following three port types with different PMDs are defined: 1000BASE-RHA, 1000BASE-RHB, and 1000BASE-RHC (collectively referred to as 1000BASE-RHx).
- EPoC operates over a point-to-multipoint (P2MP) topology composed of passive segments of coaxial media and passive taps/couplers, optionally interconnected with active coaxial amplifiers, and/or analog optical links creating a tree-and-branch topology.

Because EPoC is the first IEEE Ethernet standard that adopts QAM modulation, the development time line is needed to indicate the exact time of QAM enters Ethernet.

TABLE IV.   EPoC AND QAM MODULATION

Time	Event	QAM Modulation
2011-11	Call for Interest	Modulation was not mentioned
2012-08	PAR Approved	Modulation was not mentioned
2012-10-28	Motion 11 Approved	Support multiple downstream modulation orders up to 4096QAM. Support multiple upstream modulation orders up to 1024QAM.
2013-01-25	Motion 3 Approved	The downstream PHY Link Channel shall use a fixed modulation order of 16 QAM to carry PHY Link
2013-03-21	Motion 4 Approved	The E PoC standard shall support multiple modulation profiles for the bursting DS and US PHY and a single modulation profile for the continuous DS PHY.
2014-01-22	Motion 11 Approved	Support for 2048 and 4096 QAM in the TDD upstream shall be mandatory, using the same QAM constellation mapping as the FDD downstream.
2014-09	1st draft	
2015-03	2nd draft	
2015-10	3rd draft	
2016-11	IEEE Standard	
2018-12-11	ISO/IEC Standard	ISO/IEC/IEEE 8802-3:2017/A md 6-2018

- From current highest data rate perspective, LAN/Ethernet has advantage with top speed 40 times of WLAN.
- From the timing of adoption of QAM modulation perspective, WLAN has the advantage, adopting 64-QAM modulation in 1999, two decades ahead of LAN/Ethernet.
- In 1999, WLAN had given up QPSK and implemented 64-QAM modulation, nowadays PAM 4 (equivalent to QPSK) is still the main choice for Ethernet modulation scheme.
- Ethernet has one advantage over WLAN in the highest mandatory order with 4096-QAM compared with WLAN's 1024-QAM.
- Ethernet has also an advantage over WLAN in the highest optional order with 16384-QAM compared with WLAN's upcoming 4096-QAM in IEEE 802.11be.
- Ethernet probably has reached the highest possible QAM order in 16384, while WLAN has no plans for QAM orders over 4096.
- Ethernet has these advantages because of the favorable transmission medium.
- Facing unfavorable application and medium conditions, WLAN develops other modulation technologies such as 8 spatial stream operation which is unavailable to LAN/Ethernet systems.

TABLE V.   LAN AND WLAN MODULATION COMPARISON

Parameters	LAN/Ethernet	WLAN
Highest data rates	400G	10G
QAM modulation	2018	1999
Highest order (Mandatory)	4096-QAM	1024-QAM
Highest order (Optional)	16384-QAM	4096-QAM （planned)
Highest possible	Upto 16384-QAM	No more planned beyond 4096-QAM
Adoption	Limited application	System wide
Spatial Streams	None	8

- From current highest data rate perspective, LAN/Ethernet has advantage with top speed 40 times of WLAN.
- From the timing of adoption of QAM modulation perspective, WLAN has the advantage, adopting 64-QAM modulation in 1999, two decades ahead of LAN/Ethernet.
- In 1999, WLAN had given up QPSK and implemented 64-QAM modulation, nowadays PAM 4 (equivalent to QPSK) is still the main choice for Ethernet modulation scheme.
- Ethernet has one advantage over WLAN in the highest mandatory order with 4096-QAM compared with WLAN's 1024-QAM.
- Ethernet has also an advantage over WLAN in the highest optional order with 16384-QAM compared with WLAN's upcoming 4096-QAM in IEEE 802.11be.
- Ethernet probably has reached the highest possible QAM order in 16384, while WLAN has no plans for QAM orders over 4096.
- Ethernet has these advantages because of the favorable transmission medium.
- Facing unfavorable application and medium conditions, WLAN develops other modulation technologies such as 8 spatial stream operation which is unavailable to LAN/Ethernet systems.

III.   RESEARCH RESULTS AND FINDDINGS

A. SPECTRAL EFFICIENCY

Spectral Efficiency is one of the most important indicators of the capabilities of MCS system. [19] It affects the data rates (throughput) and bandwidth utility efficiency. In different application scenarios, however, the weight of Spectral Efficiency in the development of communication capacity varies.

IEEE Ethernet standard does not offer spectral efficiency tables for PAM modulation schemes. The following table is based on theoretical estimates:

TABLE VI.   PAM MODULATION TYPES AND APPLICATION SCENARIOS

Modulation	Application	Spectral Efficiency bps/Hz
PAM 3	100BASE-T1 100BASE-T4 1000BASE-T1	<2
PAM 4	400G	<2
PAM 5	10BASE-T 100BASE-T2 1000BASE-T	<2
PAM 16	2.5GBASE-T 5GBASE-T 10GBASE-T 25GBASE-T 50GBASE-T	3.125

This table reveals a fact that Ethernet PAM modulation has lower Spectral Efficiencies (SE) with highest SE not exceeding 4 bps/Hz.

Comparing the two major Ethernet modulation schemes, PAM modulation has much lower Spectral Efficiency rates, and QAM modulation can deliver several times higher Spectral Efficiency thus could significantly increase the capacity of Ethernet communication systems.

One observation is that in other applications fields, the evolution of MCS technology is through the path of FSK/PSK to QPSK, 16-QAM, 64-QAM, 256-QAM and 1024-QAM. [20] In Ethernet, the evolution of MCS technology is from PAM, to PAM 4, PAM 5 and PAM 16 and then to M-QAM. However, not only older Ethernet protocols continue to rely on PAM technology, the newer groups such as IEEE P802.3dcw 400 Gb/s over DWDM systems, IEEE P802.3df 400 Gb/s and 800 Gb/s Ethernet, IEEE P802.3dj 200 Gb/s, 400 Gb/s, 800 Gb/s, and 1.6 Tb/s Ethernet all adopt PAM 4 as the modulation scheme.

The major reason for not adopting higher order QAM modulation in systems over 200Gb/s Ethernet standards are the complexity factor. [21] It is not clear how long this factor will remain a barrier since higher order modulation schemes such as 256-QAM and 1024-QAM have because state of the art MCS technology and Ethernet is adopting M-QAM since 2018. It is likely that Ethernet will follow the main-stream in higher order MCS applications.

B. *Power Efficiency*

During the pre-AG 4 discussions between August 2021 and July 2022 over the issue of WLAN MCS deficiency, the trend of higher and higher MCS power consumption was one of the major factors demonstrating the need for MCS Innovation.

In IEEE 802.3 Ethernet standard, the term Energy Efficiency (EE) was used instead of Power Efficiency (PE) .The purpose of Energy Efficiency is to lower power consumption of Ethernet systems, so the term of Energy Efficiency and Power Efficiency are interchangeable.

Look at the history of 802.3 Ethernet, it is noticeable that IEEE 802.3 standard is very dedicated to achieve Energy Efficiency for Ethernet motivated by the following factors:

- Legislative pressure: legislative action worldwide is demanding improvements in energy efficiency of networked systems.
- Market pressure: energy consumption and efficiency will become a major factor in the choice of network solutions, especially in data centers.
- Cost saving: Energy costs are a major component of operating cost. The Energy efficiency solutions will not materially impact component or installation costs, and may provide cost savings opportunities.

Green Ethernet is a common name for a set of features that is designed to be environmentally friendly, and to reduce the power consumption of a device. [22] The Green Ethernet feature can reduce overall power usage in the following ways:

- Energy-Detect Mode: On an inactive link, the port moves into inactive mode, saving power while keeping the Administrative status of the port Up. Recovery from this mode to full operational mode is fast, transparent, and no frames are lost. This mode is supported on both GE and FE ports.
- Short-Reach Mode: This feature provides for power savings on a short length of cable. After cable length is analyzed, the power usage is adjusted for various cable lengths. If the cable is shorter than 30 meter for Ten

gigabit ports and 50 meter for other type of ports, the device uses less power to send frames over the cable, thus saving energy. This mode is only supported on RJ45 GE ports; it does not apply to Combo ports. This mode is disabled by default.

In addition to the above Green Ethernet features, the 802.3az Energy Efficient Ethernet is found on devices supporting GE ports. EEE reduces power consumption when there is no traffic on the port.

The differences between EEE and Green Ethernet are that the later is enabled on all devices whereas only Gigabyte ports are enabled. [23]. With EEE. [24] 802.3az EEE is designed to save power when there is no traffic on the link. And, in Green Ethernet, power is reduced when the port is down but when using 802.3az EEE, systems on both sides of the link can disable portions of their functionality and save power during periods of no traffic.

From MCS perspective, there are some observations:

- The Green Energy and EEE are out of scope, just as the Target Wake Time (TWT) energy saving technology in WLAN. [25] The Ethernet power saving technologies such as disabling port LEDs when not needed are Port Management functions irrelevant with MCS operations.
- The MCS technologies in Ethernet are similar to those employed in other applications such as WLAN in terms of power consumption in transmission of data.
- There is no power saving mechanism to reduce MCS power consumption in Ethernet standards.
- The constraints in power deficiency faced by other application fields such WLAN are also affecting Ethernet operations.
- For example, PAM 4 modulation can double the speed of Ethernet transmission, but also causes 4-5 dB penalty which has to be compensated by other technical measures such as optical amplification or FEC coding systems with higher code gains. [26] Higher order modulations schemes such as PAM 16 and M-QAM results in

more power penalties harder to compensate with other measures.

- Power consumption is one of the major factors blocking Ethernet's utilization of higher Spectral Efficiency modulation schemes. [27] Higher SNR modulation schemes for WLAN systems may be affordable due to the distributed deployment scenario. For Ethernet, in many situations such as operation centers and data storage hubs, higher power consumption may be a cost inhibitor for higher order modulations schemes.

- Ethernet may further cut operation costs if innovative MCS technologies can reduce power consumption while maintain or even increase spectral efficiency.

C. Coding Deficiency

In conventional MCS technology, the C means channel coding and usually refers to FEC coding system. [28] The deficiency of FEC coding has been discussed in 6N 17675 but a through analysis is needed to fully understand the issue and to provide guidelines for coding scheme innovation.

In Ethernet, there are three FEC coding systems used in different application scenarios. Coding gains, latency and complexity are the factors considered in Ethernet FEC coding selections.

- LDPC has higher coding gain (only 0.66 dB gain) but higher latency and complexity.
- Small code size such as RS code has lower latency.
- LDPC was used in delay insensitive network/system such as broadcast, home network, residential access network.
- LDPC is mostly used in copper and wireless system due to its good performance in these channels.
- RS has been used in fiber optical communication system, long-haul, metro and access.

MCS Coding deficiencies is a general and theoretical issue having impact over almost all ICT fields, LAN/Ethernet is no exception. AG 4 needs to have a special study on this topic. IEEE does not have a work plan to work on MCS Coding theory and innovation. There are coding related technical proposals but they are related to specific application scenarios.

IV.   DISCUSSION

LMGAR is the abbreviation for LAM MCS Gap Analysis report.[30] It will be the final gap analysis for LAN/Ethernet MCS deficiencies. The current paper is only an initial work providing some basic information as basis for further analysis.

LMGAR should be an AG 4 report with about 60 pages.[31] It will be submitted to ISO/IEC SC 6 to be reviewed at at the 47th ISO/IEC SC 6 HoDC and plenary meetings in the fall of 2024. LMGAR should be mature enough to possess the potential to be converted into a Technical Report. There are several options to develop LMGA. The following provides evaluation of each option. The industry survey contained in 6N17975 is one option to gather industry data of MCS systems. However, the industry survey is not a good option because AG 4 has enough resources for more detailed information. IEEE is the leading Standard Development Organization of LAN technology and has close cooperation with JTC 1/SC 6. If IEEE is interested in providing resources to help out with this work, it would be of great help. AG 4 can solicit contributions from the industry and researchers who can provide practical experiences, market needs and academic theoretic work to help make the analysis more accurate reflection of the gaps between technology and social demand. The final option is to work it out within AG 4. This option has one advantage: because AG 4 is working on MCS gap analysis in several other application fields, LMGA can derive comparative knowledge from other fields. IEEE is the only standard development organization relevant with LMGA project and has already assigned liaison representatives to AG 4 who are senior experts in LAN technology standardization. Therefore, no matter what option is chosen, the process will benefit from collaboration with IEEE.

Because the LMGA report will cover not only technical specifications but also broad issues such as market demands and future directions, collaboration from IEEE and other relevant entities are vital for the success of this project.

In feasibility assessment, LMGA report is more practical than other fields because of the following factors:

- Already has the complete specification（6N17882）
- Historical papers
- IEEE Liaison with ISO/IEC SC 6 and AG 4
- WLAN as comparative technology
- AG 4's resources on other fields.

TABLE VII.   TIMELINE

Time	Work	Objective
2023-08-01	Proposal	LMGA proposal is submitted
2023-08-08	6th Meeting	LMGA proposal is revised or approved
2023-12-11	AG 4 Report	LMGA is included in AG 4 report and recommendations to SC 6
2024-04-01	LMGAR	1st draft of LAN MCS Gap Analysis Report is presented to AG 4
2024-07-01	Revision	2nd draft of LMGAR is presented to AG 4
2024-09-01	Completion	Final Report on LMGAR is approved and submitted to SC 6

V.   CONCLUSIONS

Technical requirement and proposal evaluation is not in the scope of this paper. However, due to the special situation of Ethernet MCS technology, it is proper here to offer some observations and thoughts on the future cooperation on technical development between IEEE 802.3 group and ISO/IEC JTC 1/SC 6.

LMGA fills a gap in the execution plan for industry survey on MCS deficiencies. And it will provide valuable insights into the application scenarios and conditions of wired modulation and coding schemes. It can also help modulation and coding scheme innovation researchers to understand the limitations of LAN technology and market requirements. And can help modulation and coding scheme innovation development more suitable for LAN applications. LMGA can not only be used by AG 4 to help future MCS innovation activities, but can also be published by ISO/IEC (if the content is mature enough) for general audience since this is the first comprehensive introduction of LAN/Ethernet MCS technology.

This paper proposes a research topic on LAN MCS Gap Analysis for AG 4 and provides an outline as a base paper for the end product "LAN MCS Gap Analysis Report". The work will be significant because of the wide application of LAN technology and the different and complicated application scenarios and challenges for MCS systems.

An overview of the LAN/Ethernet MCS systems does reveal the complexity of Ethernet application scenarios and many differences with other ICT fields such as WLAN. Even though over the past several decades, the data rates of Ethernet has shown remarkable increase and much higher than WLAN, the spectral efficiency performance lags far behind some other ICT fields. One of the major driving force behind Ethernet date rates increase if the fast expansion of fibre-optical cable capacities. As the demand for fast data rates will continue for more decades and as fibre-optical technology is also reaching theoretical and physical limits, deployment of higher order MCS technology will be the way for the future.

On the other hand, IQ based classical Modulation technologies including M-QAM are also facing theoretical and physical limitations. Unlike other advanced fields such WLAN and Mobile Communications which are already reaching the ceiling of MCS capabilities, LAN/Ethernet still has some rooms (moving from lower order to higher order MCS) to operate. If the barriers of higher order MCS complexity and power consumption are mitigated through MCS Innovation, it will be easier to convert Ethernet into higher Spectral Efficiency systems.

REFERENCES

[1] ISO/IEC JTC 1/SC 6/AG 4 N10: Proposing an Industry Survey on MCS Deficiencies, 2022-11-16.

[2] ISO/IEC JTC 1/SC 6/AG 4 N22: Execution Plan for Industry Survey on MCS Deficiencies, 2022-12-12.

[3] ISO/IEC JTC 1/SC 6/AG 4 N30: The Prospect of Collaboration with IEEE, 2022-01-12.

[4] ISO/IEC JTC 1/SC 6/AG 4 N42: IEEE responses to AG 4 Invitation, 2022-02-14.

[5] ISO/IEC JTC1-SC6 N15595: Submission of IEEE 802.3-2012 under the ISOIEEE PSDO Agreement, 2013-04-02.

[6] ISO/IEC JTC1-SC 6 N15632: Summary of voting on 6N15595 Submission of IEEE 802.3-2012, 2013-06-05.

[7] ISO/IEC JTC1-SC 6 N15724: Liaison reply to the China NB comments on the IEEE Std 802.32012, 2013-08-01.

[8] ISO/IEC JTC1 SC 6 N15999: Submission of IEEE Std. 802.3.1-2013 under the ISOIEEE PSDO Agreement, 2014-08-06.

[9] ISO/IEC JTC1-SC 6 N16047: Summary of Voting on 6N15999 Submission of IEEE Std. 802.3.1-2013 under, 2014-10-08.

[10] ISO/IEC JTC1-SC 6 N16086: Liaison reply to China NB comment on the IEEE Std. 802.3. 1-2013, 2014-11-18.

[11] ISO/IEC JTC1-SC 6 N16429: Submission of IEEE Std. 802.3-2015 for adoption under the ISOIEEE PSDO, 2016-05-12.

[12] ISO/IEC JTC1-SC 6 N16448: Summary of Voting on 6N16429 Submission of IEEE Std 802.32015, 2016-07-18.

[13] ISO/IEC JTC1-SC 6 N16458: IEEE reply to China NB comments on IEEE Std. 802.32015 60day ballot, 2016-08-17.ISO/IEC JTC 1/SC 6 6N16635:Submission of IEEE 802.11.ah-2016, 2017-05-22.

[14] ISO/IEC JTC1-SC 6 6N16546:Submission of 802.3bn-2016 for fast-track adoption under the ISO/IEEE PSDO Agreement, 2017-02-14

[15] ISO/IEC JTC1-SC 6 N16810: Submission of IEEE Std 802.16™-2017, IEEE Standard for Air Interface for Broadband Wireless Access Systems.2018-06-01.

[16] ISO/IEC JTC 1/SC 6 N16819: ISO/IEEE PSDO Agreement 2016 - Implementation Guide, 2018-07-31.

[17] ISO/IEC JTC1-SC 6 N16892: Submission of IEEE Std 802.3-2018 IEEE Standard for Ethernet, 2019-02-14.

[18] ISO/IEC JTC1-SC 6 N16917: Summary of voting on IEEE Std. 802.3TM2018 IEEE Standard for Ethernet, 2019-04-15.

[19] ISO/IECJ TC1/SC 6 N17388: Liaison reply to China NB comments on IEEE Std. 802.3-2018 FDIS ballot，2020-11-26.

[20] ISO/IEC JTC1-SC 6 N17474: Liaison reply to China NB comments on IEEE Std. 802.3.2-2019 60-day pre-ballot, 2021-02-05.

[21] ISO/IEC JTC1-SC 6 N17451: Summary of Voting on Submission of IEEE 802.3.2-2019, 2021-01-11.

[22] ISO/IEC JTC1 SC 6 N17510: Submission of IEEE 802.11ax-2021, 2022-06-11.

[23] ISO/IEC JTC1-SC 6 N17669: Liaison reply to China NB comments on ballots IEEE Std 802.3cb-2018 802.3bt-2018 802.3cd-2018 802.3cg-2019 802.3ca-2020, 2022-02-09.

[24] ISO/IEC JTC 1/SC 6 N 17828: IEEE 802 status report to ISO/IEC JTC 1/SC 6 for SC 6 meeting in July 2022 online (shortened version for SC 6 plenary), 2022-07-01.

[25] ISO/IEC JTC 1-SC 6 N17882: Liaison of IEEE 802.3 Working Group to share IEEE 802.3-2022 standard under the PSDO agreement, 2022-11-04.

[26] ISO/IEC JTC 1-SC 6 N17931: Liaison reply to China NB (ISO/IEC-IEEE 8802-3-2021-FDAmd 12, 8802-3-2021-FDAmd 13, 8802-3-2021-FDAmd 14), 2022-12-20.

[27] ISO, ISO/IEEE PARTNER STANDARDS DEVELOPMENT ORGANIZATION (PSDO) COOPERATION AGREEMENT, 2007-12-19.

[28] Y. Lu, L. Ma, D. Mo and L. Liang, "High Gain Low Complexity Low Latency FEC Codes for Ethernet and Backplane Applications", DesignCon 2018, Santa Clara, CA, 2018.

[29] Eugene (Yuxin) Dai, FEC Choices for 802.3ca, https://www.ieee802.org/3/ca/public/meeting_archive/2017/11/dai_3ca_2a_1117.pdf，November, 2017.

[30] Jinlong Wei, Qixiang Cheng, Richard V. Penty, Ian H. White, and David G. Cunningham: 400 Gigabit Ethernet Using Advanced Modulation Formats: Performance, Complexity, and Power Dissipation, IEEE Communications Magazine, February 2015.

[31] NIKHIL JAIN，PAM & Ethernet: A Perfect Match, https://www.edn.com/pam-ethernet-a-perfect-match/, 2016-05-06.

Research on Multi-Sensor Fusion Firefighting Manpower Status Monitoring Technology

Wanying Dang
School of Computer Science and Engineering
Xi'an Technological University
Xi'an, China
E-mail: 953517076@qq.com

Changyuan Wang
School of Computer Science and Engineering
Xi'an Technological University
Xi'an, China
E-mail: cyw901@163.com

Abstract—**Firefighting soldiers are in danger during firefighting operations, and it is necessary to monitor the data of their physical indicators to ensure the safety of firefighting soldiers, improvement of the safety of firefighting personnel. A single sensor will appear the information blind spot, and has the defects of measurement limitation, low robustness and low precision, which can't satisfy the need of accurately judging the current state of the firefighting soldier. Therefore, this paper investigates the distribution characteristics of multi-dimensional data of firefighting soldiers in the process of working movement, The goal of multi-sensor information fusion is based on the separation of observations from each sensor, and its ultimate goal is to utilize the advantages of multiple sensors operating together or in conjunction to improve the effectiveness of the entire sensor system, the distribution characteristics of multi-dimensional data effectively improve the shortcomings of a single sensor. By introducing the idea of improving the local optimum of back propagation of BP neural network algorithm and the defects of network weights, this paper proposes a relevant fusion algorithm based on firefighting soldiers, establishes a kinematic physiological monitoring model based on firefighting soldiers, and realizes the physiological state monitoring of firefighting soldiers in the complex working environment. Experimental results show that this method can improve the accuracy with which data from several sensors determine the condition of firefighters, decision making for firefighting singletons' safety and security can be effectively improved by multi-sensor data fusion, and the accuracy of the improved FWA-BP data fusion algorithm model is increased by 3.64%, which improves the stability of the system.**

Keywords-Multi-Source Sensors; Firework-BP Algorithm; Data Fusion

I. INTRODUCTION

Firefighting safety is a matter of life and death, and the safety of firefighters is of paramount importance. According to the information of firefighters in recent years, the average annual death of about 30 people, to protect the lives of firefighters, in order to improve the safety of firefighters and the efficiency of performing tasks multi-sensor information fusion technology is applied to the firefighters' equipment in order to realize the comprehensive monitoring and analysis of the fire environment [1]. Multi-sensor data fusion can more accurately and graphically describe the observation object [2], providing new ideas for the safety and security of firefighters' single soldiers. Taking the research project of Xi'an University of Technology as an example, the decision-making fusion of multi-sensor data needs to be transmitted to the command center. Therefore, the first step is to complete the multi-sensor data fusion for firefighters.

The firefighting single soldier is the main body of firefighting work [3], the use of multi-sensor detection and fusion of the target, break through the limitations of single-sensor measurement, to avoid the blind spot of single-sensor information, and to improve the accuracy of measurement. We need to solve the following problems: First of all, to monitor and protect the firefighting singletons we must get their physiological data, and pulse and ECG are the basic indicators of vital signs monitoring, reflecting the firefighting singletons' physical condition and movement status; Then, only physiological sensors can not determine the

firefighting singletons' status in special cases, and we need to combine with the firefighting singletons' posture data to improve the accuracy of the results; At last, a single sensor can not guarantee the accuracy and robustness of information fusion, multi-sensor information fusion can ensure the accuracy and practicality of information fusion, through multi-level, multi-space information complementary and optimized combination of processing, multi-sensor data fusion ultimately produces a consistent interpretation of the firefighting soldier[4]. In this paper, a multi-sensor data fusion decision-making algorithm based on firefighting singletons is designed,, so as to provide scientific technical support and guidance for the practical application of firefighting singletons.

The basic principle of multi-sensor data fusion is just like the process of comprehensive information processing in human brain, it makes full use of multi-sensor resources, the complementary and redundant information of various sensors in space and time is optimized according to a certain optimization criterion, which produces a consistent interpretation and description of the observation environment. The research results of this paper include the following, the acquisition of pulse and ECG time and frequency domain indicators in physiological information, and simulation of firefighting single-armed operation intensity experiments to obtain pulse, ECG, and posture data, to extract posture features and identify and classify postures; the acquisition of the relevant physiological dataset and posture dataset to analyze the above indicators of the correlation between safety and security, in order to determine the feature indicators based on the final safety decision-making model.

II. RELATED WORK

In the Physiology and Sports Research Laboratory of a university in the U.S.A., a special fireproof shirt was designed in which a physiological state monitor-PSM was embedded[5].The purpose of this study was to test that while performing various activities related to firefighting, firefighters can accurately detect the heart rate HR and the respiratory rate RR by wearing the device, which allows for real-time analysis of firefighters' health status information to monitor the physiological status of the firefighters[6]. In 2015, a wearable smart system was proposed by the French National Institute of Higher Arts and Textile Industries. In 2020, Literature [7] provides an overview of existing technologies and solutions for smart textiles and sensing garments for physiological monitoring and suggests that this can be achieved by applying textile technology to sensing garments in which the sensors are fully embedded in the fabric.

Shufeng Yang et al [8] designed and developed a firefighter vital signs detection system for real-time firefighting singletons in the exercise state with information on respiration, heart rate, body temperature, activity intensity, and posture. In February 2016, a smart wearable system was proposed to protect firefighting singletons and to deliver real-time information on the physiological status of firefighting singletons. The proposed smart wearable system includes heart rate and temperature information detection, gas concentration sensors, and acceleration sensors, which are combined to judge and estimate the overall physical condition of the firefighter. The development of the domestic wearable sensor system in recent years is still relatively rapid, commanders need to effectively judge the on-site environment according to the equipment of the firefighter's single soldier, do a good job of surveying, and in the process of making judgments, you can use the relevant equipment to enhance the scientific nature of the command with the support of intelligent technology to ensure the safety of the on-site firefighters [9].

III. MODELS AND ALGORITHMS

A. System Composition

The firefighting single soldier safety and security system includes wearable sensor terminal, remote information transmission and intelligent control platform. The composition of this firefighting manpower safety and security system is shown in Figure 1.
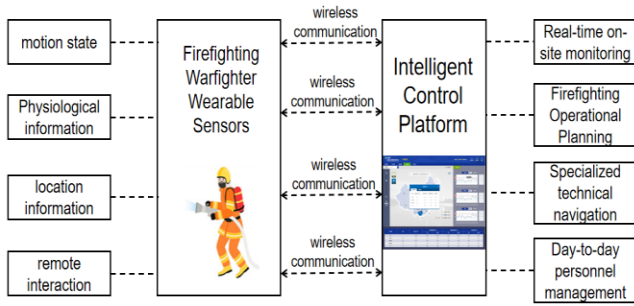
Figure 1.   Firefighting man-portable safety and security system

Wearable sensor terminal is the carrier of this system, mainly based on a variety of wearable sensors, can collect firefighting soldiers for physiological information, movement status, location information, and at the same time has the function of remote information interaction. Remote information transmission is the data interaction between the wearable sensor terminal and the control platform based on wireless communication, the combat firefighters through the sensor terminal in the form of data flow through the form of radio uploaded to the control platform, so that the control center personnel can understand and analyze the scene situation in a timely manner. The control platform will release the fire emergency plan and all kinds of instructions through wireless communication, realizing real-time interaction between firefighters and the command center.

The control platform realizes data collection, organization and analysis. Through the information interaction between combat firefighters and the control platform, it realizes the management of firefighting command and firefighting rescue. The control platform can not only monitor the scene in real time, but also has the functions of firefighting operation planning, professional and technical navigation and daily personnel management [10].

B. Physiology and Posture System Research

As shown in Figure 2, it is a flowchart of the design of the safety and security of the firefighting single soldier consisting of three components, namely the equipment needed for data acquisition, the processing of the different equipment after data acquisition and the fusion of multi-sensor data. The three components are described in detail next.

1) Data acquisition and processing process

The data acquisition and processing process is categorized into physiological and postural approaches, and the data the purpose of data preprocessing is to fill in missing values, smooth or remove abnormal values, and correct data inconsistencies [11]. The reason for feature extraction in physiological data acquisition process is the individual variability of firefighting soldiers and the different physiological functions of the human body, and then through the threshold value to the firefighting soldier's state of the division, and finally get the results of the current state; posture data acquisition process of feature recognition refers to the extraction of firefighting soldier's posture or behavior of the special information, and through the posture recognition model to the firefighting soldier's posture of the classification, and finally get the results of the current posture, the result of the current posture.
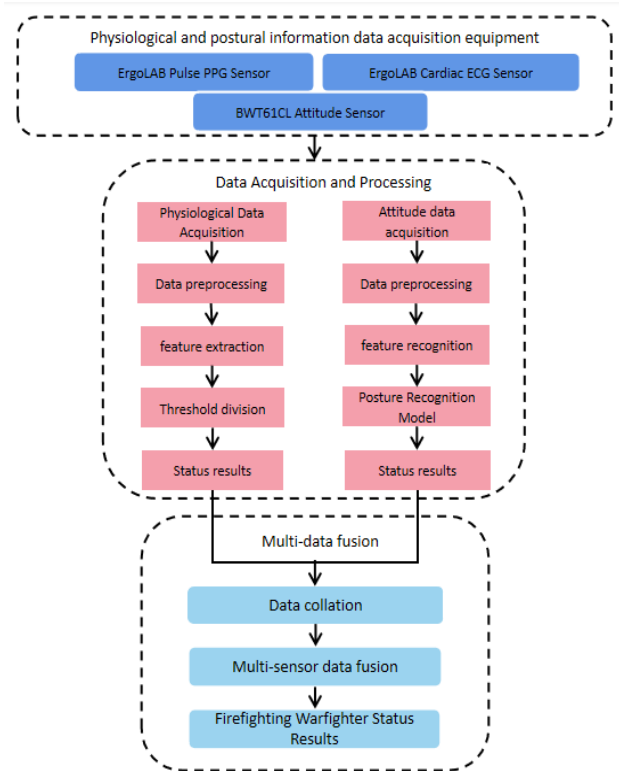

Figure 2.   Design flowchart for firefighting manpower safety

Due to the good accuracy and high sensitivity of the posture sensor, the amount of data collected in a short period of time is relatively large, so this paper chooses the support vector machine

algorithm that can solve the problem of small samples, and after pre-processing the original more than 30,000 groups of posture samples, only two thousand groups of posture samples can have a good classification effect on the two categories of non-falling and falling postures. And we choose to fix the posture sensor at the position of waist which has higher accuracy [12]. In this paper for the firefighting soldier posture recognition is mainly to improve the accuracy of judging the state of the firefighting soldier, all the use of simple binary classification with which the combination of posture features are also more obvious, the use of small samples and a simple SVM algorithm model for posture classification to give a result with an accuracy of up to 99.06%.

2) Multi-data fusion

In multi-sensor data fusion, by collecting multi-level and comprehensive information about the target and combining it with appropriate fusion methods, the final information obtained is far more comprehensive and reliable than that obtained by using a single sensor [13]. A BP neural network and an improved BP neural network are used for multi-sensor data fusion, and the states of firefighting soldiers are categorized into two major categories: "normal state" and "event state", and the "event state" is categorized in detail. The "event state" is also categorized in detail. The "ordinary state" is the safety state, and the "event state" is divided into abnormal state and warning state, i.e., safety, abnormality and warning.

C. Multi-sensor data fusion algorithms

1) Introduction to traditional BP algorithms

The bp neural network model determines the input and output levels of a contract according to the known and predicted data types. The data signals are transmitted from the input layer to the hidden layer centered in the neural network, where the data is learned and processed. The processed data signals are transmitted to the output layer. If the results do not match expectations, errors spread somewhere and hidden weights and thresholds return to expectations [14].
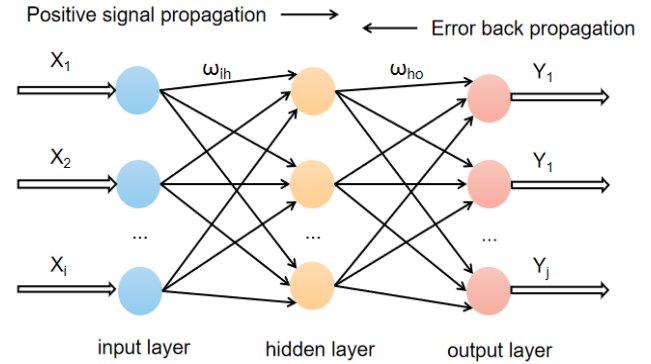

Figure 3. Schematic diagram of BP neural network and security

The problem of the traditional BP algorithm is that the BP network uses local optimization algorithm, and the objective function surface of the multilayer network structure is generally more complex, which leads to local convergence of the network, and the optimal solution of the problem cannot be obtained. Therefore, two improved methods are proposed to solve the problems of traditional BP: the improved fireworks algorithm can solve the defect of local optimization, and the fireworks algorithm is simple and has a wide search range.

2) Introduction to the improved Firework-BP algorithm

The fireworks algorithm contains three operations: explosion, variation and selection, each firework will explode and produce several sparks, some sparks have a certain probability to produce special sparks, and the sparks will be the variation sparks. Sparks are distributed randomly and evenly around the spark according to the amplitude of the current spark, while mutant sparks are generated in a normal distribution around the current spark. Each spark in the fireworks algorithm has two properties: amplitude and quantity. The brighter the fireworks (the better the target), the smaller the amplitude [15]; The brighter the spark from the explosion (the better the target), the greater the number of sparks produced by the explosion. $x_1, x_2, ..., x_i$ is the input value of the neural network, $Y_1, Y_2, ..., Y_j$ is the output value of the neural network, the number of neurons in the input layer is I, ω_{ih} is the weight of the connection between the input layer and the hidden layer, ω_{ho} is the connection weights from

the hidden layer to the output layer [16]. f_1 is the hidden layer activation function and b_1 is the hidden layer threshold. Firework is an improvement on the BP neural network back propagation.

The number of sparks in the explosion Eq (1) and (2):

$$s_i = s_{max} \frac{f_{max} - f(x_i) + \zeta}{\sum_{k=1}^{N}(f_{max} - f(x_k)) + \zeta} \qquad (1)$$

$$\hat{s}_i = \begin{cases} round(a * s_{max}), s_i < a * s_{max} \\ round(b * s_{max}), s_i > b * s_{max} \\ round(s_i), otherwise \end{cases} \qquad (2)$$

The formula (3) and (4) for the amplitude size of a spark:

$$A_i = A_{max} \frac{f(x_i) - f_{min} + \zeta}{\sum_{k=1}^{N}(f(x_k) - f_{min}) + \zeta} \qquad (3)$$

$$y_{ij} = x_{ij} + A_i * r_j \qquad (4)$$

Among them, s_{max} is the maximum number of sparks generated by the explosion, A_{max} is the maximum amplitude, ξ is a small real number, a is the minimum spark generation ratio, b is the maximum spark generation ratio, r is a random number between -1 and 1 [17].

In this paper, using the loss (Loss) and accuracy (Accuracy) of the algorithm model to evaluate. The calculation formula is as follows:

$$L = \frac{1}{2}\left\|y^{out} - y^l\right\|^2 = \frac{1}{2}\sum_{k=1}^{m}(y^{out} - y^l)^2 \qquad (5)$$

$$Acc = \frac{Number\ of\ eligible\ output\ values}{Total\ number\ of\ output\ values} * 100\% \qquad (6)$$

The flowchart of the improved Firework-BP algorithm is shown in Figure 4.
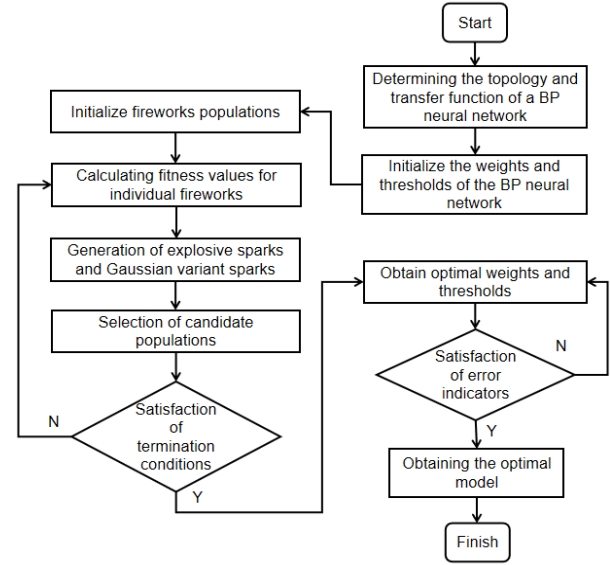

Figure 4.   Flowchart of the improved Firework-BP algorithm

IV. EXPERIMENT

A. Experimental design

Posture data collection: the sensor device needs to be worn comfortably and cannot affect the freedom of movement of the firefighting soldiers during operation. Due to the special nature of the firefighting soldiers' work and the uniqueness of the firefighting soldiers' movements during work, the position and number of wearing posture sensors should be constrained under the circumstance of guaranteeing the accuracy. Twenty subjects were selected to conduct the following experiments respectively. The BWT61CL posture sensor was fixed in the center of the back side of the subject's waist, and after many experiments, it was found that wearing it on the waist of the human body was the most ideal [18], and the posture data collection was divided into three forms: standing, free movement and falling. Each subject's data collection time for each group was 15s, four groups for each standing and activity, eight groups for the falling state, and standing and free activity were categorized as the upright state. One sample of the posture sensor contained nine data of angle x, y, z (unit: g), acceleration x, y, z (unit: °/s) and angular velocity x, y, z (unit: °).

Physiological data collection: There is a gap between the physiological state data of firefighting soldiers collected in the laboratory and the state data of real firefighting operations. In order to ensure the objectivity of the data testing, 20 male graduate students, whose height is not less than 170cm, whose weight is not more than 20% of the standard weight for men and not less than 10% of the standard weight for men, and who are in good health, were selected; all participants were provided with a written informed consent form, and was informed of the specific contents of the experiment and the precautions to be taken when collecting data, to ensure that the data collected could be effectively used for the experiment. The data were collected in a manner that ensured that the data could be used effectively in the experiments. Physiological data were collected using the ErgoLAB pulse PPG sensor and the ErgoLAB pulse ECG sensor. The pulse PPG sensor is worn with a black ear clip attached to the earlobe and a strap secured to the arm; the ECG sensor is worn with three electrode pads attached to the three electrodes of the sensor and a strap secured to the subject. In order to increase the situational variability and realism of the data, the types of data collected during the firefighting manoeuvre were categorized into low-risk, medium-risk, and medium-high-risk in order to collect a wider range of physiological state reference values.

B. Device Composition

The pulse PPG sensor is shown here, and the light intensity it detects changes pulsatilly with the heartbeat. This light intensity change signal is converted into an electrical signal, which reflects the change of the blood flow after amplification. The signals analyzed in the experiments were the R-R period, which indicates the heart rate or interbeat period, and the P-P period, which reflects the heart rate cycle of sinus rhythm, but it is difficult to accurately detect the P-P period, so the R-R period was used in the actual detection. The R-R interval is usually equal to the P-P interval.

The electrocardiographic ECG sensor, shown in the figure, detects signals as the heart is stimulated sequentially by the pacemaker, atria, and ventricles during each cardiac cycle. Along with the bioelectric changes, various forms of potential change patterns are mapped from the body surface by means of a cardiac tracer. The human heart rate (R-R spacing) fluctuates under normal conditions, and the R-R spacing generally varies by tens of milliseconds. Which responds to the changing pattern of the heart's rhythm, and is a commonly used indicator for the study of cardiac autonomic function.

The attitude sensor can recognize the attitude of all parts of the limbs and torso of the firefighting soldier, integrating a high-precision three-axis gyroscope, three-axis accelerometer and three-axis Euler angle, using a high-performance microprocessor and advanced dynamics solving and Kalman dynamic filtering algorithms [18].The output frequency in the attitude sensor is 100Hz and the baud rate is 115200bps.The X-axis, Y-axis and Z-axis in the attitude sensor correspond to roll angle, pitch angle and yaw angle respectively.

C. Experimental results

Experiments have been conducted on the data fusion decision based on the firefighting single soldier in the fireground operation of multi-sensors on the BP neural network algorithm and Firework-BP neural network algorithm. In this paper, using the loss and accuracy of the algorithm model to evaluate.

The Loss and Accuracy plots of the BP neural network for data fusion are shown in Figure 5 and Figure 6.
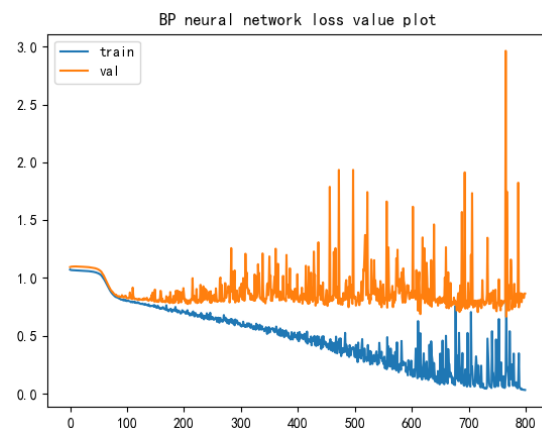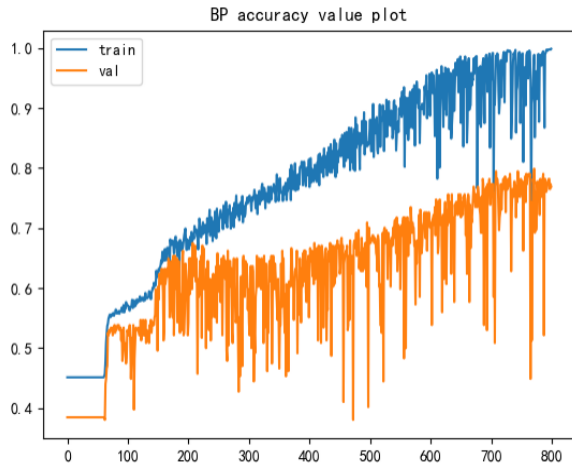

Figure 5.   Loss plots for BP data fusion

Figure 6.   Accuracy plots for BP data fusion

The Loss and Accuracy plots of the Firework-BP neural network for data fusion are shown in Figure 7 and Figure 8.
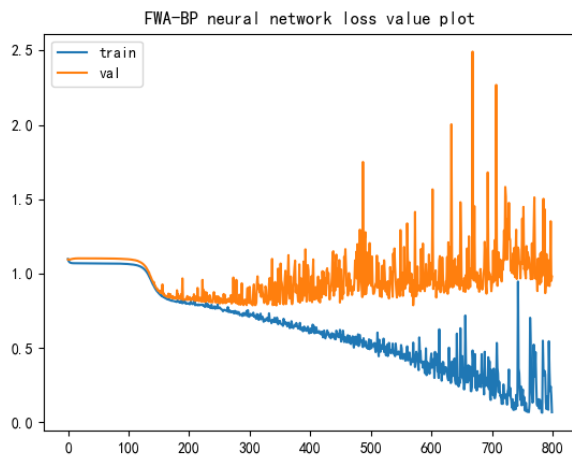

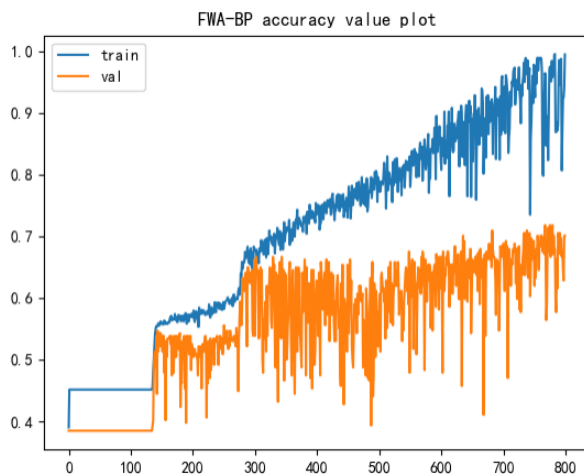Figure 7.   Loss plots for Firework-BP data fusion

Figure 8.   Accuracy plots for Firework-BP data fusion

As can be seen from the above figure, the number of iterations for both models is 800, the loss of the validation set after data fusion of the improved Firework-BP neural network model is smaller than that of the BP neural network model, and the accuracy of the validation set after data fusion of the improved Firework-BP neural network model is higher than that of the BP neural network model, which proves that the Firework-BP neural network algorithm proposed in this paper has a higher accuracy of multi-sensor data fusion. The loss decreases the fastest when the iteration is almost 100 times, the accuracy of the BP neural network model increases the fastest in the 100th and 300th times, and the accuracy of the Firework-BP neural network model increases the fastest in the 80th and 200th times, and it can be clearly seen that the stability of the improved Firework-BP neural network model is better by comparing the accuracy graphs of the two models. In this paper, the accuracy of the algorithm model is also better when the sudden failure problem of one of the sensors is considered, and the robustness of the algorithm model is better.

V. CONCLUSIONS

Firefighting singletons are the main body of firefighting work, fire safety and security system effectively protects the safety of firefighting singletons when they are operating in the fire scene, using multi-sensors for target detection and fusion, verifying the algorithm's role of enhancing firefighters' safety and task efficiency through experiments and data analysis, and providing scientific technical support and guidance for the practical application of firefighting singletons.

In this paper, multi-sensor data fusion based on Firework-BP neural network algorithm is used to judge the physical state of firefighting singletons, which not only improves the low accuracy of the judgment of a single class of sensors, but also effectively improves the stability of the BP neural network algorithm. The vital signs of firefighters are categorized into three types: safety, abnormality and warning, alert firefighters with warning vital signs, remove firefighters from the fire scene if necessary, minimizing the risk factor for single firefighters, and rescue and resuscitate

firefighters whose vital signs are in danger, and the state of firefighting singletons is predicted according to the trained model, which can effectively improve the decision-making on the safety and security of firefighting singletons through multi-sensor data fusion and improve the stability of the system. The accuracy of the improved Firework-BP data fusion algorithm model is improved by 3.64%.It is verified that the improved model proposed in this thesis is effective and reliable, and can be widely applied in the actual operation of protecting firefighting singletons, which can effectively improve the personal safety of firefighting singletons, Contribute valuable ideas and effective methods for future research in the area of protection of the firefighting unit.

REFERENCES

[1] Zhou Jinghong. Prevention and control measures of firefighters' casualties in fire-fighting and rescue [J]. Today's Firefighting, 2022, 7(08): 133-135.

[2] Shi Xiaodong,Yang Shikun. A Review of Research on Multi-Sensor Information Fusion [J]. Communication and Information Technology, 2022, 260(06): 34-41.

[3] Yu Guipeng. Research on the safety of firefighters in fire fighting and rescue work [J]. Today's Firefighting, 2023, 8(02): 124-126.

[4] Shi Xiaodong, Yang Shikun. A review of multi-sensor information fusion research [J]. Communication and Information Technology, 2022, 260(06): 34-41.

[5] Smith Denise L, Haller Jeannie M, Dolezal Brett A, Cooper Christopher B, Fehling Patricia C. Evaluation of a wearable physiological status monitor during simulated fire fighting activities. [J].Journal of occupational and environmental hygiene, 2014, 11(7): 156-160.

[6] Bu Y, Wu W, Zeng X, et al. A Wearable Intelligent System For Real Time Monitoring Firefighter's Physiological State and Predicting Dangers[C]// Hangzhou Dianzi University, Chinese Institute of Electronics. Proceedings of 2015 IEEE 16th International Conference on Communication Technology (ICCT).Institute of Electrical and Electronics Engineers, 2015: 451-454.

[7] Alessandra A, Matteo C,A. I C, et al. Smart Textiles and Sensorized Garments for Physiological Monitoring: A Review of Available Solutions and Techniques [J]. Sensors, 2021, 21(3).

[8] YANG Shufeng, SUI Hulin, LI Zhigang. Design and realization of firefighter vital signs monitoring system [J]. Fire Science and Technology, 2014, 33(03): 314-317.

[9] LI Haoze, LI Penghui. Analysis of firefighter casualty causes and prevention countermeasures in firefighting and rescue [J]. Firefighting World (Electronic Edition), 2022, 8(13):62-63.

[10] Yu Jiaming. Design of firefighter status monitoring and analysis system based on smart wearable device sensing [J]. Firefighting World (Electronic Edition), 2022, 8(06): 72-74.

[11] Zhu Juxiang, Gu Wei, Luo Danyue et al. Multi-sensor data fusion based on PSO optimized BP neural network [J]. China Test, 2022, 48(08):94-100.

[12] Ntanasis, P., Pippa, E., Özdemir, A. T., Barshan, B., & Megalooikonomou, V. (2017).Investigation of Sensor Placement for Accurate Fall Detection. Wireless Mobile Communication and Healthcare, 225–232.

[13] Zhou, T. Y.. Research on multi-sensor data fusion based on fuzzy theory and neural network [D]. Nanjing University of Information Engineering, 2022, 10(25): 124-129.

[14] Li Si-Nan, Zhao H. Human physiological state based on multi-sensor [D]. Multi-sensor based visualization technique for human physiological state discrimination [J]. Sensors and Microsystems, 2019, 38 (12):25-28+32.

[15] Ling Xiao, Xu Lushuai, Yu Jianping, Liang Rui. Corrosion rate prediction in oil pipelines based on improved BP neural network [J].Sensors and Microsystems, 2021, 40(02): 124-127.

[16] Li Y, Zhuohui L, Weijian R, et al. Improving the Drilling Parameter Optimization Method Based on the Fireworks Algorithm [J]. ACS omega, 2022, 7(42):21-26.

[17] ZHOU Lin, LEI Liping, YANG Longfeng. Multi-sensor based human behavior recognition system [J]. Sensors and Microsystems, 2016, 35(03):89-91+95.

[18] Zhang Lei, Chen Feng, Yang Wenhao, Li Hongzhen. Design of fall remote alarm system based on six-axis attitude sensor [J]. Technology and Innovation, 2022(02): 57-60.